The postcranial anatomy of pachycephalosaurs (Ornithischia: Pachycephalosauria) and its phylogenetic and myological implications

by

Bryan Moore

A thesis submitted to the Faculty of Graduate and Postdoctoral Affairs in partial fulfillment of the requirements for the degree of

Master of Science

in

Earth Sciences

Carleton University
Ottawa, Ontario

Abstract

Pachycephalosaurs are a group of small-bodied, bipedal ornithischian dinosaurs. They are best known for their characteristic fusion of the frontals and parietals into a "skull dome". This feature is the most commonly preserved element of pachycephalosaurs and therefore much research has been dedicated to their cranial anatomy. The postcranial skeleton is not often preserved and does not receive the same attention. CMN 22039 at the Canadian Museum of Nature represents a rare postcranial specimen. The goal of this study is to use CMN 22039 with other comparable specimens to investigate the postcranial anatomy of pachycephalosaurs in both a functional and phylogenetic context.

Examining CMN 22039 alongside other pachycephalosaurs revealed that new postcranial characters change the current phylogeny of pachycephalosaurs, although, it remains unclear if this is due to ontogenetic variations. Studying the postcranial anatomy of *Stegoceras validum* also facilitated the first detailed myological reconstruction of the appendicular skeleton of pachycephalosaurs.

Acknowledgements

I would like to thank my supervisors, Dr. Jordan Mallon and Dr. Tim Patterson, for their support and insights throughout this project. Thank you to my other committee members, Dr. Michael Ryan and Dr. David Evans, for their guidance and helpful feedback. I would also like to thank the Canadian Museum of Nature (CMN) and the Royal Ontario Museum (ROM) for providing access to the specimens required for this study. I am grateful to Dr. Scott Ruffalo and Alan McDonald for providing me with digital specimens when in person study was impossible due to the COVID-19 pandemic. I would like to thank Mathew Roloson for teaching me how to use 3D programs such as Blender (2018) which were essential to the completion of this study. Finally, I would like to thank Cary Woodruff for teaching me proper osteohistological procedures and methods, and Dr. Kevin Seymour, and Brian Iwama for allowing access to and guiding me through the collections facilities of the ROM.

Table of Contents

List of Tables

List of Figures

Chapter 1: Introduction

Pachycephalosauria (Figure 1) is a group of small-bodied (~2 to 6 m in length), bipedal ornithischian dinosaurs, defined as all taxa more closely related to *Pachycephalosaurus wyomingensis* (Gilmore, 1931) than to *Triceratops horridus* Marsh, 1889 (Sereno, 1997; Maryańska *et al*., 2004). Perhaps the most striking feature of the group is their characteristic fusion and thickening of the frontals and parietals, and adjacent peripheral elements, into a "skull dome". The dome is often adorned around its lateral and posterior margins by rounded nodes or spikes (Cooper, 2004; Goodwin & Horner, 2004; Maryańska *et al*., 2004). These animals are also unique among the herbivorous ornithischians of the Late Cretaceous because they display a heterodont dentition; the premaxillary teeth are peg-like and their cheek teeth are variably leaf-shaped. The rostrum terminates in a short beak. These animals had short forelimbs and hindlimbs compared to other bipedal ornithischians, such as thescelosaurids and other small ornithischians, and a wide torso and pelvic region (Maryańska *et al*., 2004). Although postcranial material is scarce, several synapomorphies have been identified within this part of the skeleton. Diagnostic postcranial features include a sigmoidal dorsal margin of the ilium, a prominent medial flange projecting from the iliac blade, a pubis that is nearly or fully excluded from the acetabulum, double ridge and groove articulations on the dorsal vertebrae, elongate sacral ribs, and the presence of a caudal basket of ossified tendons (Figure 2; Maryańska & Osmolska, 1974; Maryańska *et al*., 2004; Brown & Russell, 2012).

A

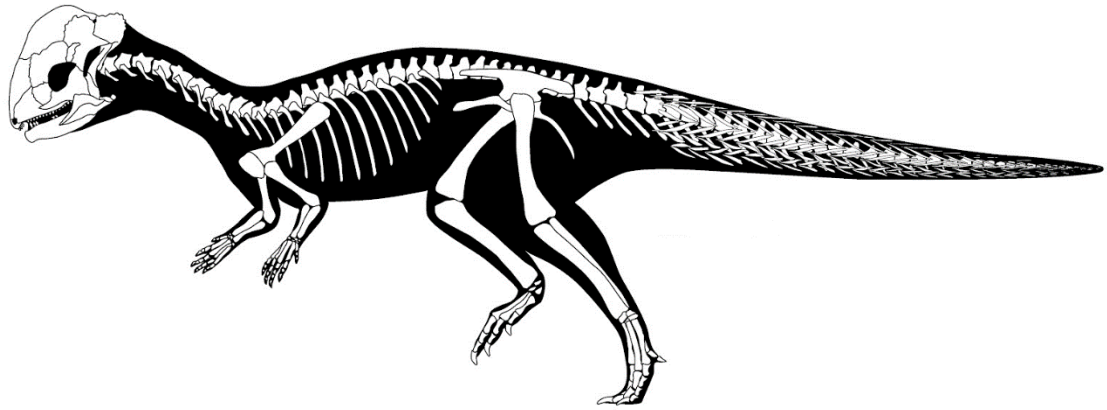

B

Figure 1. (A) Skeletal reconstruction of the general pachycephalosaurian body plan (adapted from Evans *et al*., 2013) and (B) life reconstruction of the pachycephalosaur *Stegoceras validum* in a coastal flood plain habitat (Image credit: Brett Booth).

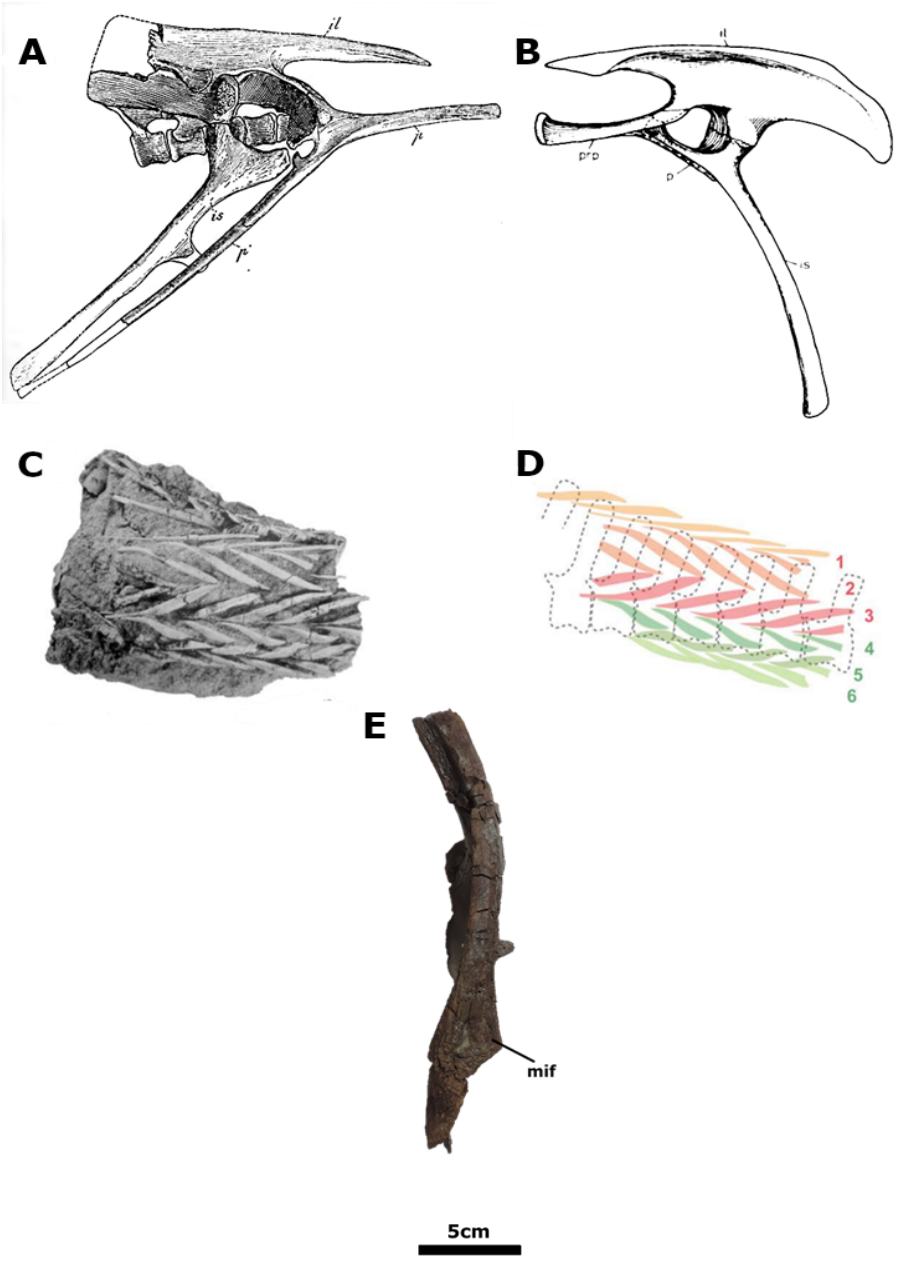

Figure 2. Diagnostic pachycephalosaurian postcranial features: (A) reconstruction of the right pelvis of *Thescelosaurus* in lateral view showing the primitive condition of the pachycephalosaurian pelvis from Gilmore (1915), (B) reconstruction of the right pelvis of *Homalocephale calathocercos* in medial view showing its reduced pubis compared to that of *Thescelosaurus* from Maryańska *et al*. (2004), (C) caudal basket of *Homalocephale* (MPC-D 100/1201), (D) reconstruction of the caudal basket of MPC-D 100/1201 in life orientation overlapping the vertebral column from Brown & Russell (2012), and (E)) Left ilium of *Pachycephalosaurus* (ROM 73555) in dorsal view showing the prominent medial flange of the iliac blade. Abbreviations: il - ilium, is - ischium, mif - medial iliac flange, p - pubis, prp - prepubic process.

Pachycephalosaur Paleogeography

Pachycephalosaurs existed from the Santonian to the Maastrichtian (~86 to 66 Ma) in North America and Asia (Butler & Sullivan, 2009). If the recent interpretation of *Heterodontosaurus* Crompton & Charig, 1962 as a basal pachycephalosaur is accepted (Dieudonné *et al*., 2020) then pachycephalosaurs may have existed as far back as the earliest Jurassic. However, this hypothesis has not yet undergone independent testing, and so will not be considered further here. Pachycephalosaurs likely originated in central Asia and migrated to North America via Beringia just prior to the late Santonian, ~83.6 Ma (Maryańska *et al*., 2004). At this time, North America and Asia had a greenhouse climate. North America was inundated by the Western Interior Seaway, which possibly regulated a subtropical climate with seasonally warm temperatures (Fricke *et al*., 2010; Wang *et al*., 2013). Asian deposits from this time consist of abundant aeolian dunes and isolated lake systems, indicating a much more arid environment (Maryańska *et al*., 2004; Wang *et al*., 2013). Areas where Asian pachycephalosaurs are found, however, such as the upper Nemegt Formation, are often characterized by a wetter climate and fluvial deposits (Evans *et al*., 2011, 2018; Eberth, 2018). Pachycephalosaurs, therefore, may have occupyied similar climates on both continents.

Pachycephalosaur Paleobiology

Much of what is known about pachycephalosaur biology is derived from the extensive research that has been done regarding their skulls. The domes of

pachycephalosaurs have inspired much debate as to their primary function. This debate has resulted in two primary hypotheses. The first states that the dome was a display structure, functioning in sexual selection and/or species recognition (Goodwin *et al*., 1998; Goodwin & Horner, 2004; Knell & Sampson, 2011). This hypothesis has been criticized, however, as the domes of pachycephalosaurs require a significant amount of material and energy investment for a relatively simple display structure (Peterson *et al*., 2013). Additionally, the domes of pachycephalosaurs have been proposed to have changed drastically over the course of ontogeny, posing difficulties for species recognition (Williamson & Carr, 2002; Goodwin & Horner, 2004; Schott *et al*., 2011; Peterson *et al*., 2013). Finally, the domes of adult pachycephalosaurs from varying species and genera are all relatively similar, once again presenting issues for the species recognition hypothesis (Hone & Naish, 2013; Peterson *et al*., 2013). The nodal ornaments surrounding the dome, however, are species specific and vary minimally through ontogeny (Schott & Evans, 2012). They may have served as display structures or functioned in species recognition (Schott & Evans, 2012).

The second hypothesis states that the dome was used as a weapon for intraspecific combat in shoving, head-butting, or flank-butting competitions with other males (Colbert, 1955; Galton, 1970; Sues; 1978, Bakker *et al*., 2006; Snively & Cox, 2008; Lehman, 2010; Longrich *et al*., 2010; Snively & Theodor, 2011; Peterson *et al*., 2013). Although debated (Goodwin and Horner, 2004; Padian & Horner, 2010), this hypothesis is mostly supported by evidence demonstrating that the structure of the dome would have been able to withstand high impacts and redistribute the energy away from the

brain (Snively & Theodor, 2011; Peterson *et al*., 2013). Further support has been found in the form of pathological features such as irregular lesions and remodeling consistent with osteological damage from head-butting competitions (Peterson *et al*., 2013).

Much about pachycephalosaur dietary habits may be inferred from their dental morphology. It has been hypothesized that their beak and peg-like premaxillary teeth were used for gripping and gathering food while their cheek teeth were used for simple chewing of vegetation (Weishampel & Norman, 1989; Fastovsky & Weishampel, 1996). Their wide gut and hip structures also suggest the presence of a fermentation chamber for digesting fibrous vegetation. This is also consistent with wear patterns found on pachycephalosaur teeth, which indicate a diet plausibly including leaves, stems, seeds, and fruits (Maryańska & Osmolska, 1974; Maryańska *et al*., 2004).

Pachycephalosaur Taphonomy

Compared to the megaherbivores of Late Cretaceous North America and Asia, pachycephalosaur postcranial remains are rare. One possible reason for the lack of pachycephalosaurian remains is their small size. Since larger skeletal elements are more robust to destructive taphonomic processes, the small fragile elements of pachycephalosaur skeletons are less likely to be preserved. In the Dinosaur Park Formation (DPF), Alberta, Canada, where many pachycephalosaur remains have been discovered, there is a significant correlation between animal size (estimated body mass) and skeletal completeness (Brown *et al*., 2013). This may reflect the meandering and

braided river palaeoenvironments that characterize the deposits of the DPF. If the remains of small-bodied taxa were exposed to fluvial systems after death, then it is likely that their individual skeletal elements would be transported, sorted, and possibly destroyed due to their fragility (Brown *et al*., 2013). As pachycephalosaurs were small dinosaurs, their representation in the fossil record is low. Most partially articulated skeletons have been discovered in Asia, likely due to its drier paleoclimate and lack of widespread transport mechanisms (Gradzinsky, 1970; Gradzinsky & Jerzykiewicz, 1974; Gradzinsky *et al*., 1977; Maryańska *et al*., 2004). Even when taking these exceptional specimens into account, the vast majority of pachycephalosaurian remains consist of isolated, robust skull domes (Table 1; Evans et al. 2013). Since the skull dome is the element that is most often preserved, its morphology is largely used to distinguish between genera and species (Snively & Theodor, 2011; Evans et al 2013).

The dearth of pachycephalosaur postcrania has complicated our understanding of their biology in several respects. First, little is known about their ontogeny, beyond the growth and fusion of the dome and its associated ornamentation (Sues, 1978; Horner & Goodwin, 2006, 2009; Schott, 2011; Schott *et al*., 2011, Schott and Evans 2012, 2017). Second, postcranial characters make up a small ratio of the overall characters used in the most recent phylogenetic studies, making up only 13 of a total 50 characters in the studies of Evans *et al*. (2013) and Williamson and Brusatte (2016), a situation that may not only bias topologies (Mounce *et al*., 2016), but also result in the poor systematic resolution of most analyses. Lastly, the myology of the postcranium is poorly known,

particularly as regards the uniquely wide pelvic girdle, reduced pubis, and medial iliac flange (Maryańska *et al*., 2004).

Thesis Layout and Goals

Recently, a new small pachycephalosaur specimen containing a significant amount of postcranial material was identified by D. Evans at the Canadian Museum of Nature (CMN 22039). Chapter 2 will describe the morphology of this important new skeleton, making comparisons to other pachycephalosaur postcrania and relevant outgroup taxa. The osteohistology of a limb bone of the specimen will also be described to better understand its ontogenetic status. Phylogenetically informative postcranial characters of this and other skeletons will be identified to update and improve the resolution of current pachycephalosaur phylogenies. Chapter 3 will present a reconstruction of the appendicular myology of a related pachycephalosaur skeleton (*Stegoceras validum*, UALVP 2) to inform our understanding of the functional morphology of the pachycephalosaur postcranium. Chapter 4 will present conclusions to the aforementioned sections, discuss the importance and limitations of my findings, and provide insight on future directions of study.

Chapter 2: Description of a juvenile pachycephalosaur (Dinosauria: Ornithischia) skeleton from the Frenchman Formation of Saskatchewan and its phylogenetic implications

Introduction

The general lack of preserved pachycephalosaur material has hindered our understanding of their osteology, growth patterns and evolutionary relationships. As new postcranial material is unearthed, it may help to fill these gaps. One such example is CMN 22039 (Figure 3) at the Canadian Museum of Nature (CMN). It is a small, partial postcranium that was collected by Dale Russell and Gilles Danis from the upper Maastrichtian Frenchman Formation of Saskatchewan in 1973. Initially assumed to belong to a juvenile *Thescelosaurus* (Russell & Manabe, 2002), the skeleton has never been described or illustrated, and is reinterpreted here as pertaining to a juvenile pachycephalosaur. This recognition cements CMN 22039 as Canada's second most complete pachycephalosaur postcranium, after UALVP 2, a largely complete skeleton of *Stegoceras validum* (Lambe 1902). In this chapter, I will illustrate and describe CMN 22039, and compare it to other pachycephalosaurs and relevant outgroup taxa. I will also conduct an osteohistological analysis of CMN 22039 to confirm its ontogenetic age and to improve our understanding of pachycephalosaur growth patterns. The specimen will then be coded into the recent character matrix of Williamson and Brusatte (2016),

including newly identified characters, to determine its phylogenetic position and the influence of these new characters on pachycephalosaur topology.

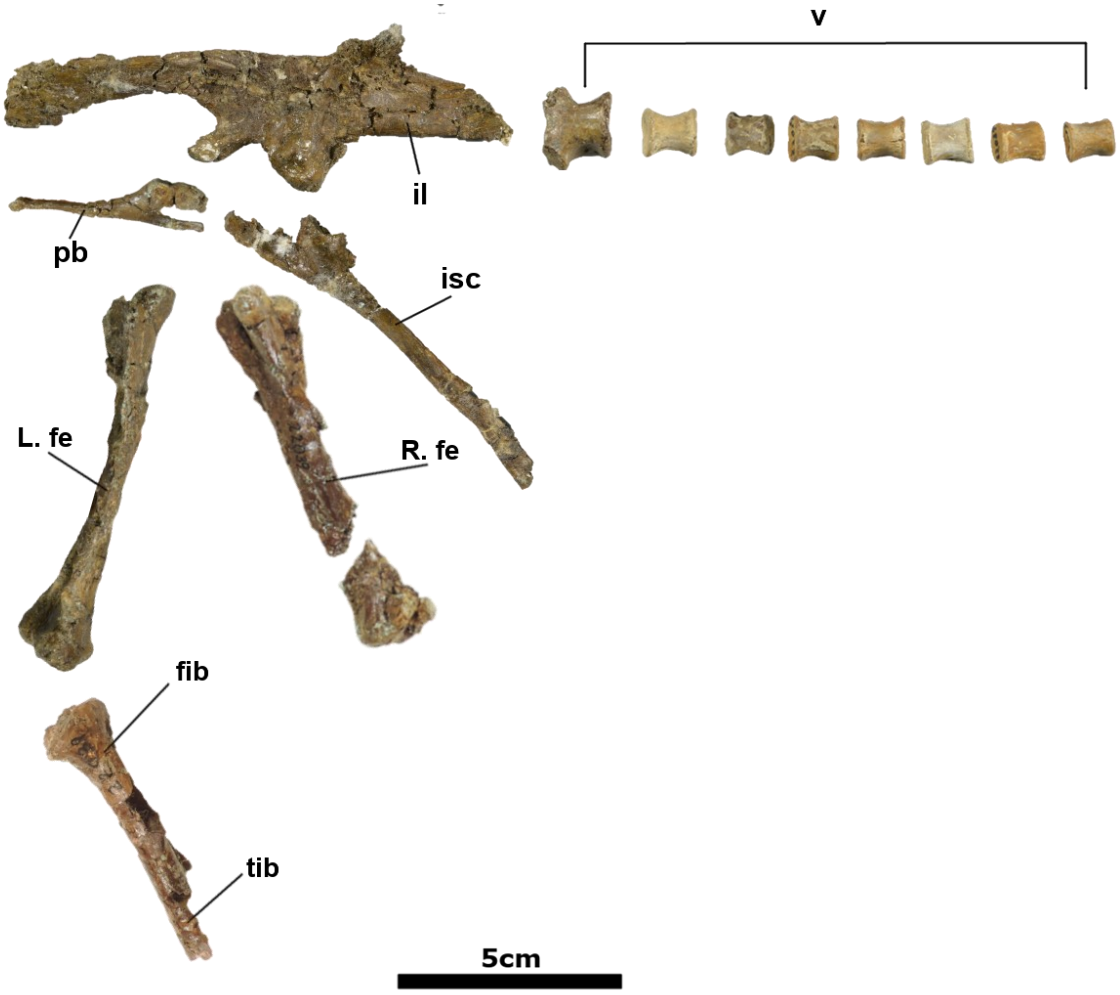

Figure 3. Major preserved elements of CMN 22039 in left lateral view. Abbreviations: fib - left fibula, il - right ilium, isc - right ischium, L. fe - left femur, R. fe - right femur, tib - left tibia, v - vertebrae.

Regional Geology

CMN 22039 was found within the Frenchman Formation, which is the youngest of five Maastrichtian formations in southern Saskatchewan (Bamforth *et al*., 2014). The

other four formations (oldest to youngest: Bearpaw, Eastend, Whitemud, and Battle) show evidence of regression of the Western Interior Sea throughout the Maastrichtian (Fraser *et al.,* 1935; Furnival, 1946; Mossop & Shetsen, 1994; Bamforth *et al*., 2014). The Frenchman Formation was deposited in a low-lying system of meandering rivers and overbank settings (McIver, 2002; Bamforth *et al*., 2014). The base of the formation borders the Battle Formation in most localities. However, in some areas, the units underlying the Frenchman Formation have been largely eroded, causing it to rest on one of the Whitemud, Eastend, or Bearpaw formations (Kupsch, 1957, Kolaceke *et al*., 2018). To the East and West, the Frenchman Formation gradually thins and overlies progressively younger units. Thinning continues towards central and eastern Saskatchewan, where the formation completely disappears (Fraser *et al*., 1935; McIver, 2002). In the northern and eastern areas of the formation, on the flanks of the Cypress Hills, up to 60 m (200 ft) of older formations have been removed through erosion (Kupsch, 1957). The erosion causing the unconformable hiatus at the base of the Frenchman Formation occurred at the beginning of the late Maastrichtian (Kupsch, 1957). The subsequent deposition of the Frenchman Formation is attributed to subsidence associated with orogeny action in the Cordillera (Catuneanu & Sweet, 1999; McIver, 2002). The top of the Frenchman Formation borders the base of the Ravenscrag Formation, marked by the Ferris Coal Seam (Fraser *et al*., 1935; Furnival, 1946; Kupsch, 1957; McIver, 2002; Bamforth *et al*., 2014). This layer is thought to be the equivalent of the Z coal observed in the Hell Creek Formation. (Baadsgaard & Lerbekmo, 1980; Baadsgaard *et al*., 1987; Lerbekmo *et al*., 1987). The overall thickness of the Frenchman

Formation varies from 8 m at its thinnest to 68 m at its thickest (McIver, 2002; Bamforth *et al*., 2014).

The lithology of the Frenchman Formation can be subdivided into two main, laterally discontinuous lithofacies (Kupsch, 1956; McIver, 2002; Bamforth *et al*., 2014; Kolaceke *et al*., 2018). The first is sand-dominated and represents fluvial deposits (mostly fine-grained lithic wackes). It contains cross-stratification, fossil plant debris, coal lenses, and some clay/silt. This facies is common in the lower portion of the Frenchman Formation; however, in some areas it occurs higher in section (Kupsch, 1956; McIver, 2002; Bamforth *et al*., 2014; Kolaceke *et al*., 2018). The second facies is dominated by silt- and claystones and ironstone lenses (Kupsch, 1956; McIver, 2002; Bamforth *et al*., 2014; Kolaceke *et al*., 2018). It commonly overlies the sandstone lithofacies; however, their order is not consistent across all localities (Kolaceke *et al*., 2018). Kolaceke *et al*. (2018) recognized two additional facies, one comprised of fine sandstone and siltstone interbedded with clay and the other made mostly of massive sandstone with interbedded siltstone and claystone. These tend to be thinner and less widespread (Kolaceke *et al*., 2018).

The Frenchman Formation preserves an assortment of vertebrate macrofossils, microfossils, and invertebrate traces. The non-dinosaurian vertebrate fossils are represented by several species of fish, freshwater turtles, crocodiles, *Champsosaurus*, amphibians, birds, squamates, chondrichthyans, and mammals (Storer, 1989; Tokaryk & James, 1989; Tokaryk 1997; Tokaryk & Bryant, 2004; Tokaryk, 2009; Tokaryk & Brinkman, 2009; Brown *et al*., 2011; Bamforth *et al*., 2014). Of the dinosaurian fossils of

the Frenchman Formation, those of *Triceratops prorsus* Marsh, 1890 are the most common (Tokaryk, 2009). Several theropod taxa (e.g., *Tyrannosaurus rex* Osborn, 1905, Ornithomimidae indet., Caenagnathidae indet., *Troodon*) are also preserved alongside the ornithischians *Edmontosaurus annectens* Lambe, 1917, *Thescelosaurus assiniboiensis* Gilmore, 1913, an unidentified ankylosaur, and, prior to CMN 22039, one definitive pachycephalosaur (cf. *Sphaerotholus buchholtzae*) (Tokaryk, 1997; Tokaryk, 2009; Brown *et al*., 2011; Bamforth *et al*., 2014; Bell *et al*., 2015; Mallon *et al*., 2015). The latter is based on a single occurrence of a left postorbital (Mallon *et al*., 2015).

CMN 22039 Locality

CMN 22039 was discovered by Dale Russell immediately outside the east block of Grasslands National Park, Saskatchewan (approximate UTM coordinates: 13U 0384904 m, 5436956 m). An attempt to relocate the original quarry was mounted by Jordan Mallon and Mat Roloson in the summer of 2020; however, they were unsuccessful. The specimen was preserved at the base of a ~6.7 m thick claystone unit of the Frenchman Formation roughly 14 meters below the Ferris Coal Seam (Figure 4). This claystone unit was likely part of a floodplain deposit.

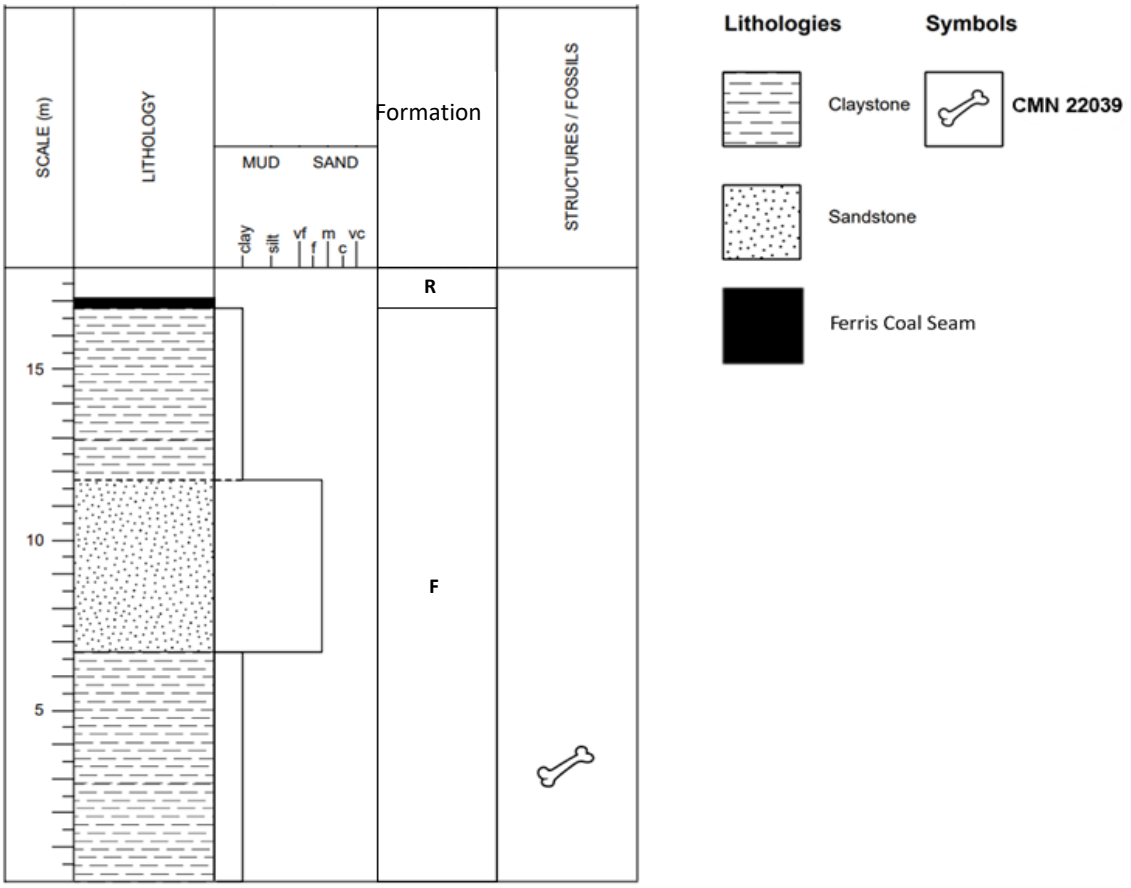

Figure 4. Stratigraphic section of the Frenchman Formation showing the geologic location of CMN 22039 as depicted in the 1973 field notes of Dale Russell (on file at the Canadian Museum of Nature). Abbreviations: F - Frenchman Formation, R - Ravenscrag Formation.

Systematic paleontology

Dinosauria Owen, 1842

Ornithischia Seeley, 1887

Pachycephalosauria, Maryánska and Osmólska, 1974

Pachycephalosauridae, Sternberg, 1945

Pachycephalosaurinae, Sternberg, 1945

Methods

Skeletal elements were measured using a tailor's measuring tape and an Empire six-inch digital electronic caliper (model 2789). Measurements of these bones are provided in Tables 1-3. All elements were described and compared to other pachycephalosaurs with postcranial material. I observed *Pachycephalosaurus sp.* (ROM 73555), *P. wyomingensis* (NSM PV 20423), and *S. validum* (UALVP 2) first-hand. Specimens studied from photographs and the literature include *Homalocephale calathocercos* Maryańska & Osmolska, 1974 (MPC-D 100/1201), *Prenocephale prenes* Maryańska & Osmolska, 1974 (MPC-D 100/1204), *Goyocephale lattimorei* Perle *et al*., 1982 (GI SPS 100/1501), and *Wannanosaurus yansiensis* Hou, 1977 (IVPP V 4447). Relevant outgroup taxa, including *Psittacosaurus mongoliensis* Osborn, 1923, *Stenopelix valdensis* Meyer, 1857, *Thescelosaurus neglectus* Gilmore, 1913, *Thescelosaurus sp.*, and *Heterodontosaurus tucki* were also used for comparison (Gilmore, 1913, 1915, 1924; Perle *et* al., 1982; Sues & Galton, 1982; Sereno, 1987; Sereno *et al*., 1988; Maryańska *et al*., 2004; Butler & Sullivan, 2009; Brown *et al*., 2011).

Table 1. Limb bone measurements of CMN 22039 (N/A indicates broken or missing material).

Element	**Proximodistal length (mm)**	**Midshaft mediolateral diameter (mm)**	**Midshaft anteroposterior diameter (mm)**	**Midshaft circumference (mm)**
Left Femur	84.5	6.5	13.0	35.1
Right Femur	100.5	12.0	6.4	34.5
Left Tibia	N/A	7.7	N/A	N/A
Left Fibula	N/A	4.2	N/A	N/A

Table 2. Pelvic girdle length measurements of CMN 22039 (an * indicates material that is partially broken or missing).

Element	**Length (mm)**
Right Ilium	107.0*
Preacetabular Process of Right Ilium	46.0
Postacetabular Process of Right Ilium	34.5*
Left Ischium	98.5*
Left Pubis	9.0

Table 3. Centrum measurements of CMN 22039.

Relative centrum position	**Anteroposterior length (mm)**	**Width of anterior face (mm)**	**Width of posterior face (mm)**	**Anterior dorsoventral height (mm)**	**Posterior dorsoventral height (mm)**
1	19.5	17.0	14.0	10.0	10.0
2	17.0	11.5	N/A	9.7	N/A
3	12.0	11.5	10.5	9.0	9.0
4	9.5	10.0	9.0	8.0	7.5
5	8.5	8.5	8.0	7.5	7.5
6	8.0	8.5	8.5	7.2	7.0
7	8.5	8.5	N/A	7.0	N/A
8	8.0	8.5	8.0	7.0	6.5
9	8.5	8.0	7.5	6.5	6.0
10	8.5	8.0	7.5	6.0	5.8
11	8.0	8.5	8.0	6.0	5.0

Axial Skeleton

Vertebrae (Figure 5). A single sacral centrum is preserved. It is larger than the preserved caudal centra and can be identified by its low ventral keel, the extreme concavity of its lateral surfaces, and its flaring superior articular processes (Maryańska & Osmólska, 1974; Maryańska *et al*., 2004).

Fourteen caudal centra are preserved, ~30% of the tail based on the preserved vertebrae of other pachycephalosaurs (Gilmore, 1913, 1915, 1924; Perle *et* al., 1982; Sues & Galton, 1982; Sereno, 1987; Sereno *et al*., 1988; Maryańska *et al*., 2004; Butler & Sullivan, 2009; Brown *et al*., 2011), dissociated from their neural arches. They can be identified as such by the combined presence of the following features: spool-shaped centra, rapid shallowing of the ventral keel in posterior caudals, and rib attachments on the centra as opposed to the transverse processes. These conditions are common to all pachycephalosaurs but do not distinguish them from the consulted outgroup taxa (Gilmore, 1913; Gilmore, 1915; Sues & Galton, 1982; Sereno, 1987; Sereno *et al*., 1988; Maryańska *et al*., 2004, Butler & Sullivan, 2009; Brown *et al*., 2011). The larger, anterior caudal vertebrae are subequal in size and possess a ventral keel that becomes increasingly shallow in the posterior caudals. The two largest, anteriormost caudal centra bear sutural surfaces on their lateral faces for attachment of the caudal ribs. These surfaces are round in outline and occur directly caudal to the anterior face of the centrum and border on the boundary between the centrum and the neural arch. The posterior caudal vertebrae are longer anteroposteriorly compared to their height but remain subequal in length and width (Table 3).

Only four disassociated neural arches are preserved well enough to be identified, all of which are incomplete and at least partially warped taphonomically. They appear to belong to dorsal vertebrae based on their robust neural spines which are subrectangular in lateral view, their caudally steep transverse processes, and an observable double

ridge and groove articulation of the pre- and post-zygapophyses (Maryańska *et al*., 2004).

Figure 5. Preserved centra of CMN 22039 in (A) dorsal and (B) ventral views.

The most complete neural spine (Figure 6) is dorsoventrally long and slightly inclined caudally at an angle of ~75°. The two pre-zygapophyses extend anteriorly and slightly dorsally from the neural arch and are concave medially. The post-zygapophyses are shorter than the pre-zygapophyses and extend directly caudally from the neural arch. Each post-zygapophysis displays a groove on its ventral surface to receive the dorsal ridge of the pre-zygapophyses of the following vertebra. This character is shared among all pachycephalosaurs with well-preserved dorsal vertebrae (*Pachycephalosaurus*, *Stegoceras*, *Homalocephale*, and *Prenocephale*) and is not present in the consulted outgroup taxa (Gilmore, 1913; Gilmore, 1915; Sues & Galton, 1982; Sereno, 1987; Sereno *et al*., 1988; Maryańska *et al*., 2004, Butler & Sullivan, 2009; Brown *et al*., 2011; Evans *et al*., 2013).

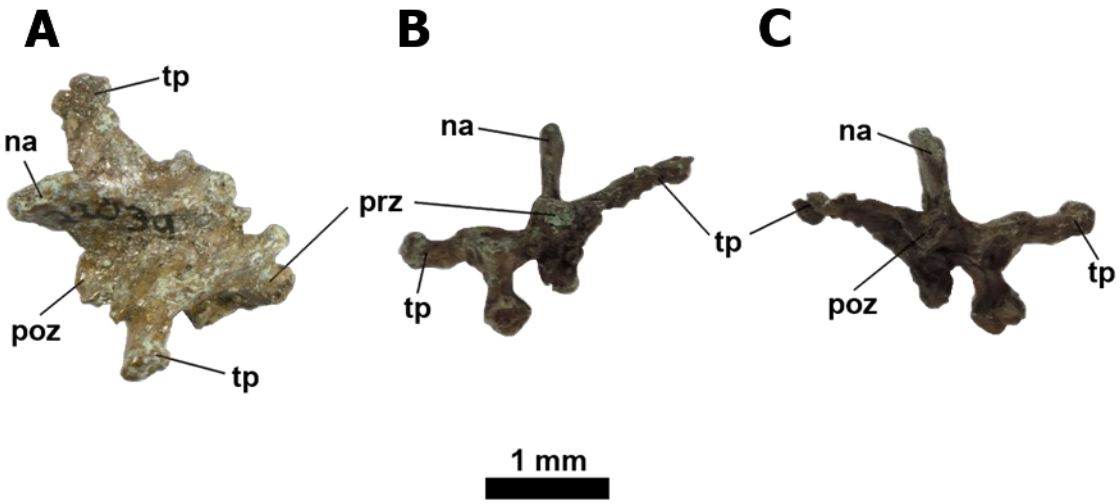

Figure 6. Best preserved dorsal neural spine of CMN 22039 in (A) dorsal, (B) anterior, and (C) posterior views. Abbreviations: na - neural arch, poz - pos-tzygapophysis, prz - pre-zygapophysis, tp - transverse process.

Ribs (Figure 7). One complete rib and several rib fragments are preserved. The complete rib is long and bowed medially at its midpoint, as is typical for the anterior caudal ribs of all known pachycephalosaurs (Butler & Sullivan, 2009; Brown & Russell, 2012). Dorsal, and sacral ribs tend to display more bowing proximally, supporting the interpretation of this element as a caudal rib. The proximal end of the rib is expanded, but the tuberculum and capitulum are not preserved. The rest of the rib is mediolaterally flattened and uniformly thin. There is a prominent medial kink at the halfway point of the body of the rib; this is likely taphonomic in origin as there is substantial cracking visible at this point.

Figure 7. Caudal rib of CMN 22039 in (A) lateral and (B) medial views. Abbreviations: h - head.

Pelvic Girdle

Ilium (Figure 8). The right ilium of CMN 22039 has been taphonomically crushed mediolaterally. Its dorsal margin is sigmoidal, as in all pachycephalosaurs (Maryańska *et al*., 2004; Evans *et al*., 2013; Williamson & Brusatte, 2016), albeit weakly. The sigmoidal curve of the ilium is not diagnostic of pachycephalosaurs, however, because the same state is observed in *Thescelosaurus* (Gilmore, 1915; Brown, 2009; Brown *et al*., 2011). The ilia of *Stenopelix* and *Psittacosaurus* do not display this feature (Sues & Galton, 1982; Sereno, 1987; Sereno *et al*., 1988; Maryańska *et al*., 2004; Butler & Sullivan, 2009). The mediolateral crushing of the element likely reduced how sigmoidal the dorsal

margin was in life by reducing the lateral and medial deviations of the pre- and postacetabular processes, respectively.

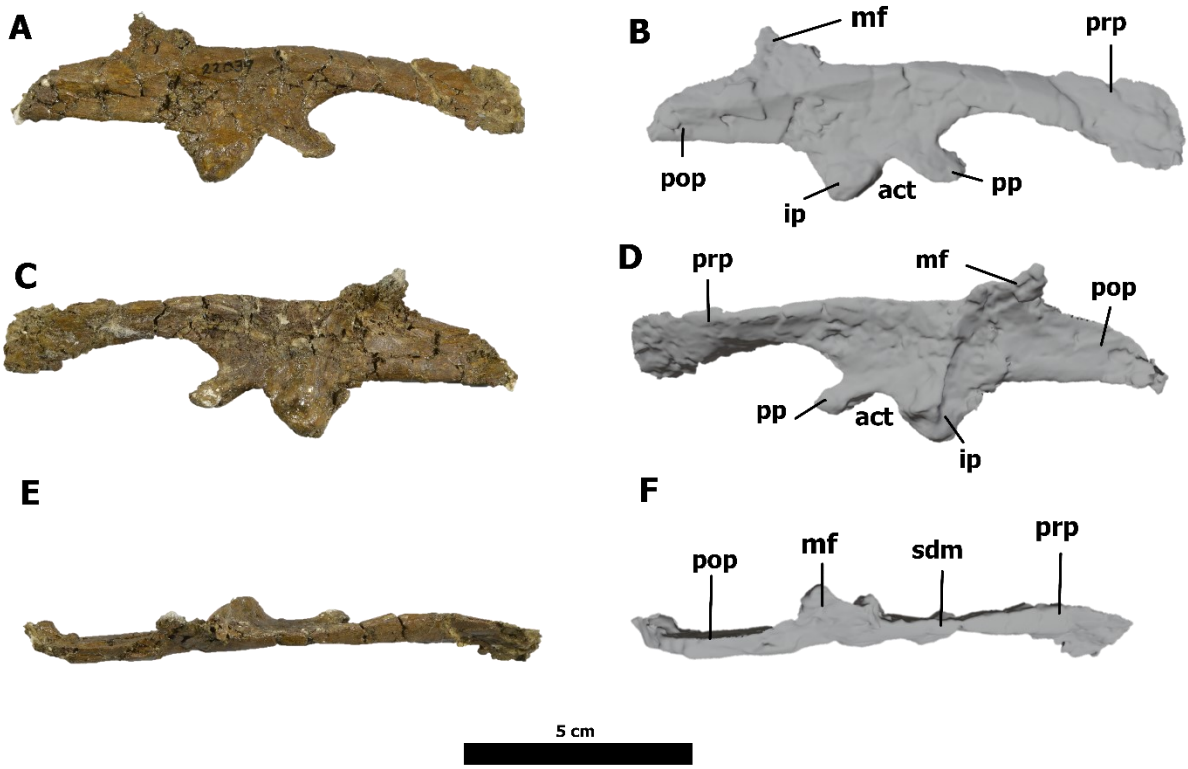

Figure 8. Right ilium and 3D scans of CMN 22039 in (AB) lateral, (CD) medial, and (EF) dorsal views. Abbreviations: act - acetabulum, ip - ischiac peduncle, mf - medial flange, pop - postacetabular process, pp - pubic peduncle, prp - preacetabular process, sdm - sigmoidal dorsal margin.

The preacetabular process is ~50% longer than the preserved postacetabular process, and mediolaterally thin. It deviates laterally from the long axis of the element at an angle of ~12°. It curves ventrally and becomes dorsoventrally taller towards its distal end.

The main body of the ilium, between the pre- and postacetabular processes, is concave on both medial and lateral surfaces. Both faces are severely cracked; however,

two faint depressions occur on the medial face, presumably for the articulation of the third and fourth sacral ribs (Maryańska *et al*., 2004). No other articular surfaces are visible. The acetabular portion of the ilium is circumscribed by smaller pubic and large ischiac peduncles. The pubic peduncle is anteroposteriorly long and widened transversely, as in*Stegoceras* and the outgroup *Thescelosaurus* (Gilmore, 1913; Gilmore, 1915; Gilmore, 1924). This condition is not observed in other pachycephalosaurs like *Pachycephalosaurus* and outgroup taxa including *Psittacosaurus* and *Stenopelix* (Sues & Galton, 1982; Sereno, 1987; Sereno *et al*., 1988; Maryańska *et al*., 2004; Butler & Sullivan, 2009; Brown *et al*., 2011). The ischiac peduncle is ~70% wider than the pubic peduncle and more uniformly rounded. The ilium of CMN 22039 also possesses the characteristic medial flange of pachycephalosaurs immediately posterior and dorsal to the acetabulum (Gilmore, 1913; Gilmore, 1915; Gilmore, 1924; Perle *et* al., 1982; Sues & Galton, 1982; Sereno, 1987; Sereno *et al*., 1988; Maryańska *et al*., 2004; Butler & Sullivan, 2009; Brown *et al*., 2011; Evans *et al*., 2013; Williamson & Brusatte, 2016). It projects from the dorsal margin of the ilium at an angle of ~70^{o} from the horizontal. Among pachycephalosaurs, this dorsal projection of the flange is unique to CMN 22039 and *S. validum* (UALVP 2). The medial flange of all other known pachycephalosaurs (*Pachycephalosaurus, Homalocephale,* and *Prenocephale*) projects horizontally (Perle *et al*., 1982; Maryańska *et al*., 2004; 2016).

The postacetabular process of the ilium deviates medially at an angle of ~17^{o} from the midline. Proximally, it exhibits the typical mediolateral curvature and subrectangular shape observed in other pachycephalosaurs (Perle *et al*., 1982;

Maryańska *et al*., 2004;) but its distal half is broken. Some pachycephalosaurs, including *P. wyomingensis* and *H. calathocercos*, possess a postacetabular process that is heavily curved ventrally (Perle *et al*., 1982). CMN 22039 displays the condition observed in other pachycephalosaurs, such as *S. validum* and *G. lattimorei*, which is a postacetabular process with little to no dorsoventral curvature (Perle *et al*., 1982).

Ischium (Figure 9). The left ischium is proximally expanded to form the pubic and ischiac peduncles. The slender pubic peduncle is anteroposteriorly elongate, likely to articulate with the pubic peduncle of the ilium, nearly excluding the pubis from the acetabulum, a trait unique to pachycephalosaurs (Maryańska and Osmólska 1974; Perle *et al*., 1982; Maryańska *et al*., 2004;). The iliac peduncle is not well preserved, and its overall morphology is impossible to determine. The ischium possesses no visible obturator process, as is the condition of all marginocephalians, including pachycephalosaurs (Butler & Sullivan, 2009). The shaft of the ischium is long, uniformly slender, gently bowed posteriorly, and slightly curved medially. This form is similar across all pachycephalosaurs. It differs from that of the outgroup taxon *S. valdensis*, which is notably kinked (Gilmore, 1924; Perle *et* al., 1982; Sues & Galton, 1982; Maryańska *et al*., 2004; Butler & Sullivan, 2009) and *Heterodontosaurus tucki* which displays no curvature (Dieudonné *et al*., 2020).

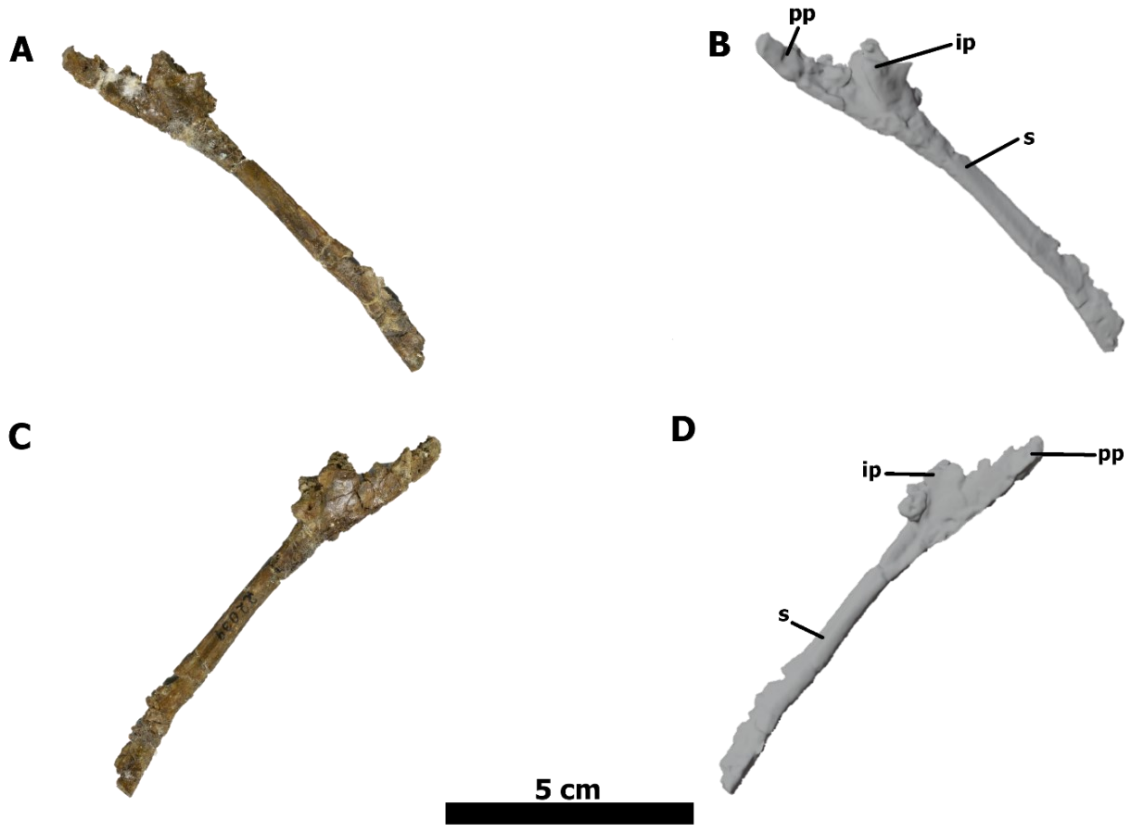

Figure 9. Left ischium and scan of the left ischium of CMN 22039 in (AB) lateral view and (CD) medial view. Abbreviations: ip - iliac peduncle, pp - pubic peduncle, s - shaft.

Pubis (Figure 10). The true pubis of CMN 22039 is extremely reduced and gracile compared to all consulted outgroup taxa (Gilmore, 1913; Gilmore, 1915; Sereno, 1987; Sereno *et al*., 1988; Brown, 2009; Brown *et al*., 2011; Dieudonné *et al*., 2020). It takes the form of a small rod extending caudally from the prepubic process, ventral to the iliac peduncle. The iliac peduncle is much larger than the true pubis and forms a rounded, convex expansion extending caudally from the prepubic process. It is the only portion of the pubis that likely contributed to the acetabulum. The prepubic process makes up the

majority of the element. It is a comparatively long and slender rod that extends anteriorly from the iliac peduncle. Proximally, the process is dorsoventrally wide and mediolaterally flattened. Distally, the element becomes much more gracile and dorsoventrally flattened. In CMN 22039, the prepubic process is straight. The prepubic processes of *Pachycephalosaurus sp.* (ROM 73555) and *H. calathocercos* (MPC-D 100/1201) by comparison are noticeably curved laterally.

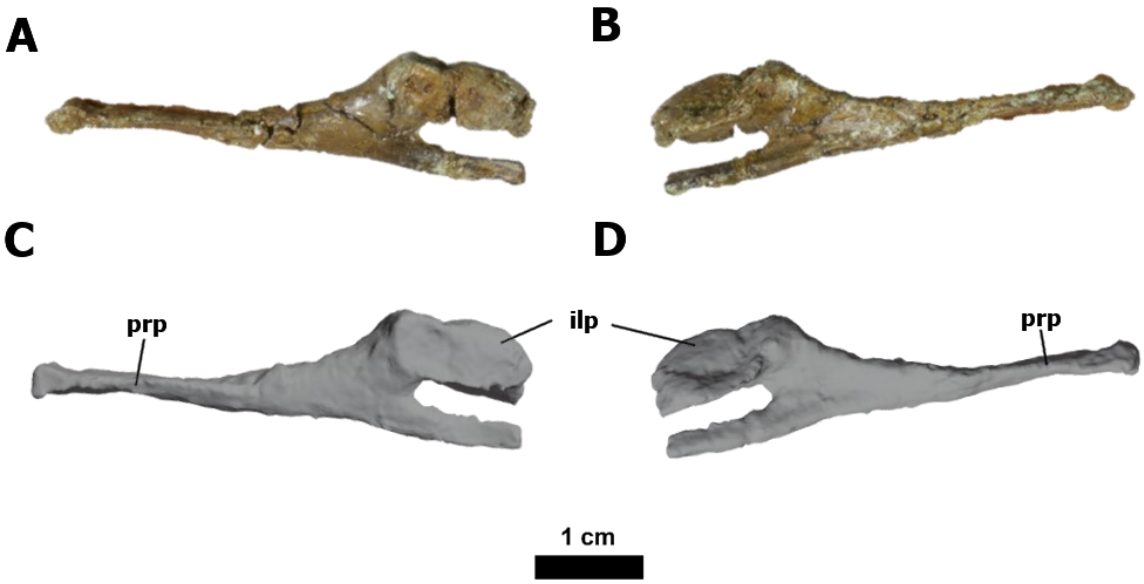

Figure 10. (AB) Left pubis of CMN 22039 in (A) lateral and (B) medial views. (CD) 3D scans of the left pubis of CMN 22039 in (C) lateral and (D) medial views. Abbreviations: ilp - iliac peduncle, prp - prepubic process.

Hindlimb

Femur (Figure 11). Both femora are present, but the left is the better preserved; there is a break in the right femur directly proximal to its distal condyles, separating them from the rest of the element. Both femora have been warped due to taphonomic processes; however, the overall morphology of the femur can be determined by examining the less deformed portions of each element. The femoral head is long,

uniformly rounded, and projects medially. It is also moderately anteroposteriorly compressed, which is common among pachycephalosaurs (Maryańska *et al*., 2004). The greater trochanter is well-developed, but slightly less so than in adult pachycephalosaurs (Gilmore, 1924; Perle *et* al., 1982; Maryańska *et al*., 2004), and lies directly lateral to the femoral head. It forms a large, rectangular expansion that widens anteroposteriorly as it progresses proximally from the shaft. It is separated from the femoral head by the deep cranial intertrochanteric groove. The lesser trochanter is either not developed or not preserved, the cracking along the surface of the element makes it impossible to discern.

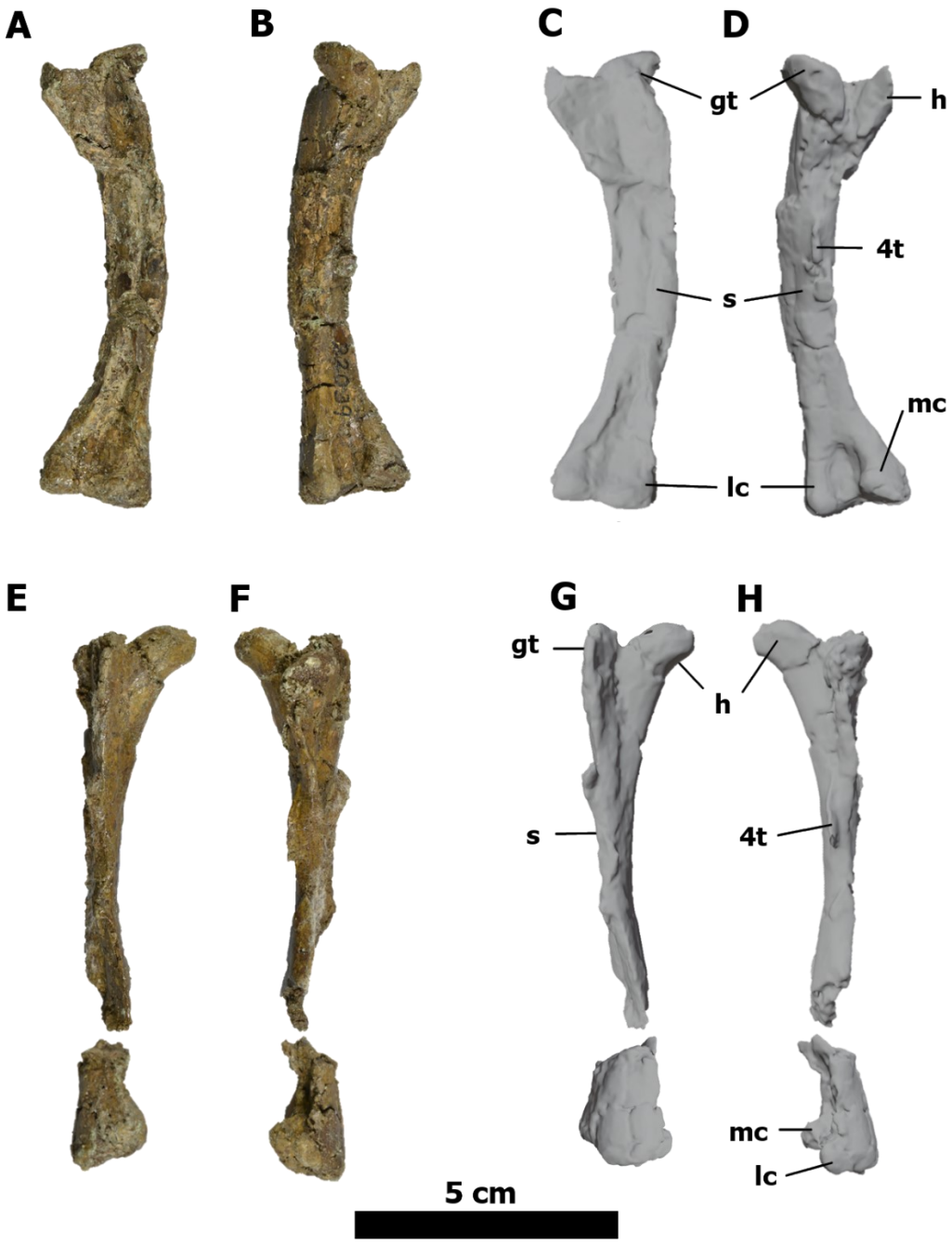

Figure 11. (AB) Left femur of CMN 22039 in (A) anterior and (B) posterior views. (CD) 3D scans of the left femur of CMN 22039 in (C) anterior and (D) posterior views. (EF) Right femur of CMN 22039 in (E) anterior and (F) posterior views. (GH) 3D scans of the right femur of CMN 22039 in (G) anterior and (H) posterior views. Abbreviations: 4t - fourth trochanter, gt - greater trochanter, h - head, lc - lateral condyle, mc - medial condyle, s - shaft.

The femoral shaft is uniformly robust, compared to the other long bones of the skeleton, and strongly bowed medially. The fourth trochanter is partially preserved, displaying a small break at its ventralmost extent, and projects from the posterior face of the shaft, approximately one-quarter down the length of the shaft. This proximal positioning of the fourth trochanter is also observed in *Pachycephalosaurus sp.* (ROM 73555), *H. calathocercos* (MPC-D 100/1201), and *Pr. prenes* (MPC-D 100/1204). In *P. wyomingensis* (NSM PV 20423) and *S. validum* (UALVP 2) it is located more distally, directly proximal to the midpoint of the shaft (Gilmore, 1924; Perle *et al*., 1982; Maryańska *et al*., 2004) and in *W. yansiensis* it is positioned directly at the midpoint (Butler & Zhao; 2009). The fourth trochanters of *Thescelosaurus*, *Psittacosaurus*, and *Stenopelix* are also proximally positioned (Koken, 1887; Gilmore, 1913; Gilmore, 1915; Sereno, 1987; Sereno *et al*., 1988; Brown, 2009; Brown *et al*., 2011). The fourth trochanter of CMN 22039 is also weakly pendant in shape. This is not observed in most other pachycephalosaurs, which generally display a non-pendant fourth trochanter, except *Pr. prenes* (MPC-D 100/1204). By comparison, the fourth trochanters observed in the outgroup taxa of *Thescelosaurus*, *Psittacosaurus*, and *Stenopelix* are all strongly pendant (Koken, 1887; Gilmore, 1913; Gilmore, 1915; Sereno, 1987; Sereno *et al*., 1988; Brown, 2009; Brown *et al*., 2011).

The distal end of the femur expands to form the prominent lateral and medial condyles. The lateral condyle is slightly larger than the medial. Both condyles are uniformly rounded except at their posterior-most extent, where they protrude strongly.

The two condyles are separated from each other by a deep, rectangular groove that gradually shallows from the posterior face of the element to its distal end.

Tibia (Figure 12). Only the left tibia is preserved. It articulates proximally with the corresponding fibula; the elements remain cemented together post-depositionally. The tibia is a long, straight element with a slender shaft and well-developed proximal and distal expansions. There is a break in the tibia separating the distal third of its shaft from its distal condyles; the intervening portion is missing. The proximal articular surface of the tibia is flat to slightly concave and is separated into a lateral and medial condyle of equal size by a shallow groove. This groove extends distally along the posterior surface of the element, gradually shallowing until it disappears where the proximal expansion merges into the shaft. The cnemial crest is subrectangular in anterior outline and extends over the anteromedial surface of the fibula. There are no significant differences in the morphology of the tibia between CMN 22039, other pachycephalosaurs and the consulted outgroup taxa (Gilmore, 1913; Gilmore, 1915; Gilmore, 1924; Perle *et* al., 1982; Sues & Galton, 1982; Sereno, 1987; Sereno *et al*., 1988; Maryańska *et al*., 2004; Butler & Sullivan, 2009; Brown *et al*., 2011). The proximal expansion gradually and uniformly thins distally towards the shaft. Where the proximal expansion and shaft meet, a significant lateral portion of the shaft has broken away, leaving a large cavity that encompasses approximately one third of the shaft's presumed length as it extends distally. The shaft gradually thins distally until its break. The distal expansion of the tibia is slightly larger than its proximal expansion. It possesses two distal condyles, the medial being slightly larger than the lateral, separated by a shallow concavity along its distal

and anterior faces. The expansion is sub-rectangular, and its distal articular surface is shallowly concave. The distal end of the fibula is not preserved.

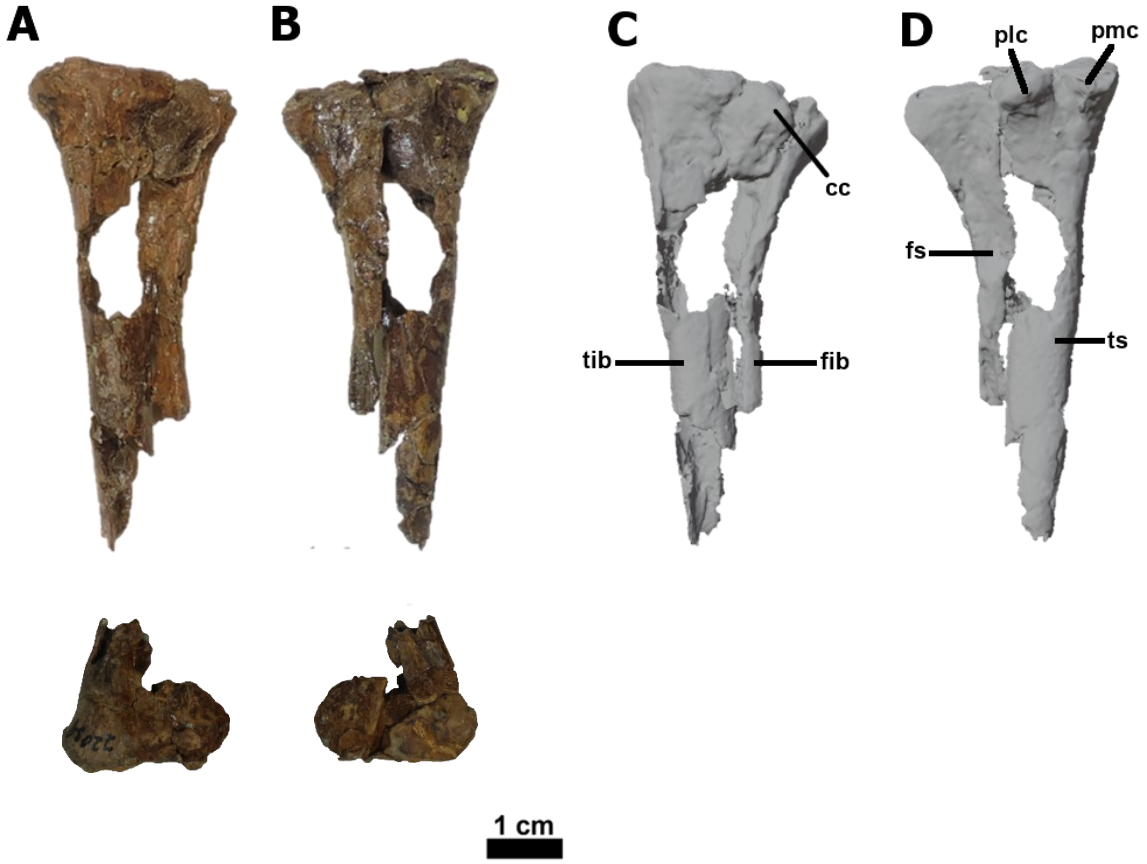

Figure 12. (AB) Left tibia and fibula of CMN 22039 in (A) anterior and (B) posterior views. (CD) 3D scans of the left tibia of CMN 22039 in (C) anterior and (D) posterior views. Abbreviations: cc - cnemial crest, fib - fibula, fs - fibular shaft, plc - proximal lateral condyle, pmc - proximal medial condyle, tib - tibia, ts - tibial shaft.

Fibula (Figure 12). Only the proximal half of the left fibula of CMN 22039 is preserved. It is more gracile than the tibia and curved laterally. The proximal end of the element is mildly expanded compared to the shaft, and gradually thins distally. The entire element is mediolaterally compressed and slightly concave on its medial surface to accept the shaft of the tibia. This overall morphology is consistent across

pachycephalosaurs and outgroup taxa (Gilmore, 1913; Gilmore, 1915; Gilmore, 1924; Perle *et* al., 1982; Sues & Galton, 1982; Sereno, 1987; Sereno *et al*., 1988; Maryańska *et al*., 2004; Butler & Sullivan, 2009; Brown *et al*., 2011).

Histological Analysis

Methods

To determine the ontogenetic age of CMN 22039, an osteohistological analysis was performed on its tibia and fibula. To accomplish this, thin sections were made of the specimen. First, a line was drawn along the shafts of the bones, at the approximate midpoint, to indicate where a cross-section needed to be made. Technovit 5071 was then applied around the line in a two parts powder to one part water ratio to stabilize the element for cutting. After the Technovit solution had hardened, a cross-section was made through the specimen using a Buehler Isomet 1000 precision saw. While the cross-section was being made, microscope slides were frosted using a 600-grit silicon carbide mixture. Once the cross-section was complete, the specimen was super-glued to the frosted microscope slide and allowed to set. The remainder of the specimen was then cut away from the microscope slide to create a thin section. Using a Hillquist thin section machine, the thin section was then ground down until light was visibly able to pass through it. The thin section was then hand ground and polished using 600- and subsequently 1000-grit silicon carbide mixtures. Finally, the completed thin sections were viewed under normal and cross-polarized light (Figure 13).

Results

The cortex of the tibia and fibula is composed entirely of highly vascularized woven bone, appearing isotropic under cross-polarized light (Francillon-Vieillot *et* al., 1990; Castanet *et al*., 2000; de Margerie *et al*., 2002; Lamm & Werning, 2013; Prieto-Márquez *et al*., 2016a; Prieto-Márquez *et al*., 2016b). Although all woven bone is disorganized (Francillon-Vieillot *et* al., 1990; Castanet *et al*., 2000; de Margerie *et al*., 2002; Lamm & Werning, 2013; Prieto-Márquez *et al*., 2016a; Prieto-Márquez *et al*., 2016b), there is a clear distinction between levels of vascularization and organization observable in the tibia of CMN 22039 (Figure 13). The bone surrounding the marrow cavity is highly disorganized and vascular trabecular bone (Figure 13). It forms a distinct boundary with the surrounding cortical bone, which abruptly becomes less vascular and more organized. This same boundary is observable in the fibula of CMN 22039, however, the abrupt change in organization and vascularity is less pronounced (Figure 13). Vascularity instead appears to be almost randomly oriented in a woven configuration and poorly organized throughout the entirety of the bones. Additionally, vascular canals open to the bone surface, indicating rapid and active growth (Redelstorff & Sander, 2009). Without any obvious, longitudinally oriented osteons, by the definition of Lamm & Werning (2013), the bone cannot therefore be described as fibrolamellar. There is also no evidence of secondary remodeling (e.g., secondary osteons) or lines of arrested growth (Francillon-Vieillot *et* al., 1990; Castanet *et al*., 2000; de Margerie *et al*., 2002; Lamm & Werning, 2013; Prieto-Márquez *et al*., 2016a; Prieto-Márquez *et al*., 2016b).

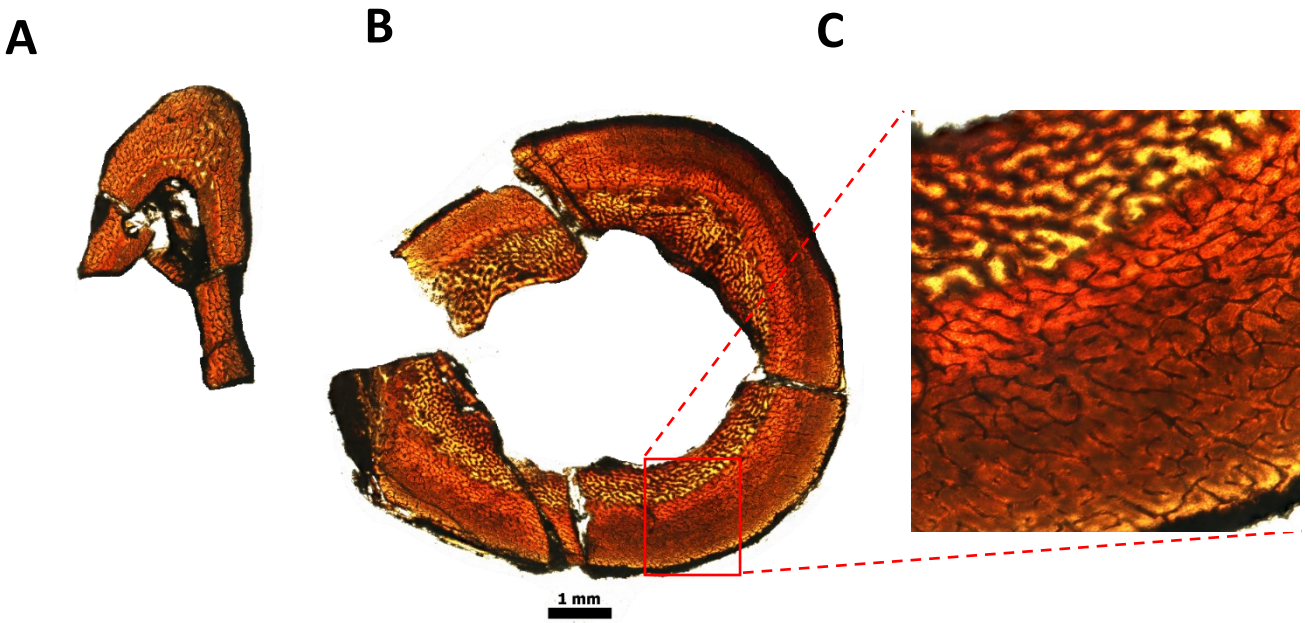

Figure 13. Cross-section of the (A) fibula and (B) tibia of CMN 22039 under normal light and 4x magnification and (C) close up of the tibial cross-section of CMN 22039.

Phylogenetic Analysis

New characters

In studying the skeleton of CMN 22039, I identified two new characters of the pachycephalosaur postcranium of potential phylogenetic significance. The first concerns the projection angle of the medial flange of the ilium. In all pachycephalosaur ilia, except those of *S. validum* (UALVP 2) and CMN 22039, the medial flange projects directly horizontal from the dorsal margin of the ilium (Figure 14). In these two specimens, however, the medial flange projects dorsomedially, at an angle of ~40^{o} to the horizontal in UALVP 2 and ~70^{o} in CMN 22039 (Figure 14). Although there is some deformation around the base of the flange in CMN 22039, it does not appear to have

been severe enough to cause a 70° deflection from the horizontal. In life, it is more likely that the medial flange projected at a similar angle to that of UALVP 2.

Figure 14. Right ilium of CMN 22039 and ROM 73555 (*Pachycephalosaurus sp.*) in (A,B) medial and (C,D) dorsal views showing the difference in medial flange projection angles. The medial flange of CMN 22039 (A,C) projects at an angle ~ 70° from the frontal plane while that of ROM 73555 (B,D) is parallel with the frontal plane. Abbreviations: mf - medial flange.

The second character concerns the shape of the femoral fourth trochanter (Figure 15). Among the pachycephalosaurs analyzed, CMN 22039 and *Pr. prenes* exhibit a weakly pendant trochanter morphology, while the rest exhibit a non-pendant morphology. In marginocephalians, the ancestral condition is a strongly pendant fourth trochanter. More derived forms display a non-pendant morphology (Persons & Currie, 2020). This morphology does not appear to vary through ontogeny in at least some basal marginocephalians, as the condition does not change in extremely young to adult

specimens of *Protoceratops* (Fastovsky *et al*., 2011; Slowiak *et al*., 2019; Persons & Currie, 2020).

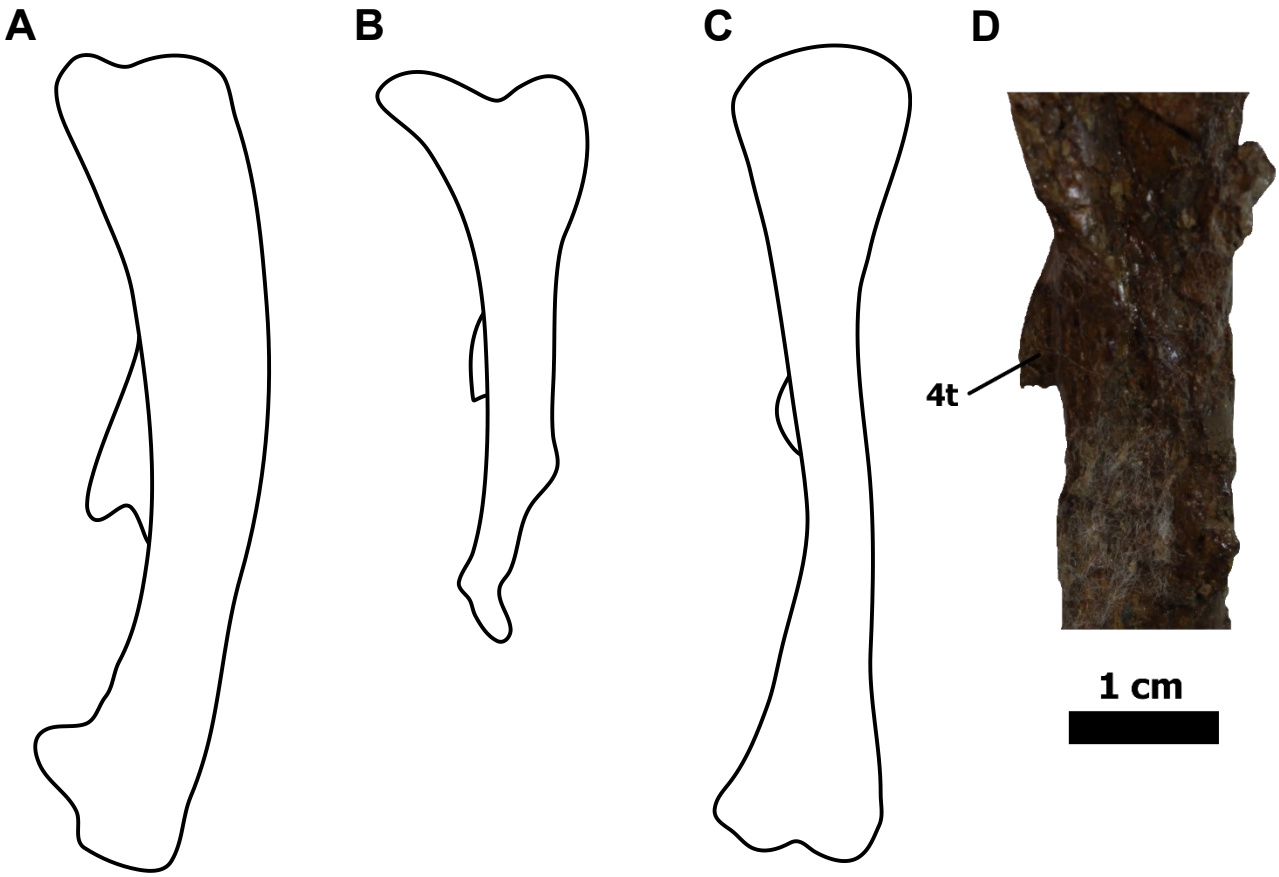

Figure 15. Scaled outlines of the femora of (A) *Thescelosaurus*, (B) CMN 22039, and (C) *Stegoceras* in medio-posterior view, showing their three distinct fourth trochanter morphologies: (A) strongly pendant fourth trochanter, (B) weakly pendant fourth trochanter, and (C) non-pendant fourth trochanter. (D) Close up of the fourth trochanter morphology of CMN 22039 in medio-posterior view. Abbreviations: 4t - fourth trochanter.

Additionally, a third possibly phylogenetically relevant character was identified concerning the proximodistal position of the fourth trochanter. In all pachycephalosaurs which preserve this feature, the fourth trochanter is located at a proximal position on the femoral shaft, with the exception of *W. yansiensis, S. validum,* and *P. wyomingensis*.

In these taxa, the fourth trochanter is shifted distally towards the proximodistal midpoint of the shaft. This character may, however, vary ontogenetically. Although there is no direct evidence that the positioning of the fourth trochanter varies with age in marginocephalians, it has been found to vary in other dinosaur groups (Persons & Currie, 2020). In derived therizinosaurids and juvenile sauropods, the fourth trochanter migrates distally through ontogeny (McIntosh, 1990; Kundrát *et al*., 2008; Persons & Currie, 2020). As such, the usefulness of this trait in phylogenetic analyses is limited and it was not included in the phylogenetic analysis.

Methods

The above characters were coded into the phylogenetic analysis of Williamson and Brusatte (2016). Several characters of the genus *Pachycephalosaurus* were updated to account for the postcranial material of ROM 73555, which was not yet published at the time of the study of Williamson and Brusatte. All the updated characters were previously scored as missing data. *Pachycephalosaurus* was rescored as follows: character 2, the shape of the distal end of the preacetabular process, is now scored as "1" (dorsoventrally flattened and expanded distally). Character 6, the form of the zygapophyseal articulations, is now scored as "1" (grooved). Character 9, the lateral deflection of the preacetabular process, is now scored as "1" (marked). Character 10, the position of the medial tab on the iliac blade, is now scored as "2" (on the postacetabular process). Character 11, the shape of the postacetabular process of the ilium, is now scored as "1" (deep and downturned distally, with an arcuate dorsal margin). Character 12, the shape of the ischial pubic peduncle, is now scored as "1"

(transversely flattened). Finally, character 13, the state of the pubic body, is now scored as “1” (reduced and nearly excluded from the acetabulum). The updated character matrix of Williamson and Brusatte (2016) is available in the appendix.

The revised dataset was subjected to a cladistic parsimony analysis in TNT v. 1.5 (Goloboff & Catalano, 2016) using the same settings as those of Williamson and Brusatte (2016), to facilitate comparison. Two analyses were run: one including CMN 22039 and one excluding CMN 22039, to isolate results caused by the addition of a new taxon versus the results of adding new characters. I used the “New-Technology search” option, with the sectorial search, ratchet, tree drift, and tree fuse options selected with default settings. The resulting consensus trees were then subjected to bootstrap analyses under the resampling option of TNT (Goloboff & Catalano, 2016) using 1000 replicates and a traditional search. This was done to estimate branch support in the most parsimonious trees. Bremer support values were also calculated in TNT to determine node support. Characters were then analyzed using the INFO command in TNT to determine which characters were uninformative.

Results

CMN 22039 was scored for nine postcranial characters. The strict consensus analysis including CMN 22039 resulted in recognition of the three most parsimonious trees, each with 85 steps (consistency index = 0.639, retention index = 0.643). The strict consensus analysis excluding CMN 22039 resulted in four most parsimonious trees, each with 82 steps (consistency index = 0.633, retention index = 0.633). The resulting strict

consensus trees are displayed in Figure 16. A total of 11 characters were uninformative, including eight cranial and three postcranial characters. None of the uninformative postcranial characters were new characters added in this study.

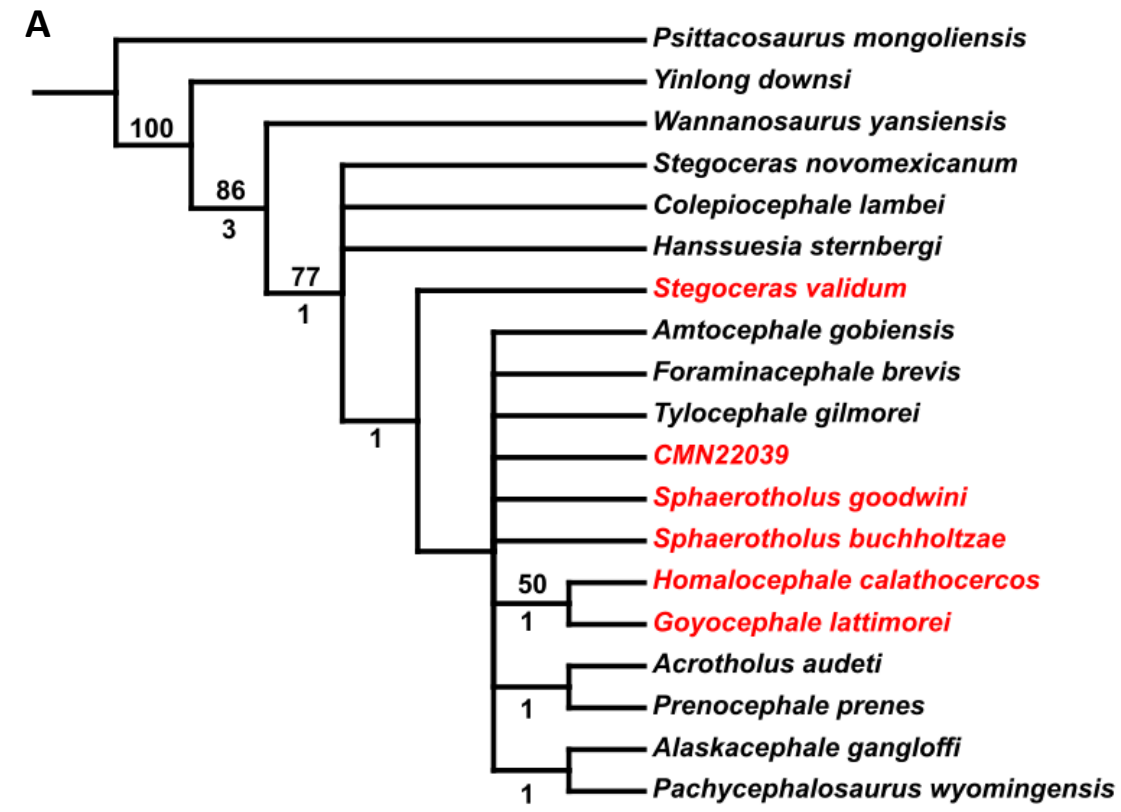
A
Psittacosaurus mongoliensis
Yinlong downsi
Wannanosaurus yansiensis
Stegoceras novomexicanum
Colepiocephale lambei
Hanssuesia sternbergi
Stegoceras validum
Amtocephale gobiensis
Foraminacephale brevis
Tylocephale gilmorei
CMN22039
Sphaerotholus goodwini
Sphaerotholus buchholtzae
Homalocephale calathocercos
Goyocephale lattimorei
Acrotholus audeti
Prenocephale prenes
Alaskacephale gangloffi
Pachycephalosaurus wyomingensis
100
86
3
77
1
1
50
1
1
1

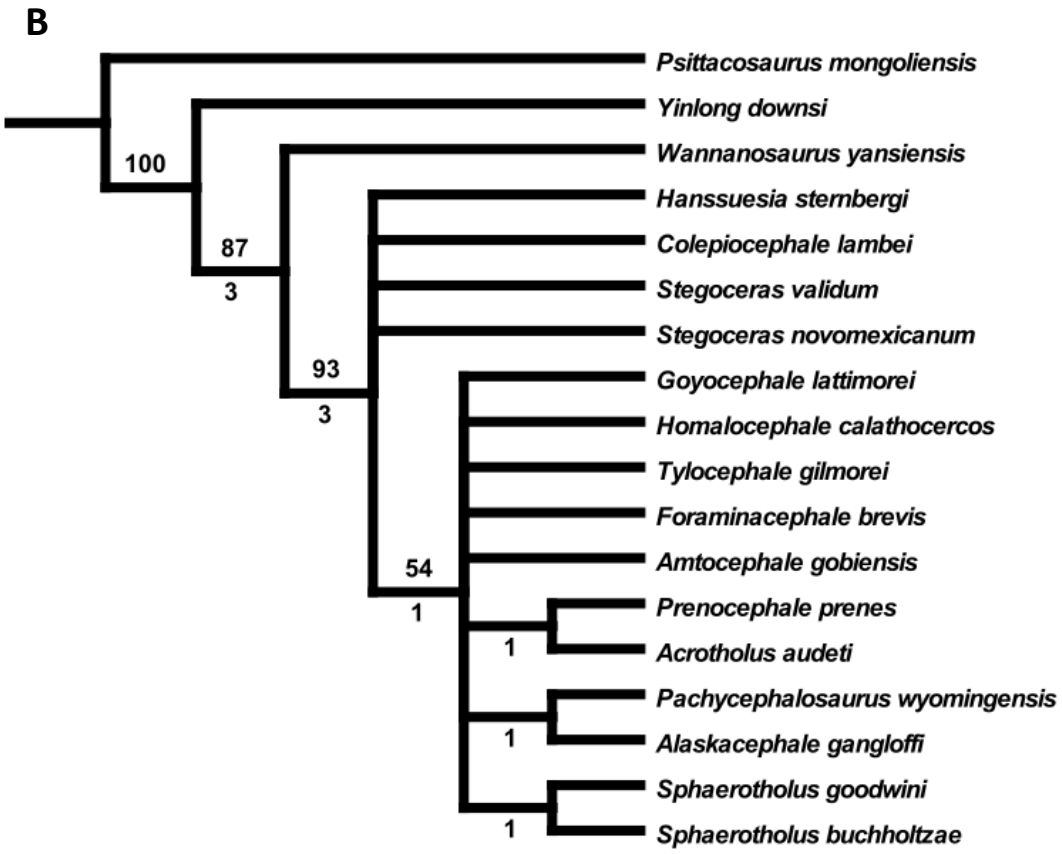
B
Psittacosaurus mongoliensis
Yinlong downsi
Wannanosaurus yansiensis
Hanssuesia sternbergi
Colepiocephale lambei
Stegoceras validum
Stegoceras novomexicanum
Goyocephale lattimorei
Homalocephale calathocercos
Tylocephale gilmorei
Foraminacephale brevis
Amtocephale gobiensis
Prenocephale prenes
Acrotholus audeti
Pachycephalosaurus wyomingensis
Alaskacephale gangloffi
Sphaerotholus goodwini
Sphaerotholus buchholtzae
100
87
3
93
3
54
1
1
1
1

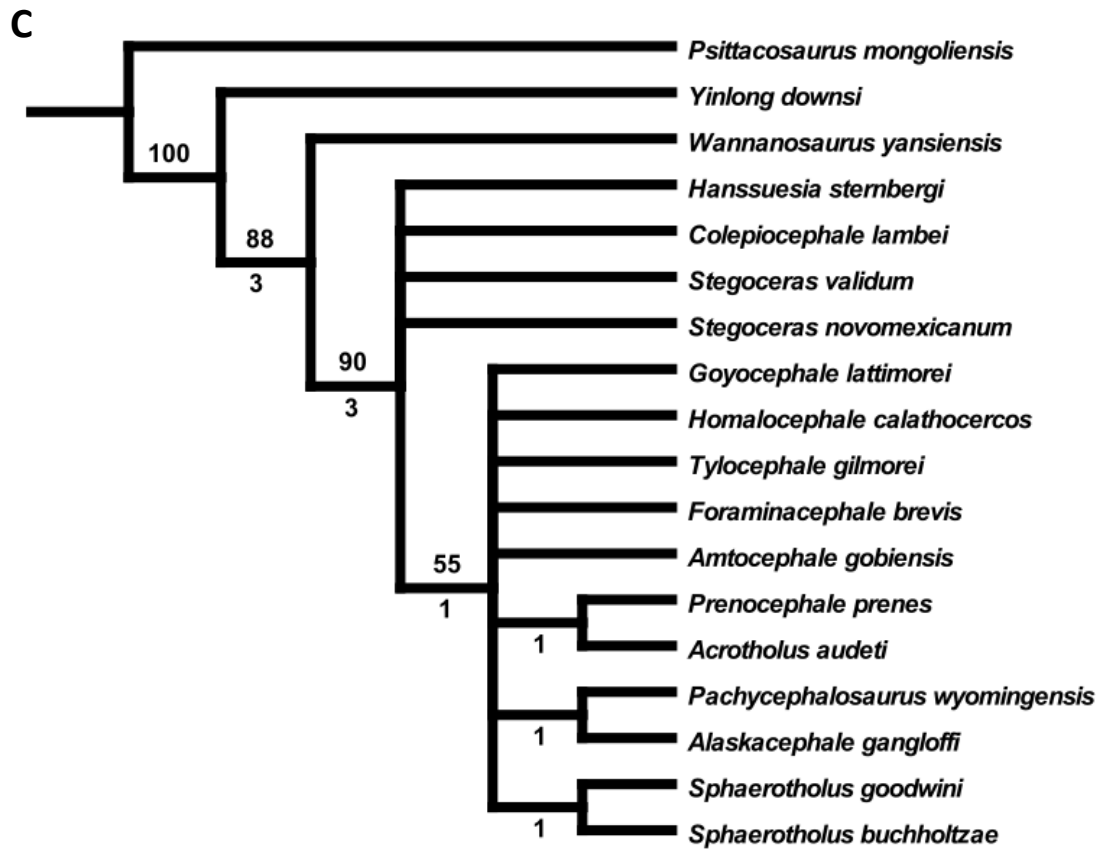

Figure 16. Phylogeny of Pachycephalosauria. (A) Strict consensus tree including CMN 22039 and new and updated postcranial data (consistency index = 0.639, retention index = 0.643). (B) Strict consensus tree including new and updated postcranial data and excluding CMN 22039 (consistency index = 0.633, retention index = 0.633). (C) Williamson and Brusatte (2016) strict consensus tree (consistency index = 0.753, retention index = 0.796). Numbers above nodes are absolute bootstrap frequencies and numbers below nodes are Bremer support values. Differences from the tree of Williamson and Brusatte are highlighted in red.

There are no changes in the phylogenetic positions of any taxa when comparing the strict consensus tree including only the new postcranial data to that of Williamson and Brusatte (2016).

Several notable changes exist between the strict consensus tree including CMN 22039 (Figure 16) and the previous phylogeny of Williamson and Brusatte (2016; Figure 16). The first is that *S. validum* is no longer part of the same polytomy as *Stegoceras novomexicanum*, *Colepiocephale lambei* (Sullivan, 2003), and *Hanssuesia sternbergi* (Brown & Schlaikjer, 1943), suggesting that *S. novomexicanum* is not congeneric with *S. valium*. Instead, *S. validum* is now shown as more derived and a sister taxon to the second large polytomy. *S. validum* differs from *S. novomexicanum* in character 28 (supratemporal fenestra is open or closed). Additionally, *S. novomexicanum* is missing data for characters 40 (number of nodes in the primary parietosquamosal node row), 41 (presence/absence of irregular tuberculate ornamentation on the caudal surface of the squamosal below the primary node row), and 43 (presence/absence of enlarged, medialmost nodes in the primary parietosquamosal node row) which are not missing for *S. validum*. This missing data could have contributed to the new position of *S. validum* by creating artificial character differences between *S. validum* and *S. novomexicanum*. The second major difference between the phylogenies of this study and that of Williamson and Brusatte (2016) is that the sister-taxon pair of *Sphaerotholus goodwini* and *Sp. buchholtzae* Williamson and Carr, 2002 no longer exists. These taxa are now part of the second large polytomy. Finally, a new sister-taxon pair has formed between *H. calathocercos* and *G. lattimorei*, supported by eight synapomorphies. Furthermore, there is the new addition of CMN 22039 to the phylogeny, which is placed within the polytomy including *Tylocephale gilmorei* Maryańska & Osmolska, 1974,

Foraminacephale brevis (Schott & Evans, 2016), *Sp. goodwini*, *Sp. buchholtzae*, and *Amtocephale gobiensis* Tsogtbaatar & Sullivan, 2011. Taxa which are placed in this polytomy have shared character states, or missing data, for characters 7, 13, 27, 28, 29, 32, 35, 42, 46, and 48. Unfortunately, of these characters, CMN 22039 only possesses data for character 13: having a highly reduced pubis. As such, the placement of CMN 22039 in this polytomy is not well-supported by synapomorphies. Additionally, low Bremer support frequencies of 1 indicate that this node can easily degrade. The tenuous relationships observed in the strict consensus analysis (Figure 16) are due to a lack of data for many character states across many taxa and cannot be resolved until more data has been collected.

Discussion

Ontogenetic age of CMN 22039

The ontogenetic stage of pachycephalosaurs is usually determined by examining cranial features (Schott, 2011; Schott *et al*., 2011). Some such features include the development and fusion of the fronto-parietal dome, the presence/absence of tubercles on the frontals and parietals, the shape of the postorbitals and supraorbitals, and the convexity of the frontonasal boss (Schott, 2011; Schott *et al*., 2011). Unfortunately, none of these characters are preserved in CMN 22039, so its ontogenetic age must be inferred from alternative sources. The postcranial skeleton of CMN 22039 displays several features which are indicative of a young individual. The most notable of these is the overall size of the skeleton. CMN 22039 is extremely small, with its largest limb bone

(the right femur) measuring just over 100 mm in length. Pachycephalosaurs are small animals among dinosaurs, however, this skeleton constitutes one of the smallest pachycephalosaurs ever discovered, including young individuals such as *Homalocephale calathocercos* (MPC-D 100/1201) whose femur measures 212 mm in length (Perle *et* al., 1982; Evans *et al*., 2011; Goodwin & Evans, 2016). CMN 22039 also displays completely unfused neurocentral sutures on its caudal centra. All its centra are dissociated from their respective neural arches, suggesting that the animal died before neurocentral fusion could take place. This lack of fusion in the vertebrae is a common indication of a juvenile life stage among dinosaurs and most tetrapods (Brochu, 1996; Hoffman & Sander, 2014).

Further evidence supporting a juvenile life stage for CMN 22039 was obtained from an osteohistological analysis of its tibia and fibula (Figure 14). These two elements are composed entirely of highly vascularized woven bone. This is the fastest deposited type of bone tissue and is only found in fast-growing, immature animals and bone breakage sites (Francillon-Vieillot *et* al., 1990; Castanet *et al*., 2000; de Margerie *et al*., 2002; Lamm & Werning, 2013; Prieto-Márquez *et al*., 2016a; Prieto-Márquez *et al*., 2016b). Additionally, features which would be present in older animals, such as secondary remodeling and secondary osteons (Francillon-Vieillot *et* al., 1990; Castanet *et al*., 2000; de Margerie *et al*., 2002; Lamm & Werning, 2013; Prieto-Márquez *et al*., 2016a; Prieto-Márquez *et al*., 2016b), are not present in the tibia and fibula of CMN 22039 (Figure 14), further supporting a juvenile growth stage. The cross-sections of

these elements also do not display any lines of arrested growth (LAGs), perhaps indicating that the animal died before it had reached 1 year of age.

On the basis of the above-described skeletal and histological features, CMN 22039 can be accurately identified as a juvenile animal, potentially even within its first year of age.

Taxonomic identity of CMN 22039

Contrary to the initial finding of Russell and Manabe (2002), CMN 22039 is not *Thescelosaurus*, but is instead attributable to Pachycephalosauria, based on the presence of a few established synapomorphies. These include: (1) a double ridge and groove articulation of the pre- and postzygapophyses on the large caudal vertebrae; (2) a medial flange on the postacetabular process of the ilium; and (3) a highly reduced pubis that only minimally contributes to the margin of the acetabulum (Maryańska et al., 2004). Characters deemed diagnostic of *Thescelosaurus* are all isolated to the cranium (Boyd *et al*., 2009), which is absent in CMN 22039. The original assignment to *Thescelosaurus* therefore appears to be unjustified. Unfortunately, the lack of cranial material also makes confident identification of CMN 22039 beyond the family level impossible. However, based on phylogenetic, geographic, stratigraphic, and morphological considerations, a tentative identification might be made.

In the phylogenetic analysis (Figure 16), *Stegoceras*, *Colepiocephale*, and *Hanssuesia* are recovered basal to CMN 22039. Given the juvenile status of the specimen (see above), and the fact that juveniles of even highly derived species tend to

plot basally on cladograms due to a lack of derived characters (Kluge, 1985; Barrantes & Everhard, 2010; Carballido & Sander, 2014), the relatively derived nature of CMN 22039 argues against its assignment to any of the above genera. The specimen is also unlikely to be attributable to any Asian genus (*Goyocephale*, *Prenocephale*, *Tylocephale*, *Amtocephale*, *Homalocephale*), given that pachycephalosaur genera are not known to span continents; however, this argument must not be relied upon too heavily, in light of the fact that some other dinosaur genera do (e.g., *Saurolophus*). If the remaining Campanian taxa (e.g., *Sp. goodwini*, *Foraminacephale* Evans *et al*., 2013) are rejected on the basis of their older stratigraphic age, that leaves the Maastrichtian-aged *Alaskacephale* Sullivan, 2006, *Sp. buchholtzae*, and *Pachycephalosaurus* (including *Stygimoloch* and *Dracorex*) (Brown & Schlaikjer, 1943; Galton & Sues, 1983; Williamson & Carr, 2002; Bakker, 2006; Sullivan, 2006; Horner & Goodwin, 2009; Longrich *et al*., 2010; Mallon *et al*., 2014). CMN 22039 shares no overlapping material with either *Alaskacephale* or *Sphaerotholus*, and so cannot be compared on this basis. The specimen is distinct from *Pachycephalosaurus* in its possession of a dorsal projection of the medial iliac flange (which projects medially in *Pachycephalosaurus*), and a proximally positioned fourth trochanter (which is positioned centrally in *Pachycephalosaurus*). These conflicting character states make it unlikely that CMN 22039 belongs to *Pachycephalosaurus*, unless the characters vary ontogenetically. If the proximodistal position of the fourth trochanter shifts through ontogeny in marginocephalians as it does in some sauropods and therizinosaurs (McIntosh, 1990; Kundrát *et al*., 2008; Persons & Currie, 2020), then the proximodistal position of the fourth trochanter cannot

be used reliably to distinguish between these taxa. At least in basal marginocephalians such as *Protoceratops andrewsi*, however, this character does not appear to undergo any ontogenetic changes (Slowiak *et al*., 2019). Ontogenetic variation of the iliac medial flange is entirely unknown in pachycephalosaurs. *Sphaerotholus buchholtzae* and *Alaskacephale* therefore appear to be the two most likely candidates for the taxonomic identity of CMN 22039. The fact that, of these two species, only cf. *Sp. buccholtzae* has been described from the Frenchman Formation previously (Mallon *et al*., 2014) gives some reason for thinking that CMN 22039 might be attributable to that species. However, more extensive sampling of the formation is clearly needed to clarify the nature of its faunal assemblage.

Systematic considerations

When comparing the strict consensus tree excluding CMN 22039 (Figure 16) to that of Williamson and Brusatte (2016; Figure 16), there are no phylogenetic differences. These findings call into question the changes observed in the tree which includes CMN 22039 because the observed changes were caused by the addition of a new operational taxonomic unit (OTU) and not the addition of new postcranial character data. Adding new postcranial data caused a decrease in the consistency and retention indices, indicating increased homoplasy. Bremer support values remained the same and there were only minor differences in absolute bootstrap frequencies. Since these values did not significantly change, solely adding postcranial data to the matrix of Williamson and Brusatte (2016) did not improve or reduce clade support. Since solely adding postcranial data did not change the phylogenetic relationships of any taxa nor

significantly alter support measures, it is likely that the added postcranial data either have no effect on the evolutionary relationships of pachycephalosaurs or are harmonious with the phylogenetic signal(s) of the cranial data. If the effects of the new characters were conflicting with the phylogenetic signal(s) of the cranial data, it is likely that some nodes would have collapsed, especially for more derived clades where Bremer support values are minimal. That being said, only two new characters were added to the analysis so any effects would be minor. Another source of new postcranial data added to the analysis includes updated characters for *Pachycephalosaurus*. A total of seven postcranial characters were updated from having no data for this taxon in addition to the two new characters that were added for all taxa. Given that the position of *P. wyomingensis* remains the same across all strict consensus trees presented in this study (Figure 16), it is likely that the phylogenetic signal of the new postcranial data for this taxon is harmonious with that of the cranial data.

When comparing the strict consensus tree including CMN 22039 (Figure 16) to that of Williamson and Brusatte (2016; Figure 16), most of the phylogenetic relationships within Pachycephalosauria are retained. There are several differences, however. *Stegoceras validum* is now placed on its own branch in a more derived position than its previous polytomy with *S. novomexicanum*, implying that the monophyly of *Stegoceras* may no longer be valid. The sister taxon pair containing *Sp. goodwini* and *Sp. buchholtzae* from the analysis of Williamson and Brusatte (2016) has collapsed into a polytomy. Upon further examination, these two species share three distinct characters (described above) which are not present in the other members of the

polytomy and are only separated from each other on the basis of the character state for character 37 in *Sp. goodwini*. The sister taxon pair of *H. calathocercos* and *G. lattimorei* re-emerges similar to the group proposed by the phylogeny of Longrich *et al*. (2010) containing *Homalocephale*, *Goyocephale*, and *Wannanosaurus* and the original family Homalocephalidae proposed by Perle *et al*. (1982). This reappearance is supported by eight cranial synapomorphies: (1) having open supratemporal fenestrae, (2) having a flat skull dome, (3) the postorbital and supraorbital II not contributing to the skull dome, (4) having the caudal margin of the skull dome blend with the parietosquamosal shelf in lateral view, (5) having irregular tuberculate ornamentation on the caudal surface of the squamosal, (6) having enlarged medial nodes in the primary parietosquamosal node row however, (7) not having a secondary corner node medial to the lateroventral corner node, and (8) not having a postorbital node row (Evans *et al*., 2013). These characters, however, have been found to vary with ontogeny (Evans *et al*., 2013) and so more research is necessary before the sister-taxon pair of *Homalocephale* and *Goyocephale* can be confidently accepted. The branch supporting this clade also displays a low bootstrap value of 52 on the strict consensus tree (Figure 16). Overall, the pachycephalosaur phylogeny of this study (Figure 16) remains at a similar resolution to that of Williamson and Brusatte (2016). Although areas of high and low resolution have shifted, many taxa remain part of unresolved polytomies.

Conclusions

CMN 22039 has been confidently identified as a juvenile pachycephalosaur. This conclusion is supported by the presence of pachycephalosaur synapomorphies including: (1) a double ridge and groove articulation of the pre- and postzygapophyses on the large caudal vertebrae; (2) a medial flange on the postacetabular process of the ilium; and (3) a highly reduced pubis that only minimally contributes to the margin of the acetabulum (Maryańska et al., 2004). Its juvenile life stage is supported by: (1) its small size; (2) unfused neurocentral sutures of the dorsal and caudal vertebrae; (3) an immature woven bone texture of the tibia and fibula; and (4) a lack of any secondary mature osteohistological features. Comparisons between this new pachycephalosaur postcranial skeleton, pre-existing pachycephalosaur specimens with comparable material, and relevant outgroup taxa led to the discovery of several new postcranial characters which vary between taxa. Such characters include: (1) the angle of projection of the medial iliac flange, (2) the shape of the fourth trochanter, and (3) the proximodistal position of the fourth trochanter along the femoral shaft. Of these new characters, the position of the fourth trochanter along the femoral shaft potentially varies with ontogeny and is therefore of limited use. Until more pachycephalosaur postcranial material is discovered, it is impossible to determine if this variation is due to ontogenetic changes or taxonomic differences. No other significant postcranial characters were found to vary through ontogeny.

Adding new postcranial data and characters to the character matrix of Williamson and Brusatte (2016) while excluding CMN 22039 results in no changes to the

pachycephalosaur phylogeny. It is therefore likely that the changes observed in the strict consensus analysis including CMN 22039 were a result of the addition of a new OTU and not of new postcranial data. Since clade support is unaffected by adding two new postcranial characters to the matrix, it is likely that the phylogenetic signals of these characters do not conflict with the signal(s) of previous data. A total of nine postcranial characters were added or updated for *P. wyomingensis* and its phylogenetic position does not change across all three strict consensus trees. This further solidifies its position in the pachycephalosaur phylogeny and indicates that the added postcranial data for this taxon aligns with the signals of previous data.

Adding the data from CMN 22039 to the character matrix of Williamson and Brusatte (2016), along with new postcranial data and characters for other pachycephalosaurs, places it within a large polytomy more derived than *S. validum* and more basal to the sister-taxon pairs of *Homalocephale* and *Goyocephale*, *Acrotholus* and *Prenocephale*, and *Pachycephalosaurus* and *Alaskacephale*. Taking its ontogenetic age into account, it may in fact occupy a more derived position (Kluge, 1985; Barrantes & Everhard, 2010; Carballido & Sander, 2014), although this is impossible to determine without more data. Through the addition of postcranial characters to phylogenetic analyses, it is evident that our understanding of the evolutionary relationships of pachycephalosaurs has changed. This is made clear by the addition of new clades , the disappearance of previously supported clades, and the appearance of new clades (Figure 16). Overall, the resolution of the pachycephalosaur phylogeny remains the same, however, isolated areas of high resolution and homoplasy have shifted. *H.*

calathocercos once again forms a clade with *G. latimorei*, *S. validum* is now isolated on its own branch, and the sister-taxon pair of *Sp. goodwini* and *Sp. buchholtzae* has degraded into a polytomy.

Although much uncertainty exists surrounding the postcranial skeleton of pachycephalosaurs, postcranial characters have been found to vary in the few taxa represented by comparable postcranial material. As such, the postcranial skeleton of pachycephalosaurs cannot be ignored when assessing the evolutionary relationships of these animals.

Chapter 3: A reconstruction of the appendicular myology of *Stegoceras validum* (Ornithischia: Pachycephalosauridae) with comments on functional morphology

Introduction

Pachycephalosauria is a group of generally small, bipedal dinosaurs which are known mostly from cranial material (Sereno, 1997; Maryańska *et al*., 2004). These domes are thick and robust and preserve much more easily in the fossil record than the delicate pachycephalosaur postcranial skeleton. As a result, much research about these animals has been concentrated on this feature and its function. The most popular hypothesis for the purpose of the pachycephalosaur skull dome is that it served as a weapon during intraspecific combat involving shoving, head-butting, shoving, or flank-butting (Colbert, 1955; Galton, 1970b; Sues; 1978, Bakker *et al*., 2006; Snively & Cox, 2008; Lehman, 2010; Longrich *et al*., 2010; Snively & Theodor, 2011; Peterson *et al*., 2013). Due to the attention received by the skull dome, the postcranium is often ignored, even though it too displays odd morphologies for a small, bipedal ornithischian. For example, it is the only dinosaur group which displays a medial flange projecting from the dorsal margin of the ilium and a pubis that is so reduced that it is almost entirely excluded from the acetabulum (Maryańska *et al*., 2004). Despite these strikingly odd structures, no research to date has been performed to determine their functions. In this chapter, features such as those described above will be used to inform the first

appendicular muscular reconstruction of a pachycephalosaur and investigate the functions of unique postcranial morphologies.

Only a select few pachycephalosaurs have preserved elements from the postcranial skeleton. These include *P. wyomingensis*, *Pachycephalosaurus sp.*, *S. validum*, *H. calathocercos*, *Pr. prenes*, *G. lattimorei*, and *W. yansiensis*. By observing the postcranial material of these animals, several odd adaptations become apparent. One such adaptation is present in the dorsal and anteriormost caudal vertebrae. The pre- and postzygapophyses articulate in a double ridge and groove structure in which the prezygapophyses of the posterior vertebra possess small ridges on their dorsal surfaces which articulate with grooves on the ventral surfaces of the postzygapophyses of the anterior vertebra. Such articulations would allow for minimal lateral movement in the vertebral column, creating a very rigid structure.

This is not the only odd pachycephalosaur adaptation which would have contributed to stiffness in the vertebral column. Pachycephalosaurs also possess a basket of ossified myoseptal tendons in their tails surrounding the caudal vertebrae (Brown & Russell, 2012). Just like the double ridge and groove structure present in the dorsal and anteriormost caudal vertebrae, these ossifications would have limited mobility in the tail, creating a stiff and rigid structure. It has been hypothesized that having a rigid tail may have been an adaptation associated with the proposed head-butting behaviour of these animals. This theory claims that the tail may have been used in a tripodal stance during intraspecific combat, and so having a rigid tail resistant to

torsional loading would provide more stability (Brown & Russell, 2012). However, this is very much still speculative.

The odd postcranial adaptations of pachycephalosaurs are not only limited to the axial column. The pelvic structure also displays several unique characters. Of these, the most noticeable is the transversely broad pelvis. In ornithischians, a broadened ilium is usually correlated with quadrupedality (Maidment & Barrett, 2014), however, the pachycephalosaur forelimb is too small and gracile for weight-bearing, meaning pachycephalosaurs were certainly bipedal. Not only do they display an oddly wide pelvis, but the structure is also formed differently from that of any other ornithischian dinosaur. Most quadrupedal ornithischians display a lateral folding or thickening of the ilium, resulting in a broad pelvis (Maidment & Barrett, 2014). Pachycephalosaurs instead developed a medially-projecting flange on the dorsal margin of the ilium. The reason for this flange and the resulting broad pelvis of pachycephalosaurs remains unknown.

The acetabular structure is also oddly adapted in pachycephalosaurs in that the pubis is either completely or partially excluded from the acetabulum (Maryańska *et al*., 2004). This results from an elongate pubic peduncle of the ischium which forms an articulation with the pubic peduncle of the ilium. Additionally, the pubis itself is extremely reduced, only measuring roughly half the length of the prepubic process and barely extending past the iliac peduncle posteriorly.

Pachycephalosaur hindlimbs are also strange when compared to other ornithischians. In general, quadrupedal ornithischians (such as ceratopsids, stegosaurs,

and ankylosaurs) have a femur longer than the tibia while the reverse is true in bipeds such as hypsilophodontids, *Lesothosaurus*, and *Abrictosaurus* (Maidment & Barrett, 2014). Pachycephalosaurs are the only unambiguous bipedal ornithischians to break this pattern by having a femur longer than the tibia (Maidment & Barrett, 2014).

To date, these postcranial oddities have been useful in identifying pachycephalosaur postcranial material but have never been thoroughly investigated as to their functional purpose. This is in part due to the poor fossil record of pachycephalosaurs resulting in a lack of study material. However, with the continuous discovery of new material and reidentification of old specimens as pachycephalosaurs, there is now a significant data base of pachycephalosaur postcranial remains which can be used to investigate these strange structures. Included in this material is an exceptional specimen of *S. validum* (UALVP 2), which preserves an entire forelimb and hindlimb as well as nearly complete pectoral and pelvic girdles. In this chapter, I will investigate the interactions between odd pachycephalosaur postcranial skeletal adaptations and their appendicular musculature. This will be accomplished by first examining the appendicular skeleton of UALVP 2 for muscle scars. These will then be contrasted to the appendicular musculature of the extant phylogenetic bracket of dinosaurs (crocodilians and birds) through comparisons with the literature. Finally, an appendicular muscular reconstruction of UALVP 2 will be performed with comments on the effects and function of the aforementioned odd pachycephalosaur skeletal adaptations.

Methods

Muscles generally do not preserve in the fossil record, making it exceedingly difficult to understand the myology of fossil organisms. Luckily, direct evidence of muscles is often preserved by the surface texture of bones. Osteological correlates of muscles are created as a muscle exerts stress on the underlying bone (Bryant & Seymour, 1990; Frankel & Nordin, 2001; Voegele *et al*., 2020; Voegele *et al*., 2021). Such textures indicate where muscles would have attached to the bone, the minimum size of the attachment area, and even the type of attachment. Unfortunately, not all muscles will produce visible texturing, nor will the entire attachment area be preserved (Bryant & Seymour, 1990; Dilkes *et al*., 2000; Dilkes *et al*., 2012; Voegele *et al*., 2020; Voegele *et al*., 2021). As such, when reconstructing the myology of fossil organisms, it is often necessary to rely on comparisons with the extant phylogenetic bracket (EPB). By observing the myology of the EPB, one can make inferences about where and how muscles may have attached in fossil organisms (Witmer, 1995; Tsuihiji, 2010; Voegele *et al*., 2020; Voegele *et al*., 2021). Of course, this method of reconstruction is not foolproof, as extant organisms often have different body plans than their fossil predecessors and have likely modified their myology as a result (Witmer, 1995; Tsuihiji, 2010).

To reconstruct the appendicular musculature of UALVP 2, a combination of the above-described methods was used. First, casts of UALVP 2 were analyzed alongside photographs and 3D scans of the original material to identify any osteological correlates (striations, pitted/rugose textures, raised structures, etc.). These observations were

then compared to the musculature of the EPB of non-avian dinosaurs (modern crocodilians and birds) and muscular reconstructions of fossil dinosaurs in the literature (von Huene, 1929; Galton, 1969; Galton, 1970a; Borsuk-Bialynicka, 1977; Coombs, 1978; Norman, 1986; Dilkes, 2000; Jasinoski *et al*., 2006; Harris, 2007; Curry Rogers, 2009; Otero, 2010; Maidment & Barrett, 2011; Burch, 2014; Poropat *et al*., 2015; Otero, 2018; Voegele *et al*., 2020; Voegele *et al*., 2021) to verify their agreement. Because muscles do not always create surface texturing, and when they do it is usually not over their entire attachment site (Bryant and Seymour, 1990; Dilkes et al., 2012; Voegele *et al*., 2020; Voegele *et al*., 2021), muscles for UALVP 2 were only reconstructed over the area of their corresponding osteological correlate. This leads to a highly conservative reconstruction with a muscle distribution pattern that is likely sparser than it was in life. Still, examining osteological correlates can provide valuable information on myological stress patterns when studying related taxa (Voegele *et al*., 2020). Muscle terminology will follow that of recent dinosaur myological reconstructions including Voegele *et al*. (2020) and Voegele *et al*. (2021).

When reconstructing the myology of extinct animals, there is always a degree of uncertainty. To aid in understanding the degree to which such reconstructions can be trusted, Witmer (1995) identified several levels of inference. These will be used here to when describing the musculature of *S. validum*. Level 1 inferences are those with the highest degree of certainty in which both the soft tissue and the osteological correlate(s) are present in the EPB. Level 1’ inferences are those where the soft tissue is present in the EPB, but the osteological correlate is not or differs between taxa. Less

confidence is given to cases where the soft tissue and osteological correlate(s) are present in only some of the EPB taxa: level 2 inferences. The least reliable instance that will be discussed here, a level 2' inference, is when there is no observable osteological correlate in any of the EPB taxa.

Results

The appendicular skeleton of UALVP 2 preserves elements of the pectoral girdle, pelvic girdle, forelimb, and hindlimb. These elements include the right scapula, right coracoid, right humerus, right radius, right ulna, right ilium, right ischium, left and right femora, left tibia, and left and right fibulae. The following reconstruction will describe the muscles that attached to each of these elements and infer muscle attachments for elements of the appendicular skeleton which were not preserved based on comparisons with the extant phylogenetic bracket. Reconstructed muscle origins and insertions for *S. validum* are displayed in Tables 4 and 5.

Table 4. Reconstructed origins and insertions of the pectoral and forelimb musculature of *Stegoceras validum*.

Muscle	**Origin and inference level**	**Insertion and inference level**
Levator Scapulae (LS)	Cranial cervical ribs (2)	Dorsal edge of distal scapula (2)
Rhomboideus (RH)	Faschia of the cervico-thoracic region and neural spines of the posterior cervical and anterior dorsal vertebrae (1')	Distomedial scapula (1')
Serratus superficialis (SRS)	Lateral surfaces of the anterior dorsal ribs (1)	Posteroventral margin of the distal scapula (1')

Serratus Profundus (SRP)	Lateral surfaces of the anterior dorsal ribs (1)	Posteroventral medial surface of the distal scapula (1)
Deltoideus scapularis (DSC)	Lateral surface of the distal scapula (1')	Lateral surface of the deltopectoral crest (1)
Deltoideus clavicularis (DCL)	Acromial ridge of the scapula (1)	Lateral surface of the deltopectoral crest, distal to the DSC
Subscapularis (SBS)	Medial scapular blade proximal to the RH and SRP (1)	Proximomedial surface of the humerus (1)
Subcoracoideus (SBC)	Medial coracoid surrounding the coracoid foramen (2)	Shared with the SBS (1)
Scapulohumeralis posterior (SHP)	Lateral scapular blade (1')	Posterior humerus distal to the internal tuberosity (1)
Scapulohumeralis anterior (SHA)	Proximal posteroventral margin of the scapular blade (2)	Posterior humerus distolateral to the internal tuberosity (2)
Supracoracoideus (SC)	Scapula along the coracoid articulation (1') and medial ventral margin of the coracoid (2)	Proximolateral deltopectoral crest (1')
Coracobrachialis (CB)	Posteroventral lateral surface of the coracoid (1)	Proximoanterior surface of humerus (1)
Triceps brachii (TB)	Proximoventral scapula (1) and posteromedial humeral shaft (1)	Olecranon process of the ulna (1)
Biceps brachii (BB)	Lateral coracoid anteroventral to the coracoid foramen and dorsal to the CB (1)	Posterolateral surface of the proximal radius (1)
Pectoralis (P)	N/A	Apex of the deltopectoral crest (1)
Brachialis (BR)	Anterolateral humeral shaft distal to the deltopectoral crest (1')	Shared with BB (1)

Latissimus dorsi (LD)	Neural spines of posterior cervical and anterior dorsal vertebrae (1)	Proximolateral portion of the posterior humeral shaft (1)
Anconeus (AN)	Distal humeral ectepicondyle (1')	Lateral ulnar shaft (1)
Extensor carpi ulnaris (ECU)	Distal humeral ectepicondyle (1')	N/A
Supinator (SU)	Proximal humeral ectepicondyle (1')	Anterolateral radius (1)
Extensor carpi radialis (ECR)	Humeral ectepicondyle between the SU and extensor digitorum longus (1')	Radiale (1')
Extensor digitorum longus (EDL)	Middle of the humeral ectepicondyle (1)	Base of metacarpals I-IV (1)
Abductor radialis (AR)	Humeral ectepicondyle lateral to the ECR (2)	Proximolateral radius (1')
Abductor pollicis longus (APL)	Lateral ulnar shaft and distomedial radial shaft (1)	Metacarpal I (1')
Pronator teres (PT)	Proximal entepicondyle (1)	Anteromedial radius (1')
Pronator quadratus (PQ)	Medial ulnar shaft (1')	Ulnar-facing radius (1')
Flexor carpi ulnaris (FCU)	Distal humeral entepicondyle (1')	Pisiform (1)
Flexor digitorum longus superficialis (FDLS)	Middle of humeral entepicondyle (1)	Ventral distal phalanges (1')
Flexor digitorum longus profundus (FDLP)	Medial ulnar shaft (1')	Shared with FDLS (1')

Table 5. Reconstructed origins and insertions of the pelvic and hindlimb musculature of *Stegoceras validum*.

Muscle	**Origin and inference level**	**Insertion and inference level**
Iliocaudalis (ILC)	Posterolateral postacetabular process of the ilium (1)	Transverse processes and haemal spines of the anterior caudal vertebrae (1)

Ischiocaudalis (ISC)	Distolateral ischial shaft (1)	Shared with the ILC (1)
Puboischiofemoralis internus 1 (PIFI 1)	Medial preacetabular process of the ilium (1)	Posteromedial femur medial to the caudofemoralis longus (1)
Puboischiofemoralis internus 2 (PIFI 2)	Lateral surfaces of dorsal vertebrae (1)	Lesser trochanter of femur (1)
Iliofemoralis (ILFE)	Supracetabular region of the lateral ilium (1')	Shared with PIFI 2 (1')
Puboischiofemoralis externus 3 (PIFE 3)	Lateral ischium (2)	Posterolateral greater trochanter of the femur (1)
Iliotibialis (ILT)	Dorsal margin of the ilium (1)	Anteromedial cnemial crest of the tibia (1)
Iliofibularis (ILF)	Dorsolateral margin of the postacetabular process of the ilium (1)	Anterolateral fibula (1)
Flexor tibialis internus 3 (FTI 3)	Lateral ischium just distal to the iliac peduncle (1')	Posteromedial tibia (1)
Flexor tibialis externus (FTE)	Lateral postacetabular process of the ilium posteroventral to the ILF (1)	Shared with the FTI 3 (1)
Caudofemoralis brevis (CFB)	Ventrolateral postacetabular process of the ilium (1)	Posterior femur lateral to the fourth trochanter (1)
Caudofemoralis longus (CFL)	Lateral caudal centra (1')	Posterior femur medial to the fourth trochanter (1)
Adductor femoralis 1 (ADF 1)	Dorsolateral ischial shaft (1')	Posterodistal femur between the lateral and medial condyles (1)
Adductor femoralis 2 (ADF 2)	Ventrolateral ischial shaft (1')	Shared with ADF 1 (1)
Ischiotrochantericus (ISTR)	Dorsomedial ischial shaft (1')	Posterolateral femur just distal to the PIFE complex (1')

Ambiens (AMB)	Proximolateral prepubis (2)	Shared with the ILT and femorotibiales (1)
Femorotibialis lateralis (FMTL)	Lateral surfaces of the anterior and posterior femoral shaft (1')	Shared with the ILT and AMB (1)
Femorotibialis medialis (FMTML)	Medial surfaces of the anterior and posterior femoral shaft (1')	Shared with the ILT and AMB (1)
Gastrocnemius lateralis (GSCL)	Posteromedial lateral condyle of the femur (1)	Ventral surfaces of metatarsals II-IV (1)
Gastrocnemius medialis (GSCM)	Posteromedial medial condyle of the femur (1)	Shared with the GSCL (1)
Fibularis (FB)	Lateral fibular shaft (1')	Ventral calcaneum and distoventral metatarsal V (1)
Extensor digitorum longus (EDL)	Lateral surface of the lateral distal condyle of the femur and anterior cnemial crest (1')	Dorsal unguals and phalanges (1')
Extensor digitorum brevis (EDB)	Dorsal surface of the proximal tarsals (1')	Shared with EDL (1')
Flexor digitorum longus (FDL)	Proximal posteromedial fibula (1')	Ventral unguals and phalanges II-IV (1)
Popliteus (POP)	Posterior cnemial pocket of the tibia (1')	Proximomedial fibula (1)
Tibialis anterior (TBA)	Anterior cnemial pocket of the tibia (1')	Proximolateral metatarsals (II-IV)
Interosseus cruris (IOC)	Distal anterolateral tibial shaft (1)	Distomedial fibula (1)
Pronator profundus (PP)	Distal posteromedial tibia (1) and distal posteromedial fibula (2)	Ventromedial metatarsal II (1)

Pectoral and Brachial Musculature

Levator scapulae (LS). The presence of the levator scapulae is debated in dinosaurs (Dilkes, 2000; Burch, 2014; Otero, 2018; Voegele *et al*., 2020) because it is present in modern crocodilians but not in birds (Howell, 1937; Jasinoski *et al*., 2006; Meers, 2003; Burch 2014). It has been reconstructed in dinosaurs such as *Dreadnoughtus schrani* Lacovara *et al*., 2014 (Voegele, *et al*., 2020), *Opisthocoelicaudia skarzynskii* (Borsuk-Bialynicka, 1977), and *Tawa hallae* Nesbitt *et al*., 2009 (Burch, 2014), but has been left out in others, such as dromaeosaurids (Jasinoski *et al*., 2006). In crocodilians and the aforementioned dinosaurs for which this muscle has been reconstructed, its superficial insertion is always found along the anterior/dorsal edge (depending on the orientation of the bone in the animal) of the scapular blade with a corresponding osteological correlate (Howell, 1937; Borsuk-Bialynicka, 1977; Meers, 2003; Jasinoski *et al*., 2006; Burch 2014; Voegele, *et al*., 2020). Based on the presence of striations in this area in UALVP 2, the insertion site of the muscle in crocodilians, and its reconstruction in numerous groups of non-avian dinosaurs, the levator scapulae is reconstructed in *S. validum* as a level 2 inference inserting along the distal third and dorsal edge of the scapular blade (Figure 17). The origin of the levator scapulae is equivocal in dinosaurs but would likely be on the cranial cervical ribs as it is in crocodilians, a level 2 inference (Meers, 2003; Burch, 2014). This muscle would have acted to rotate the scapular blade and laterally flex the neck (Burch, 2014). If present, the trapezius would have inserted with the levator scapulae; however, the trapezius has no osteological origin in archosaurs (Jasinoski *et al*., 2006; Burch, 2004; Voegele *et al*.,

2020). Instead, it originates from the underlying cervico thoracic musculature. Without an osteological origin, the trapezius is not reconstructed here in *S. validum*.

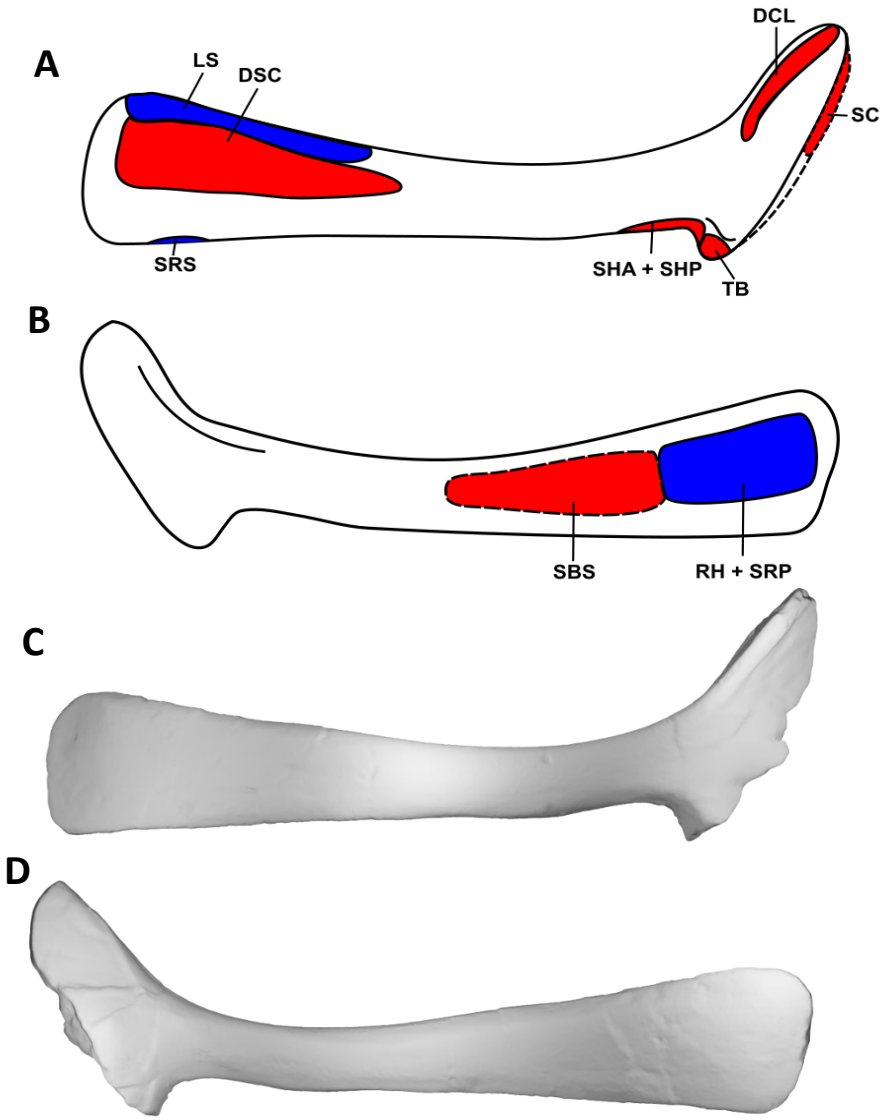

Figure 17. Myological reconstruction and scans of the right scapula of *Stegoceras validum*. (A) Lateral reconstruction, (B) medial reconstruction, (C) lateral scan, and (D) medial scan. Areas of red indicate muscle origins. Areas of blue indicate muscle insertions. Dashed lines indicate muscles that were reconstructed entirely based on EPB comparisons. Abbreviations: DCL - deltoideus clavicularis, DSC - deltoideus scapularis, LS - levator scapulae, RH - rhomboideus, SBS - subscapularis, SC - supracoracoideus, SHA - scapulohumeralis anterior, SHO - scapulohumeralis posterior, SRP - serratus profundus, SRS – serratus superficialis, TB - triceps brachii.

Rhomboideus (RH). The presence of the rhomboideus is unequivocal in dinosaurs, however, its number of divisions is equivocal (Dilkes, 2000; Meers, 2003; Jasinoski *et al*., 2006; Burch, 2014; Otero, 2018; Voegele *et al*., 2020). A profundus division is only found in birds and is reconstructed in dromaeosaurids (Jasinoski *et al*., 2006; Burch, 2014) based on the sub-horizontal position of the scapula. There are no osteological correlates directly supporting the presence of a profundus division of the rhomboideus in UALVP 2. A horizontal scapular position also results in an insertion of the rhomboideus superficialis along the medial side of the anterodorsal edge of the distal half of the scapular blade (Jasinoski *et al*., 2006; Burch, 2014). In crocodilians and ancestral theropods, the scapula is oriented sub-vertically and possesses no profundus division (Senter, 2006; Burch, 2014). The more vertical scapular orientation also leads to a lower insertion of the rhomboideus on the medial surface of the distal half of the scapula (Senter, 2006; Burch, 2014). In pachycephalosaurs, the scapula would have been oriented intermediate between the avian and crocodilian positions (Sereno, 1987; Sues & Galton, 1987; Sereno, 2000; Butler & Sullivan, 2009). As such, it is likely that the rhomboideus superficialis would have inserted at an intermediate position between the dorsal margin and medial surface of the scapular blade, a level 1' inference, similar to that proposed for *T. hallae* (Burch, 2014). This is supported by the presence of parallel striations in this location on the scapula of UALVP 2. With an intermediate scapular orientation, it is likely that the origin of the rhomboideus was also intermediate between the conditions of crocodilians and birds, attaching to the fascia of the dorsal cervico-thoracic region and the neural spines of the posterior cervical and anterior

dorsal vertebrae, a level 1' inference (Burch, 2014). Based on the proposed orientation of the scapula and morphology of the rhomboideus, this muscle would have functioned in protracting the scapula (Burch, 2014).

Serratus (SR). The presence of the serratus musculature is unequivocal in dinosaurs (Dilkes, 2000; Jasinoski *et al*., 2006; Burch, 2014; Otero, 2018; Voegele *et al*., 2020). It originates from the lateral surfaces of the anterior dorsal ribs in both birds and crocodilians (Jasinoski, 2006; Burch, 2014). With no opposing evidence, there is no reason to think this was not the case in *S. validum*, a level 1 inference. The insertion point(s) of the serratus superficialis (SRS) in dinosaurs are equivocal (Jasinoski *et al*., 2006; Burch, 2014; Voegele *et* al.,2020). Jasinoski *et al*. (2006) proposed two points of insertion for dromaeosaurids based on a tubercle present in neognath birds and *Ingenia yanshini*. More conservative models such as those for *T. hallae* (Burch, 2014) and *Dreadnoughtus schrani* (Voegele *et al*., 2020) propose a single elongated attachment site along the posteroventral margin of the distal half of the scapula. In UALVP 2, the only osteological correlate in this area is a small rugosity at the distal end of the posteroventral margin of the scapular blade. As such, the insertion of the serratus superficialis is conservatively reconstructed here as being limited to this correlate (Figure 17). This is a level 1' inference.

The serratus profundus (SRP) inserts on the medial surface of the distal end of the scapular blade in both birds and crocodilians (Jasinosky *et al*., 2006; Burch, 2014). Similar insertions have been proposed for *T. hallae* (Burch, 2014) and *Dreadnoughtus schrani* (Voegele *et al*., 2020). This area displays a striated texture on the scapula of

UALVP 2. Part of this area has already been allocated for the insertion of the rhomboideus. However, given its large surface area, it is unlikely that this entire area correlates solely with this muscle. Here, the posteroventral portion of this area in *S. validum* is allocated to the serratus profundus as a level 1 inference, while the anterodorsal portion is allocated to the rhomboideus (Figure 17).

Deltoideus scapularis (DSC). In crocodilians, the deltoideus scapularis originates on a broad area of the lateral surface of the distal half of the scapula. The avian homolog is highly modified and originates more proximally on the acromion process (Jalinoski *et al*., 2006; Burch, 2014). This means that it can no longer act as a major abductor of the humerus and must be compensated for by a highly developed supracoracoideus (Burch, 2014). This morphology is not reported in any non-avian dinosaur myological reconstructions (Borsuk-Bialynicka, 1977; Jalinoski *et al*., 2006; Otero, 2010; Burch, 2014; Klinkhamer *et al*., 2019; Veogele *et al*., 2020) and so it is much more likely that the deltoideus scapularis retained its ancestral archosaur morphology in *S. validum*. This is further supported by the expanded distal end of the scapula and its large lateral surface area. There are minor striations visible on this area of the scapula of UALVP 2 which likely correspond to the origin of the DSC (Figure 17). It is therefore reconstructed at this location in *S. validum* as a level 1' inference.

In the EPB, the deltoideus scapularis inserts on the lateral surface of the humerus proximal to the insertion of the deltoideus clavicularis (Meers, 2003; Maidment & Barrett, 2011). In birds, this attachment is found on the lateral surface of the deltopectoral crest; it attaches more proximal in crocodilians (Dilkes, 2000; Burch,

2014). The deltopectoral crest bears striations on its lateral surface in basal ornithischians such as *Heterodontosaurus* and *Scutellosaurus*, and is therefore acknowledged as the insertion area for the deltoid muscles (Maidment & Barrett, 2011). Sauropods, including *Dreadnoughtus* and *Opisthocoelicaudia*, likewise display scarring on this part of the humerus which is also attributed to the deltoideus scapularis and deltoideus clavicularis in muscular reconstructions (Borsuk-Bialynicka, 1977; Voegele *et al*., 2020). Other reconstructions, such as that of *Diamantinasaurus*, however, place this muscle in a more proximal position on the proximolateral humeral head, similar to that seen in crocodilians (Klinkhamer *et al*., 2019). This is similar to reconstructions of the theropod genus *Tawa* in which the deltoid scapularis is found to insert in a small oval depression just distal to the greater tubercle (Burch, 2014). UALVP 2 displays no such feature but does bear a distinct pitted texture on the lateral surface of the deltopectoral crest. *S. validum* is therefore reconstructed here with the basal ornithischian condition, a level 1 inference, in which the deltoid scapularis inserts on the proximal half of this area (Figure 18). Assuming this morphology, the deltoideus scapularis would have still functioned in the abduction and retraction of the humerus (Burch, 2014).

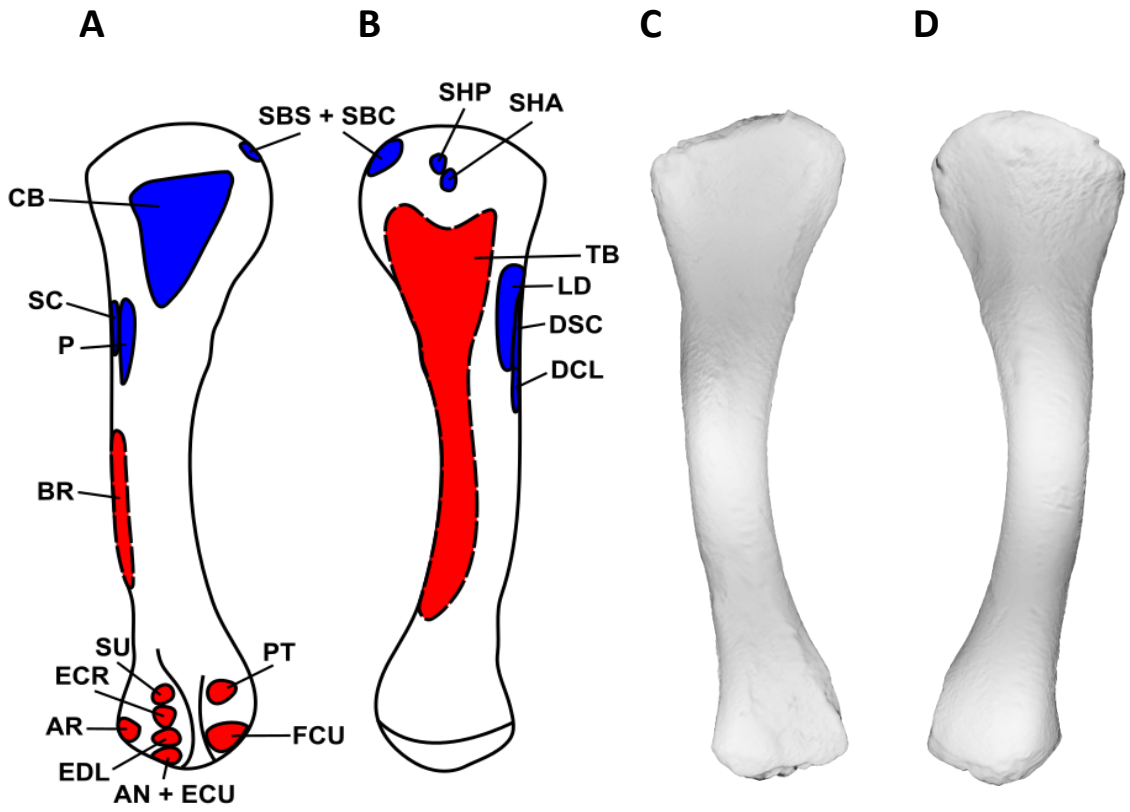

Figure 18. Myological reconstructions and scans of the right humerus of *Stegoceras validum*. (A) Anterior reconstruction, (B) posterior reconstruction, (C) anterior scan, and (D) posterior scan. Areas of red indicate muscle origins. Areas of blue indicate muscle insertions. Dashed lines indicate muscles that were reconstructed entirely based on EPB comparisons. Abbreviations: AN - anconeus, AR - abductor radialis, BR - brachialis, CB - coracobrachialis, DCL - deltoideus clavicularis, DSC - deltoideus scapularis, ECR - extensor carpi radialis, ECU - extensor carpi ulnaris, EDL - extensor digitorum longus, FCU - flexor carpi ulnaris, LD - latissimus dorsi, P - pectoralis, PT - pronator teres, SBC - subcoracoideus, SBS - subscapularis, SC - supracoracoideus, SHA - scapulohumeralis anterior, SHP - scapulohumeralis posterior, SU - supinator, TB - triceps brachii.

Deltoideus clavicularis (DCL). The deltoideus clavicularis has been highly modified in birds to the propatagialis which functions in elbow flexion of the wing (Howell, 1937; Sullivan, 1962; Burch, 2014). Some birds and all crocodilians share an origin for these

homologous muscles on the acromial ridge of the scapula (Burch, 2014). Previous myological reconstructions of a variety of dinosaurs also place the origin for the deltoideus clavicularis along this ridge (Burch, 2014; Klinkhamer *et al*., 2019; Voegele *et al*., 2020). The acromial ridge of UALVP 2 is well-defined and highly pitted, suggesting that this was indeed the site of origin for the deltoideus clavicularis in *S. validum*, a level 1 inference. Some myological reconstructions of dinosaurs extend the origin of this muscle to the acromial depression (Jasinoski *et al*., 2006), however, UALVP 2 possesses only a minor depression with no observable muscle scarring, so it is unlikely that the origin of this muscle extended beyond the acromial ridge in *S. validum* (Figure 17).

As discussed above, the deltoideus clavicularis and its homolog in birds is found to insert on the lateral surface of the deltopectoral crest just distal to the insertion of the deltoideus scapularis in the EPB (Meers, 2003; Maidment & Barrett, 2011; Burch, 2014; Voegele *et al*., 2020). This area displays osteological correlates across a variety of dinosaurs including basal ornithischians, theropods, and sauropods (Jasinoski *et al*., 2006; Maidment & Barrett, 2011; Burch, 2014; Voegele *et al*., 2020). This, too, is observed in UALVP 2. As such, the deltoideus clavicularis is reconstructed in this position for *S. validum*, a level 1 inference (Figure 18). With such a morphology, the deltoideus clavicularis would have mainly functioned to abduct the humerus in *Stegoceras* (Burch, 2014).

Subscapularis (SBS). The subscapularis unequivocally originates from the medial surface of the scapular blade in archosaurs (Burch, 2014). Exactly where it originates on the medial surface is debated. Jasinoski *et al*. (2006) argue for an origin along the

proximal half of the scapular blade on the basis of a ridge in this area which defines the dorsal edge of the subscapularis. However, this ridge is also present in crocodilians and instead defines the origin of the scapulohumeralis posterior (Meers, 2003). Burch (2014) argues that the ventrally shifted ridge in *T. hallae* would cause too much of a reduction in surface area for the attachment of the subscapularis and instead proposes an origin along the flaring blade of the scapula as in crocodilians. In sauropods, it has been proposed that the M subscapularis and subcoracoideus are divisions of the subcoracoscapularis which originates from a raised knob on the medial medial side of the proximal half of the scapula (Abdala & Diego, 2010; Otero, 2018; Voegele *et al*., 2020). UALVP 2 displays no ridges or knobs on the medial surface of the scapula; however, it does display a flared scapular blade. As such, the subscapularis is reconstructed for *S. validum* here as a level 1 inference directly proximal to the rhomboideus and serratus profundus along the medial surface of the scapular blade (Figure 17).

The insertion of the subscapularis in the EPB is tendinous and shared with the subcoracoideus. The tendon inserts unequivocally on the medial tuberosity of the humerus (Meers, 2003; Jasinoski *et al*., 2006; Maidment & Barrett, 2011; Burch, 2014). This area often displays well-defined osteological correlates, ranging from a prominent tuberosity to pitted or striated textures, across a wide array of dinosaurs and is attributed to this same insertion (Borsuk-Bialynicka, 1977; Jasinoski *et al*., 2006; Maidment & Barrett, 2011; Burch, 2014; Klinkhamer *et al*., 2019; Voegele *et al*., 2020). The humerus of UALVP 2 does not display any obvious tuberosity but does have a highly

rugose medial corner of the proximal surface of the humerus. This area is therefore attributed to the tendinous insertion of the subscapularis and subcoracoideus in *S. validum* as a level 1 inference (Figure 18). This morphology would result in a muscle which retracts and rotates the humerus (Burch, 2014).

Subcoracoideus (SBC). The subcoracoideus is fused to the subscapularis in crocodilians and has no independent osteological attachments (Meers, 2003; Burch, 2014). Birds and lepidosaurs retain an independent subcoracoideus, however, there is some variation in its structure. In the majority of neognath birds, this muscle is divided into two heads, the caput dorsale and caput ventrale (Jasinoski *et al*., 2006). Some species, however, lack the ventral head (George & Berger, 1966; McGowan, 1986; Jasinoski *et al*., 2006). The dorsal head originates from the medial side of the coracoid, overlapping the coracoid foramen (Jasinoski *et al*., 2006) while the ventral head originates from the anterior edge of the coracoid (Jasinoski *et al*., 2006). There are no osteological correlates around these areas in UALVP 2. Due to the variability of this muscle in the EPB and the lack of osteological correlates in UALVP 2, it is tentatively reconstructed here as a level 2 inference and having only the dorsal head and an origin surrounding the coracoid foramen (Figure 19). As discussed above, the insertion for the subcoracoideus would have been tendinous on the medial corner of the proximal surface of the humerus, a level 1 inference. These attachment sites would have resulted in a muscle which adducted and laterally rotated the humerus (Burch, 2014).

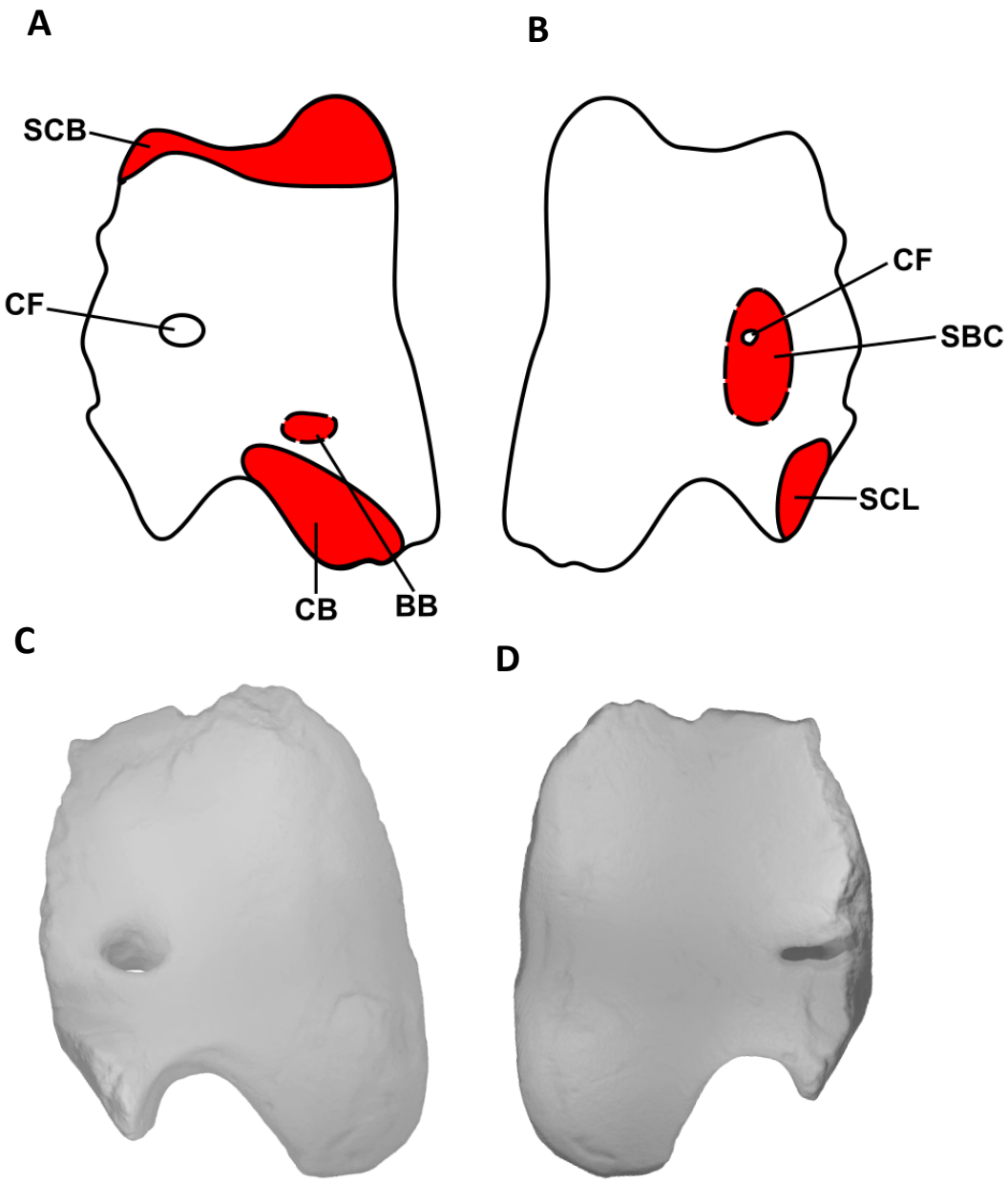

Figure 19. Myological reconstructions and scans of the right coracoid of *Stegoceras validum*. (A) lateral reconstruction, (B) medial reconstruction, (C) lateral scan, and (D) medial scan. Areas of red indicate muscle origins. Dashed lines indicate muscles that were reconstructed entirely based on EPB comparisons. Abbreviations: BB - biceps brachii, CB - coracobrachialis, CF - coracoid foramen, SBC - subcoracoideus, SCB - supracoracoideus brevis, SCL - supracoracoideus longus.

Scapulohumeralis posterior (SHP). The scapulohumeralis posterior is found in both crocodilians and birds and is therefore unequivocal in non-avian dinosaurs (Jasinoski *et al*., 2006; Burch, 2014; Voegele *et al*., 2020). In both EPB clades, the muscle originates on the lateral side of the posteroventral edge of the proximal half of the scapular blade. In birds however, the muscle usually extends far more distally, except in *Struthio*, where the origin is much more like that of crocodilians (Jasinoski *et al*., 2006; Burch, 2014). The crocodilian scapulohumeralis posterior also extends to the medial side of the scapula, inserting ventral to its medial ridge (Meers, 2003). This same ridge is present in many theropods, and so the origin of the scapulohumeralis likely extended to the medial surface in these taxa (Burch, 2014). No such ridge is present in UALVP 2. As such, the scapulohumeralis is conservatively shown here as originating only from the lateral surface of the scapular blade where the origins of the EPB taxa overlap, a level 1' inference (Figure 17). This is supported by a mild rugose texture in this area on the scapula of UALVP 2.

The insertion of the scapulohumeralis posterior is found on the posterior surface of the humerus just distal to the internal tuberosity in the EPB (Meers, 2003; Burch, 2014). It can be extensive in crocodilians but is reserved in birds (Meers, 2003; Jasinoski *et al*., 2006; Burch, 2014). It has been reconstructed in this area with the conservative morphology of birds in theropods and basal ornithischians based on striated or rugose texturing (Jasinoski *et al*., 2006; Maidment & Barrett, 2011; Burch, 2014). The area just distal to the internal tuberosity of UALVP 2 is heavily pitted, supporting the notion that this area would have served as the insertion site for the scapulohumeralis posterior in *S.*

validum, a level 1 inference (Figure 18). With this morphology, the scapulohumeralis posterior would have retracted the humerus (Maidment & Barrett, 2011).

Scapulohumeralis anterior (SHA). The scapulohumeralis anterior is present in birds but not in crocodilians (Jasinoski *et al*., 2006; Burch, 2014; Voegele *et al*., 2020). It has been hypothesized that modern crocodilians may have apomorphically lost the muscle and may not exhibit the ancestral archosauromorph condition (Sereno, 1991; Brusatte et al., 2010; Crawford et al., 2015; Voegele *et al*., 2020). As such, myological reconstructions of this muscle in dinosaurs have largely been based on its presence in birds and lepidosaurs (Jasinoski *et al*., 2006; Burch, 2014; Otero, 2018; Voegele *et al*., 2020). In these taxa, the scapulohumeralis anterior originates, at least partially, on the posteroventral margin of the scapular blade at its proximal-most extent (Jasinoski *et al*., 2006; Burch, 2014; Otero, 2018; Voegele *et al*., 2020). In lepidosaurs, this origin also extends to the lateral surface of the scapula (Dilkes, 2000; Voegele *et al*., 2020). On the scapula of UALVP 2, there is a slight rugosity corresponding to the area of origin for the scapulohumeralis anterior in birds. This rugosity, however, cannot be differentiated from that attributed to the SHP. It is likely that the SHA originated in *S. validum* from the proximal-most extent of the posteroventral margin of the scapular blade, just proximal to the SHP and that the observed rugosity corresponds to both muscles, a level 2 inference (Figure 17).

In birds, the tendinous insertion for the scapulohumeralis anterior is found just distolateral to that of the scapulohumeralis posterior. It is denoted in the EPB by the pneumatic fossa, which is not present in dinosaurs (Jasinoski *et al*., 2006; Burch, 2014).

Theropod reconstructions of this muscle are based entirely on the EPB and do not display any osteological correlates (Jasinoski *et al*., 2006; Burch, 2014). Some sauropods display a bulge on the proximolateral edge of the deltopectoral crest which has been attributed to the insertion of the scapulohumeralis anterior (Borsuk-Bialynicka, 1977; Voegele *et al*., 2020) while others display a rugose texture in this same area (Sanz *et al*., 1999). UALVP 2 displays no such features but does have a rugose texture directly distolateral to the insertion of the scapulohumeralis posterior. As such, the scapulohumeralis anterior is proposed here as a level 2 inference to have attached on the posterior surface of the humerus, distolateral to the internal tuberosity, as is the condition in birds and non-avian theropods (Figure 18). Similar to its posterior counterpart, the scapulohumeralis anterior would have also functioned to retract the humerus, given this morphology (Burch, 2014).

Supracoracoideus (SC). The supracoracoideus originates primarily from the coracoid in the EPB but attaches to the scapula in crocodilians and to the sternum in neognath birds (Burch, 2014). Additionally, crocodilians have three well-developed heads (supracoracoideus longus, intermedius, and brevis) of the supracoracoideus while birds have only one (Meers, 2003; Maidment & Barrett, 2014). The supracoracoideus longus (SCL) originates on the medial surfaces of the scapula and coracoid along their posteroventral and articular margins (Meers, 2003). On the lateral surface, the supracoracoideus brevis (SCB) arises from the coracoid dorsal to the coracoid foramen, and the supracoracoideus intermedius (SCI) arises along the dorsal articulation of the scapulocoracoid complex (Meers, 2003). In theropods, it has been proposed that this

muscle complex minimally originates from the coracoid and mainly attaches to the subacromial depression of the scapula (Jasinoski *et al*., 2006; Burch, 2014). Moegele *et al*. (2020) propose a more conservative scapular attachment in sauropods confined to the anterior margin of the scapula based on striations on the coracoid articulation. This is consistent with the myological reconstruction of basal ornithischians by Maidment & Barrett (2011). Unfortunately, the coracoid articulation of the scapula is not fully preserved in UALVP 2 and what is preserved does not display any obvious osteological correlates. The subacromial depression, however, is fully preserved and displays no evidence for the attachment of the supracoracoideus. This suggests that the supracoracoideus would have attached to the scapula along the coracoid articulation in *S. validum* as it does in crocodilians, sauropods, and basal ornithischians, as opposed to the acromial depression as seen in theropods, a level 1' inference (Figure 17) (Meers, 2003; Jasinoski *et al*., 2006; Maidment & Barrett, 2011; Burch, 2014; Voegele *et al*., 2020).

The coracoid origin of the supracoracoideus is difficult to locate in *S. validum*. All the margins of the element, save for part of the ventral margin, are mostly broken. Where preserved, striations are visible along the lateral face of the dorsal margin, possibly corresponding to the origin of the supracoracoideus brevis (SCB). Minimal striations are also preserved on the medial surface of the ventral margin of the element, bordering on the scapulocoracoid articulation. The area corresponds with part of the origin of the supracoracoideus longus (SCL) in crocodilians (Meers, 2003). As such, these areas have been reconstructed as origin sites for the supracoracoideus complex as a

level 2 inference in *S. validum* (Figure 19). There are no visible osteological correlates for the supracoracoideus intermedius on UALVP 2, as the part of the bone that would potentially support this muscle is not preserved. Therefore, the supracoracoideus intermedius is excluded from the myological reconstruction here.

The insertion of the supracoracoideus is equivocal in the EPB. Crocodilians display a tendinous insertion on the apex of the deltopectoral crest while birds have one on the greater tubercle (Meers, 2003; Jasinoski *et al*., 2006; Maidment *et al*., 2011; Burch, 2014). The avian attachment has been highly modified as the supracoracoideus functions in the elevation and rotation of the wing during the upstroke (Poore *et al*., 1997; Burch, 2014). As such, it is highly unlikely that the supracoracoideus would display such a modification in non-avian dinosaurs. Burch (2014) instead reconstructed the supracoracoideus of *Tawa* as inserting along the proximolateral edge of the deltopectoral crest on the basis of a small ovoid depression. The humerus of UALVP 2 possesses this same feature with a highly rugose surface texture. The supracoracoideus of *S. validum* therefore likely inserted at this same area (Figure 18). This is a level 1' inference. Such a morphology would result in a muscle which protracted the humerus (Burch, 2014).

Coracobrachialis (CB). The coracobrachialis is well-known in the EPB and unequivocal in dinosaurs (Dilkes, 2000; Meers, 2003; Jasinoski et al., 2006; Maidment and Barrett, 2011; Burch, 2014; Otero, 2018; Voegele *et al*., 2020). Its origin is located on the posteroventral portion of the lateral surface of the coracoid in both crocodilians and paleognath birds (Jasinoski *et al*., 2006; Burch, 2014). It has been reconstructed in

this general position in theropods (Jasinoski *et al*., 2006, Bruch, 2014), sauropods (Borsuk-Bialynicka, 1977; Langer *et al*., 2007; Klinkhamer *et al*., 2019; Voegele *et al*., 2020), and basal ornithischians (Maidment & Barrett, 2011). UALVP 2 displays notable striations in this same area which are attributed to the coracobrachialis origin as a level 1 inference (Figure 19).

The insertion of the coracobrachialis is also unequivocal in the EPB and is found on the anterior face of the humerus distal to the proximal articular surface (Burch, 2014). It extends distally, reaching the medial surface of the deltopectoral crest (Burch, 2014). In theropods, this area is defined by a large triangular depression with a distally facing apex which is attributed to the insertion of the coracobrachialis (Burch, 2014). This same morphology and proposed insertion are present in sauropods and basal ornithischians (Maidment & Barrett, 2011; Voegele *et al*., 2020). UALVP 2 displays a similar depression with rugose scarring on its proximal half and faint striations on its distal half. The medial surface of the deltopectoral crest also displays a heavily pitted texture. Based on these osteological correlates and the EPB condition (Maidment & Barrett, 2011; Burch, 2014; Voegele *et al*., 2020), this area is attributed to the insertion of the coracobrachialis in *S. validum* as a level 1 inference (Figure 18). This muscle would have protracted the humerus with the proposed morphology.

Triceps brachii (TB). The triceps brachii is present in all archosaurs but the number of heads varies in the EPB (Dilkes, 2000; Meers, 2003; Jasinoski et al., 2006; Abdala and Diogo, 2010; Maidment and Barrett, 2011; Burch, 2014; Otero, 2018; Voegele *et al*., 2020). Both birds and crocodilians have the scapular and medial heads,

but birds have a vestigial coracoid head and have lost the lateral head (Burch, 2014). Across all archosaurs and lepidosaurs, the scapular head has a small tendinous origin posterodorsal to the scapular contribution to the glenoid fossa, often associated with a rugose tubercle (Borsuk-Bialynicka, 1977; Jasinoski *et al*., 2006; Burch, 2014; Poropat *et al*., 2015; Voegele *et al*., 2020). This area of the scapula is partially broken on UALVP 2. However, the uppermost margin of a rugose tubercle is preserved, suggesting that *S. validum* displayed a similar scapular origin of the triceps brachii, a level 1 inference (Figure 17). Unfortunately, the extent of the attachment area is impossible to know.

The medial head of the triceps brachii originates on the posteromedial surface of the humeral shaft in both birds and crocodilians (Meers, 2003; Jasinoski *et al*., 2006; Burch, 2014). It is a fleshy attachment which bifurcates proximally, around the scapulohumeralis posterior in crocodilians and anterior in birds, and almost completely covers the humeral shaft (Jasinoski *et al*., 2006; Maidment & Barrett, 2011; Burch, 2014). This area lacks osteological correlates in dinosaurs (Jasinoski *et al*., 2006; Maidment & Barrett, 2011; Burch, 2014; Voegele *et al*., 2020), including UALVP 2. As such, the medial head of the triceps brachii is reconstructed here as a level 1 inference and covering the posterolateral humeral shaft based entirely on EPB comparisons (Figure 18).

UALVP 2 displays no osteological correlate for the lateral head of the TB. Since there is no direct evidence for the presence of the triceps brachii lateralis in UALVP 2, and this muscle is equivocal in the EPB, it is not reconstructed here in *S. validum*.

The heads of the triceps brachii share a single tendinous insertion on the posterior surface of the olecranon process of the ulna in the EPB (Meers, 2003; Jasinoski *et al*., 2006; Maidment & Barrett, 2011; Burch, 2014; Voegele *et al*., 2020). Most dinosaurs display some form of osteological correlate on the olecranon process which has been attributed to the insertion of the triceps brachii (Jasinoski *et al*., 2006; Maidment & Barrett, 2011; Burch, 2014; Voegele *et al*., 2020). UALVP 2 also displays distinct striations on the olecranon process which are attributed here to the tendon of the triceps brachii, a level 1 inference (Figure 20). The muscle would have therefore functioned in the extension of the humerus and antebrachium (Burch, 2014).

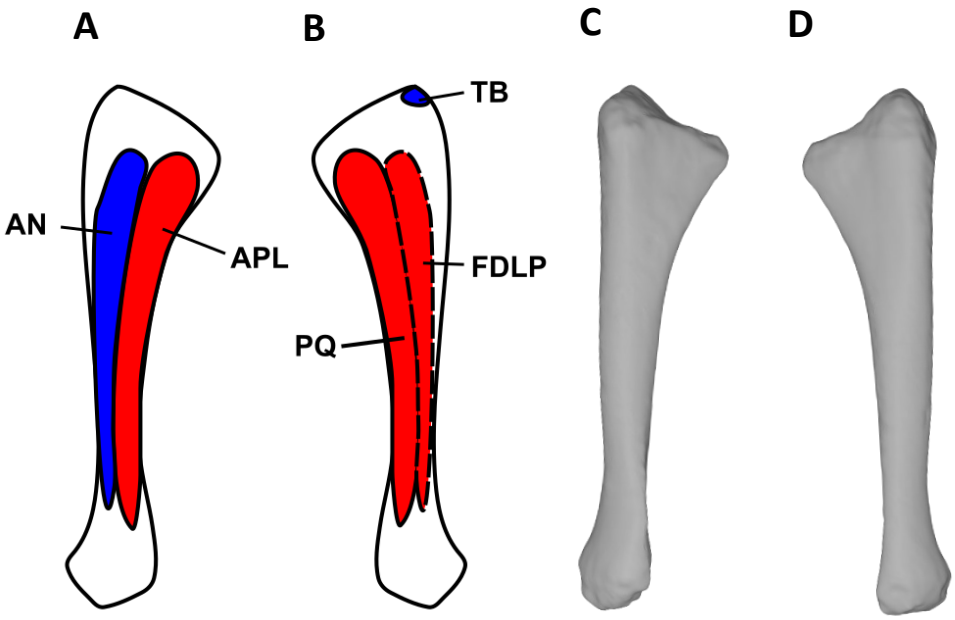

Figure 20. Myological reconstructions and scans of the right ulna of *Stegoceras validum.* (A) Lateral reconstruction, (B) medial reconstruction, (C) lateral scan, and (D) medial scan. Areas of red indicate muscle origins. Areas of blue indicate muscle insertions. Dashed lines indicate muscles that were reconstructed entirely based on EPB comparisons. Abbreviations: AN - anconeus, APL - abductor pollicis longus, FDLP - flexor digitorum longus profundus, PQ - pronator quadratus, TB - triceps brachii.

Biceps brachii (BB). The primary head of the biceps brachii arises from the coracoid in the EPB. Its tendinous origin attaches to a tubercle anterior to the glenoid fossa in both birds and crocodilians (Burch, 2014). Such a tubercle is also present in theropod dinosaurs and is assumed to be the site of origin (Jasinoski *et al*., 2006; Burch, 2014). Many sauropods display a ridge at this same area instead of a tubercle, which has also been attributed to the origin of the biceps brachii (von Huene, 1929; Borsuk-Bialynicka, 1977; Harris, 2007; Curry Rogers, 2009; Otero, 2010; Otero, 2018; Voegele *et al*., 2020). Basal ornithischians are reported as displaying no such feature by Maidment & Barrett (2011), however, ornithopods such as *Mantellisaurus* (Paul, 2007) and *Maiasaura* Horner & Makela, 1979 display a ridge and tubercle, respectively. In UALVP 2, no such osteological correlates are visible on the lateral surface of the coracoid. Given that coracoid origin of this muscle is almost unanimously reconstructed in the same position as the EPB in dinosaurs, it is reconstructed here for *S. validum* in the same position, a level 1 inference, anteroventral to the coracoid foramen and dorsal to the origin of the coracobrachialis (Figure 19). Birds and non-avian theropods also possess a humeral head of the biceps brachii, which is denoted by a rounded area on the anterior surface of the internal tuberosity (Jasinoski *et al*., 2006; Burch, 2014). This feature is not present in basal ornithischians (Maidment & Barrett, 2011) nor UALVP 2, and so is not reconstructed for *S. validum*.

The tendinous insertion of the biceps brachii is equivocal in the EPB (Dilkes, 2000; Meers, 2003; Jasinoski et al., 2006; Maidment and Barrett, 2011; Burch, 2014; Otero, 2018; Voegele *et al*., 2020). Birds display two insertions for this muscle, one on

the proximal end of the radius and the other on the ulna. Crocodilians, however, possess only the radial insertion (Meers, 2003; Jasinoski *et al*., 2006; Burch, 2014; Voegele *et al*., 2020). The ulnar insertion of the biceps brachii has been reconstructed in theropods and basal ornithischians based on EPB comparisons and varying osteological correlates (Maidment & Barrett, 2011; Burch, 2014). Its presence varies in sauropods (Borsuk-Bialynicka, 1977; Langer *et al*., 2007; Otero, 2018; Klinkhamer *et al*., 2019; Voegele *et al*., 2020). The ulna of UALVP 2 shows no distinct osteological correlate for the insertion of the biceps brachii, and since it is assumed that the origin of this muscle resembles the crocodilian morphology in *S. validum*, it is likely that this would be the case for its insertions as well. The radius, however, shows distinct striations on the proximal portion of its posterolateral surface which likely corresponded to this muscle. As such, *Stegoceras* is shown here as having no ulnar insertion and a radial insertion of the biceps brachii on the posterolateral surface of the proximal radius, a level 1 inference (Figure 21). It is still possible that *Stegoceras* had an ulnar insertion of the biceps because this insertion often leaves no visible scar (Burch, 2014). The muscle would have acted to flex the antebrachium (Burch, 2014).

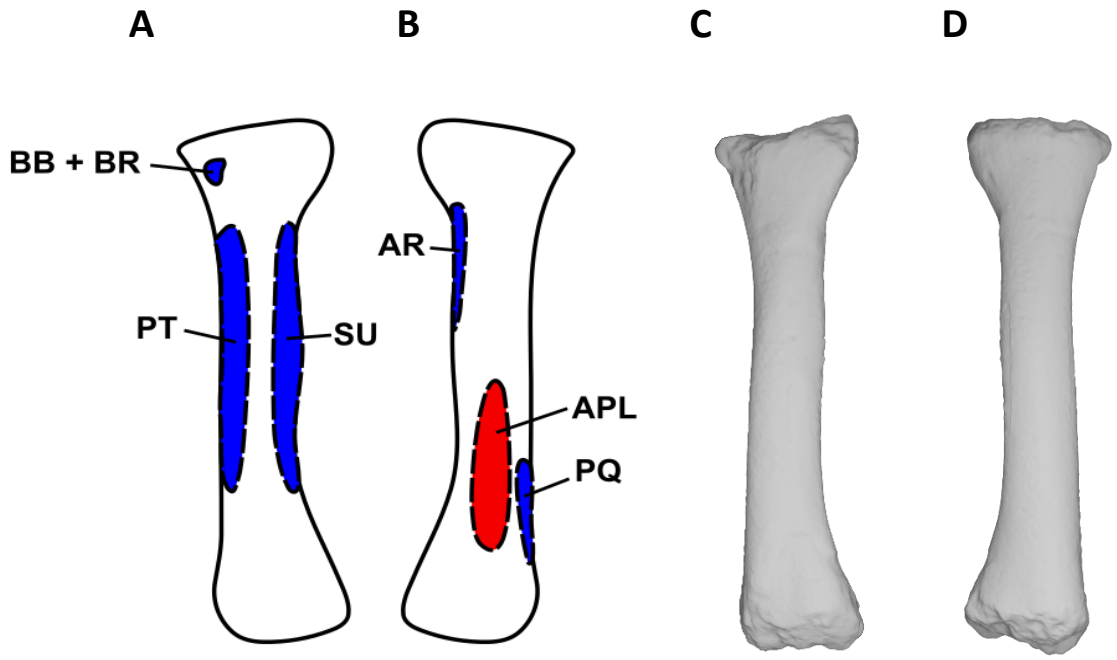

Figure 21. Myological reconstructions and scans of the right radius of *Stegoceras validum*. (A) Lateral reconstruction, (B) medial reconstruction, (C) lateral scan, and (D) medial scan. Areas of red indicate muscle origins. Areas of blue indicate muscle insertions. Dashed lines indicate muscles that were reconstructed entirely based on EPB comparisons. Abbreviations: APL - abductor pollicis longus, AR - abductor radialis, BB - biceps brachii, BR - brachialis, PQ - pronator quadratus, PT - pronator teres, SU - supinator.

Pectoralis (P). The origin of the pectoralis involves a variety of elements in archosaurs (Burch, 2014). In the EPB, one common origin is on the ventral face of the sternum. Additional origins are found on the sternal ribs in crocodilians and the coracoid in birds (Jasinoski *et al*., 2006; Burch, 2014). There is no evidence for an origin on the coracoid of UALVP 2. Without elements of the sternum preserved in UALVP 2, it is also impossible to determine if this was indeed the origin site for the pectoralis in *S. validum*.

The insertion of the pectoralis is found on the apex of the deltopectoral crest of both birds and crocodilians (Meers, 2003; Jasinoski *et al*., 2006; Maidment & Barrett,

2011; Burch, 2014; Voegele *et al*., 2020). Significant rugose scarring is visible on the deltopectoral apex in UALVP 2, making it likely that this was also the case in *S. validum*. The pectoralis is therefore reconstructed here as a level 1 inference inserting on the apex of the deltopectoral crest (Figure 18). Assuming an origin from a sternum or sternal ribs, this muscle would have acted to adduct the humerus in *S. validum*.

Humeroradialis (HR). The humeroradialis of crocodilians is homologized with the propatagialis of birds based on them sharing an embryological origin (Meers, 2003; Burch, 2014). The humeroradialis of crocodilians originates from an area distolateral to the deltopectoral crest (Meers, 2003; Jasinoski *et al*., 2006; Burch, 2014). Osteological correlates have been found near this area on the humeri of theropods and sauropods, resulting in reconstructions displaying the crocodilian morphology (Jasinoski *et al*., 2006; Bruch, 2014; Voegele *et al*., 2020). Maidment & Barrett (2011) elected to exclude this muscle from their reconstruction of basal ornithischian locomotor musculature due to its questionable homology and a lack of osteological correlates. UALVP 2 also displays no osteological correlate of the humeroradialis on the humerus.

The insertion of the humeroradialis is marked by a distinct tubercle on the posterior surface of the radius in crocodilians (Meers, 2003). No such osteological correlate is visible in UALVP 2. Due to a lack of evidence and an unresolved homology for the archosaurian humeroradialis, it is not included here in the myology of *S. validum*.

Brachialis (BR). The brachialis in crocodilians arises from an elongate region on the anterolateral surface of the humeral shaft, distal to the deltopectoral crest and

proximal to the distal condyles (Meers, 2003; Maidment & Barrett, 2011; Burch, 2014). This condition is also seen in lepidosaurs and turtles (Russell & Bauer, 2008; Walker, 1973). Birds possess the fossa musculus brachialis on the anterior surface of the humerus just proximal to the condyles for the attachment of this muscle (Baumel *et al*., 1993; Maidment & Barrett, 2011; Burch, 2014). Although the humerus of UALVP 2 displays a broad anterior intercondylar depression, there is no evidence for a distinct fossa as seen in birds. There are also no osteological correlates along the anterolateral margin of the humerus, distal to the deltopectoral crest. Because most dinosaurs are conservatively reconstructed with the assumed primitive crocodilian morphology (Jasinoski *et al*., 2006; Maidment & Barrett, 2011; Burch, 2014; Voegele *et al*., 2020), this structure is also assumed here for *S. validum* as a level 1' inference (Figure 18).

The brachialis inserts with the biceps brachii on the proximal ends of the radius and ulna in birds, but only on the radius in crocodilians (Meers, 2003; Maidment & Barrett, 2011; Burch, 2014; Voegele *et al*., 2020). As with the biceps brachii, there is no evidence for an ulnar insertion in *S. validum*. The brachialis is therefore reconstructed as inserting with the biceps brachii on the proximal end of the radius in *S. validum*, a level 1 inference (Figure 21). With this morphology, the muscle would have flexed the forearm (Burch, 2014).

Latissimus dorsi (LD). The latissimus dorsi arises from the neural spines of the last cervical vertebra and the first 6-7 dorsal vertebrae in the EPB (Meers, 2003; Maidment & Barrett, 2011; Burch, 2014). It is thus inferred to have the same origin in *S. validum*, a level 1' inference.

The insertion of the latissimus dorsi is found on the proximoposterior surface of the humeral shaft, lateral to the midline in both birds and crocodilians (Sullivan, 1962; Meers, 2003; Maidment & Barrett, 2011). An ovoid rugose scar is observed in this area on the humerus of UALVP 2. Similar scars have been observed in stegosaurs (Maidment & Barrett, 2011), sauropods (Borsuk-Bialynicka, 1977; Otero, 2010; Poropat *et al*., 2015; Otero, 2018), *Ankylosaurus* Brown, 1908 (Coombs, 1978), *Mantellisaurus* (Norman, 1986), dromaeosaurids (Jasinoski *et al*., 2006), and *Maiasaura* (Dilkes, 2000). Based on the observed osteological correlates in a variety of dinosaurs, the insertion in the EPB taxa, and the scar present in UALVP 2, the insertion of the latissimus dorsi is located on the proximolateral portion of the posterior surface of humeral shaft in *S. validum*, a level 1 inference (Figure 18). Such a morphology means that this muscle would have acted to retract the humerus (Burch, 2014).

Teres major (TM). The teres major occurs in crocodilians but not in birds (Howell, 1936; Romer 1944; Jasinoski *et al*., 2006). In crocodilians, its origin is located on the lateral surface of the posterodorsal scapular blade ventral to the DSC and its insertion is shared with the latissimus dorsi on the proximal humerus. There is no visible scarring corresponding the origin of the TM on the scapular blade of UALVP 2. Since there is no observable osteological correlate for this muscle in UALVP 2 and it is not present in all EPB taxa, it is not reconstructed here in *S. validum*.

Antebrachial Musculature

Anconeus (AN). The anconeus muscle originates on the ectepicondyle of the humerus in the EPB (Burch, 2014). It is referred to as the ectepicondylo-ulnaris in birds (Vanden Berge, & Zweers, 1993) and as the flexor ulnaris in crocodilians by Meers (2003). Of the muscles which attach to the ectepicondyle, the anconeus attaches the most distally (Burch, 2014). Ancestral Aves have a fused tendinous origin for the anconeus and extensor carpi ulnaris (Burch, 2014). Crocodilians lack the extensor carpi ulnaris entirely (Meers, 2003; Burch, 2014). Squamates also lack this muscle and turtles display a similar fusion to that of birds (Haines, 1939; Walker, 1973; Abdala *et al*., 2008; Burch, 2014). This inconsistency in modern reptiles makes it difficult to determine which morphology was more likely in non-avian dinosaurs. The ectepicondyle of UALVP 2 is highly pitted with no way of differentiating individual muscle scars. As such, both the anconeus and extensor carpi ulnaris are reconstructed here for *S. validum* as attaching to the distal portion of the humeral ectepicondyle, a level 1' inference (Figure 18). However, differentiating the origins of these muscles remains impossible.

The insertion of the AN is found on the lateral surface of the ulna in archosaurs (Burch, 2014). The insertion extends the entire length of the ulnar shaft in the EPB (Burch, 2014). Prominent striations on the lateral surface of the ulna at its proximal end support such an attachment in *S. validum*, a level 1 inference (Figure 20). This muscle would have acted to flex the forearm (Burch, 2014).

Extensor carpi ulnaris (ECU). As discussed above, the extensor carpi ulnaris is tentatively reconstructed here as attaching to the distal ectepicondyle of the humerus, along with the anconeus (Figure 18).

The ECR has multiple tendinous insertions on various carpals and metacarpals in the EPB (Burch, 2014). These attachments vary in modern reptiles and there is no way to tell how this muscle may have inserted in *S. validum* without preserved carpals and metacarpals. As such, the insertion points of the ECR remain uncertain in *Stegoceras*.

Supinator (SU). The supinator has the most proximal origin of the muscles which attach to the ectepicondyle in crocodilians (Haines, 1939; Burch, 2014). In birds, it attaches more distally, and the proximal position is taken by the extensor carpi radialis (Burch, 2014). The avian positioning is specialized to aid in flight adjustments of the wing (Vazquez, 1994; Burch, 2014), and so it is likely that the ancestral archosaurian condition is more like that of crocodilians. Once again, it is impossible to separate the muscle attachments to the ectepicondyle in UALVP 2, so the origin the supinator in *S. validum* is assumed to be the same as that observed in crocodilians, a level 1' inference (Figure 18).

The insertion of the supinator is located on the anterolateral surface of the radius in the EPB, adjacent to that of the pronator teres (George & Berger, 1966; Meers, 2003; Burch, 2014). It usually covers almost the entire length of the radial shaft (Burch, 2014). Although there are no correlates for this muscle on the radius of UALVP 2, it is reconstructed here with the same morphology as the EPB in *S. validum*, a level 1'

inference (Figure 21). This muscle would have functioned in the flexion of the forearm (Burch, 2014).

Extensor carpi radialis (ECR). In crocodilians, the extensor carpi radialis arises from the ectepicondyle of the humerus between the supinator and extensor digitorum longus (Burch, 2014). Birds display a more proximal origin (Baumel *et al*., 1993; Burch, 2014). This positioning serves to better flex and extend the wrist and elbow of the avian wing during flight (Vazquez, 1994; Burch, 2014). It is unlikely that non-avian dinosaurs had a use for such an adaptation, so it is assumed that the origin of the extensor carpi radialis of *S. validum* resembled that of crocodilians (Figure 18). This is a level 1' inference.

In crocodilians, the ECR inserts on the radiale (Meers, 2003). In birds, it inserts on the carpometacarpus on metacarpal I (Burch, 2014). Unfortunately, there is no preserved radiale or metacarpal I in UALVP 2. Since the avian wrist has been highly modified and non-avian dinosaurs display a morphology much closer to that of crocodilians, it is assumed that the ECR of *S. validum* would have inserted on the radiale as it does in crocodilians, a level 1' inference. This muscle would have acted to flex the forearm and extend and adduct the wrist (Burch, 2014).

Extensor Digitorum Longus (EDL). The origin of the EDL shows little variation in the EPB, almost always arising from the middle of the ectepicondyle of the humerus between the ECR and AN (Burch, 2014). As previously discussed, the entire ectepicondyle of UALVP 2 is highly rugose. As such, the EDL is reconstructed here as a

level 1 inference originating between the ECR and SU, as it does in modern archosaurs (Figure 18).

The EDL unequivocally inserts via tendons on the base of metacarpals I-IV in the EPB (Burch, 2014). As the metacarpals of UALVP 2 are not preserved, it is impossible to determine if this was the case in *S. validum*. It is assumed here that *S. validum* would have shared the same condition as all extant archosaurs, a level 1 inference.

Abductor radialis (AR). The abductor radialis originates lateral to the extensor carpi radialis on the ectepicondyle of the humerus in crocodilians (Meers, 2003; Burch, 2014). This muscle is not present in birds but is sometimes homologized with the second head of the extensor carpi radialis observed in some species (George & Berger, 1966; Burch, 2014). Due to the modifications for flight in the dorsal division muscles of birds, it is inferred that *S. validum* possessed an independent abductor radialis which arose from a similar position as that of crocodilians, a level 2 inference (Figure 18).

The AR has a shared tendinous insertion with the ECR on the carpometacarpus of birds, and an independent insertion on the proximal half of the radial shaft medial to the supinator in crocodilians (Meers, 2003; Burch, 2014). Given the highly modified avian wrist morphology, it is unlikely that their associated muscular attachments were shared by non-avian dinosaurs. Although there are no osteological correlates for the AR on the radius of UALVP 2, it is inferred that the musculature of *Stegoceras* would have been more similar here to that of crocodilians, a level 1’ inference. As such, the AR is reconstructed as inserting on the entire lateral surface of the proximal half of the radius

in *S. validum* (Figure 21). This morphology would result in a muscle functioning in the abduction of the forearm (Burch, 2014).

Abductor pollicis longus (APL). The abductor pollicis longus (extensor longus alulae in birds) is found in both birds and crocodilians. It has two heads, one originating from the from the lateral ulnar shaft anterior to the AN, and the other from the distomedial radial shaft (George & Berger, 1966; Meers, 2003; Burch, 2014). The ulnar head usually attaches to the full length of the shaft while the radial head only attaches to the distal half (Burch, 2014). There are no osteological correlates present on the radial shaft of UALVP 2, but there are minor striations present on the proximal and distal ends of the ulnar shaft. The APL is reconstructed here as having the same origin in *Stegoceras* as the EPB because of partial osteological correlates, a level 1 inference (Figures 20 & 21).

The insertion sites for the APL differ between birds and crocodilians. This muscle inserts on the developmental equivalent to metacarpal I in birds and on the radiale in crocodilians (Meers, 2003; Kundrát, 2009; Burch, 2014). The insertion on metacarpal I is also shared with turtles and lepidosaurs (Walker, 1973; Russell & Bauer, 2008), making it likely that this is the ancestral condition. Since there is no preserved radiale or metacarpals in UALVP 2, the insertion of the APL would have been the same in *Stegoceras* as it is in birds, turtles, and lepidosaurs, a level 1’ inference. The muscle would have therefore functioned in the extension and abduction of the wrist, and abduction of digit I (Burch, 2014).

Pronator teres (PT). The pronator teres is present in most EPB taxa and has the most proximal origin of muscles attaching to the entepicondyle of the humerus (Hudson *et al*., 1959; Zusi & Bentz, 1978; Livezey, 1990; Burch, 2014). As with the ectepicondyle, the entepicondyle of UALVP 2 is highly rugose with no visible differentiation of scar textures. Therefore, the muscles attaching to this structure will entirely be based on EPB comparisons. The pronator teres is reconstructed here as a level 1 inference attaching to the proximal margin of the entepicondyle in *S. validum* (Figure 18).

The insertion for the pronator teres is found on the anteromedial surface of the radius in the EPB (Burch, 2014). The extent of its insertion, however, varies. In all crocodilians and paleognath birds, the muscle inserts over most of the length of the radial shaft. Neognaths, to the contrary, have a shorter insertion on less than half of the proximal radius (Burch, 2014). With no osteological correlates present on the radial shaft of UALVP 2, it is inferred that the PT would have had a long insertion on the anteromedial face of the radius, a level 1' inference, as it does in the majority of EPB taxa (Figure 21).

Pronator accessorius (PA). The pronator accessorius is absent in all crocodilians and paleognath birds (Hudson *et al*., 1972; Burch, 2014). It is, however, present in neognaths, squamates, and turtles (Burch, 2014). Unfortunately, this means that its presence in non-avian dinosaurs is uncertain. With no direct evidence for the origin or insertion of this muscle on the humerus or radius of UALVP 2, it has been excluded from the appendicular musculature of *S. validum*.

Pronator quadratus (PQ). The pronator quadratus is present in crocodilians and is assumed to be homologous with the ulnimetacarpalis ventralis of birds (Sullivan, 1962; Meers, 2003; Burch, 2014; Maidment & Barrett, 2011; Voegele *et al*., 2020). It always originates along the medial surface of the ulna; however, its total area of attachment varies (Walker, 1973; Meers, 2003; Russell & Bauer, 2008; Burch, 2014). The attachment covers more than half of the ulnar shaft in crocodilians but is restricted to the distal half in most birds (George & Berger, 1966; Burch, 2014). It has been reconstructed with the crocodilian morphology in theropods (Burch, 2014) and sauropods (Voegele *et al*., 2020). The ulna of UALVP 2 exhibits striations at its proximal and distal articulations, which extend down onto the proximal and distal ends of the shaft, although the rest of the shaft displays no osteological correlates. It is possible that these striations are related to a proximal origin of the PQ, as seen in crocodilians. As such, the origin of the PQ is inferred here to have attached over the full length of the medial surface of the ulnar shaft, a level 1' inference (Figure 20).

In crocodilians and most other reptiles, the PQ inserts onto the ulnar-facing side of the radial shaft (Meers, 2003; Russell & Bauer, 2008; Burch, 2014). In turtles and birds, the insertion extends to the carpals (Straus, 1942; Haines, 1950; Walker, 1973; Berger-Dell'Mour, 1983' Burch, 2014). The radius of UALVP 2 displays no osteological correlates associated with the PQ on the radius, however, it is inferred that there would have still been an insertion on its lateral surface, based on the EPB. Unfortunately, without preserved carpals, it is impossible to say whether this insertion extended beyond the radius in *S. validum*. It is therefore conservatively constructed here as only

being present on the radius, a level 1’ inference (Figure 21). With such a morphology, this muscle would have acted to pronate the antebrachium (Burch, 2014).

Epitrochleoanconeus (EA). Known as the entepicondylo-ulnaris in birds, this muscle is not present in crocodilians but is present in other reptiles, including turtles and lepidosaurs (Abdala & Diogo, 2010; Burch, 2014). Among these reptiles, its morphology is highly varied (Burch, 2014). With little consistency in extant reptiles, the highly modified wing musculature of birds, and no direct osteological correlate for this muscle on UALVP 2, the epitrochleoanconeus is excluded from this myological reconstruction of *S. validum*.

Flexor carpi ulnaris (FCU). The flexor carpi ulnaris is found in the consulted EPB taxa and has a tendinous origin on the distal portion of the humeral entepicondyle (Burch, 2014). It has a small second tendinous attachment in many birds, which is usually associated with controlling secondary flight feathers (George & Berger, 1966; Burch, 2014). This configuration would serve no purpose in non-avian dinosaurs, so the flexor carpi ulnaris is presented here for *S. validum* with the same morphology observed in crocodilians, a level 1’ inference (Figure 18).

The flexor carpi ulnaris has an unequivocal insertion on the pisiform in the EPB (Burch, 2014). Birds, however, possess an additional insertion on the ulnare, which is not homologous to the ulnare of crocodilians (Kundrát, 2009; Burch, 2014). Because this element is not present in non-avian dinosaurs, it can be inferred from the EPB that the FCU of *Stegoceras* would have solely attached to the pisiform, a level 1 inference. This

morphology would have resulted in a muscle that flexed and adducted the wrist (Meers, 2003).

Flexor digitorum longus superficialis (FDLS). The flexor digitorum longus superficialis is present in all crocodilians and birds except ratites (McGowan, 1982; Burch, 2014). Its origin is tendinous and located between those of the flexor carpi ulnaris and the pronator teres (Burch, 2014). With no ambiguity in the EPB taxa, this origin is reconstructed with the same position in *S. validum* (Figure 18). This is a level 1 inference.

The FDLS shares tendinous insertions with the flexor digitorum longus profundus in the EPB (Burch, 2014). In modern reptiles, including turtles and lepidosaurs, these tendons attach to the ventral surfaces of all the distal phalanges (Walker, 1973; Russell & Bauer, 2008; Burch, 2014). Crocodilians have reduced digits IV and V, and so the FDLS only attaches to the other three phalanges in these animals (Meers, 2003). Birds have a highly fused and modified manus in which there is only one tendinous attachment for the FDLS on digit II (Bever *et al*., 2011; Burch, 2014). Given the modified nature of the digits of the EPB, it is difficult to reconstruct this attachment in *Stegoceras* with no preserved elements of the manus. It is tentatively reconstructed here as having tendinous insertions on the ventral side of all the distal phalanges, a level 1' inference. The FDLS would have acted to flex the wrist and digits (Burch, 2014).

Flexor digitorum longus profundus (FDLP). The presence of the FDLP is unequivocal in the EPB (Burch, 2014). It originates over the entire length of the medial

ulnar shaft in crocodilians and is posterior to the PQ. In birds, the origin of the FDLP is halted distally by the PQ (George & Berger, 1966; Burch, 2014). This reduction is likely linked to the reduction of the digits in birds, and so this muscle is not required as much to flex the digits (Burch, 2014). There are no osteological correlates on the ulnar shaft which can be specifically attributed to the FDLP in UALVP 2. Therefore, the origin of the FDLP is reconstructed in *S. validum* as having the crocodilian morphology, a level 1' inference, since the manus of pachycephalosaurs was not as highly modified as that of modern birds (Figure 20).

As stated above, the FDLP shares insertions with the FDLS, and is reconstructed as such in *S. validum*.

Pelvic Musculature

Iliocaudalis (ILC). The iliocaudalis is found in both birds and crocodilians, and is therefore unequivocally present in dinosaurs (Dilkes, 2000; Persons & Currie,2011; Voegele *et al*., 2021). This muscle originates from the posterior region of the postacetabular process of the ilium on its lateral surface in the EPB (Dilkes, 2000; Persons & Currie, 2011; Voegele, 2021), and has been reconstructed this way for dinosaurs such as *Maiasaura* (Dilkes, 2000), *Dreadnoughtus* (Voegele *et al*., 2021), *Opisthocoelicaudia* (Borsuk-Bialynicka, 1977), *Rapetosaurus* (Curry Rogers, 2009), and *Tyrannosaurus* (Persons & Currie, 2011). UALVP 2 displays distinct striations on this region at a rough midpoint dorsoventrally. It is inferred from the EPB and previous

dinosaurian reconstructions that this would have served as the origin site for the ILC in *S. validum* (Figure 22). This is a level 1 inference.

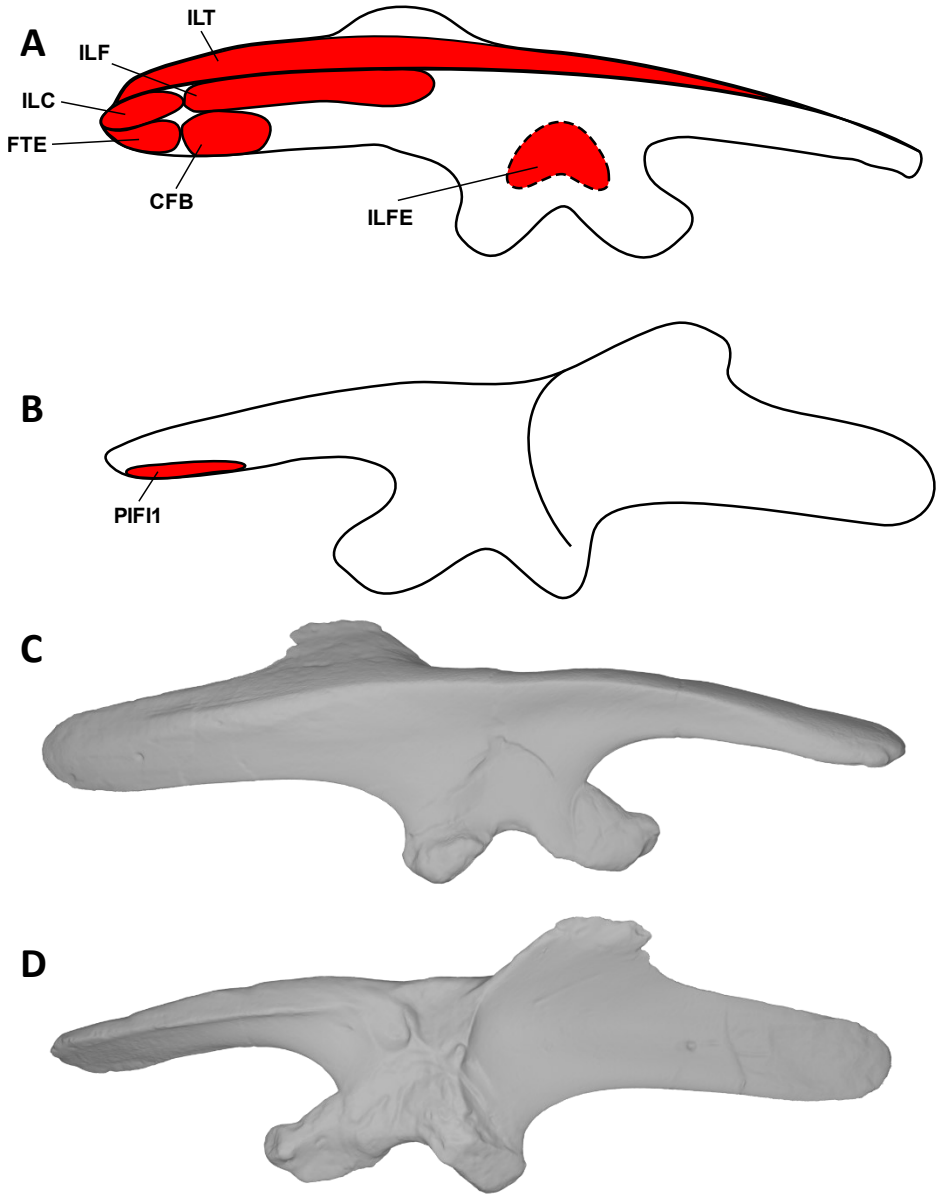

Figure 22. Myological reconstructions and scans of the right ilium of *Stegoceras validum*. (A) Lateral reconstruction, (B) medial reconstruction, (C) lateral scan, and (D) medial scan. Areas of red indicate muscle origins. Dashed lines indicate muscles that were reconstructed entirely based on EPB comparisons. Abbreviations: CFB - caudofemoralis brevis, FTE - flexor tibialis externus, ILC - iliocaudalis, ILF - iliofibularis, ILFE - iliofemoralis, ILT - iliotibialis, PIFI1 - puboischiofemoralis internus 1.

The ILC shares insertions with the ischiocaudalis on the anterior caudal vertebrae in crocodilians (Persons & Currie, 2011). Attachments are found on the lateral and ventral surfaces of the caudal ribs and on the ventral tips of the haemal spines (Persons & Currie, 2011). Although many caudal vertebrae are preserved in UALVP 2, they either do not display any obvious osteological correlates for these insertions or do not preserve transverse processes or haemal spines. As such, it is assumed as a level 1' inference, based on the EPB, that these attachments were present in *S. validum*. If this is the case, then the form of the ILC, along with other muscles which attach to the base of the tail in archosaurs such as the ischiocaudalis and caudofemoralis, may have been influenced by the tail and pelvic structure of pachycephalosaurs. The posterior pelvic structure and base of the tail of pachycephalosaurs are transversely wide when compared to other dinosaurs (Maryańska *et al*., 2004; Maidment & Barrett, 2014) resulting from the medially projecting flange of the ilium and long sacral and caudal ribs. Such structures would have allowed for larger muscles with more mass at the base of the tail (Persons & Currie, 2010). As a result, these muscles were likely strong and well-developed in pachycephalosaurs.

Ischiocaudalis (ISC). If the homology of the pubocaudalis of birds to the ischiocaudalis of crocodilians is accepted, then the presence of the ischiocaudalis in dinosaurs is unequivocal (Dilkes, 2000; Persons & Currie, 2011; Voegele *et al*., 2021). The muscle originates from the distal shaft of the ischium on its lateral surface in the EPB, just lateral to the attachment of the puboischiofemoralis externus III (Dilkes, 2000; Persons & Currie, 2011; Voegele *et al*., 2021). UALVP 2 displays distinct striations in this

region of the ischium, however attachments for the ISC and the puboischiofemoralis externus cannot be distinguished from each other. Therefore, the distal portion of this area is assigned to the origin of the ISC in *S. validum* as a level 1 inference (Figure 23).

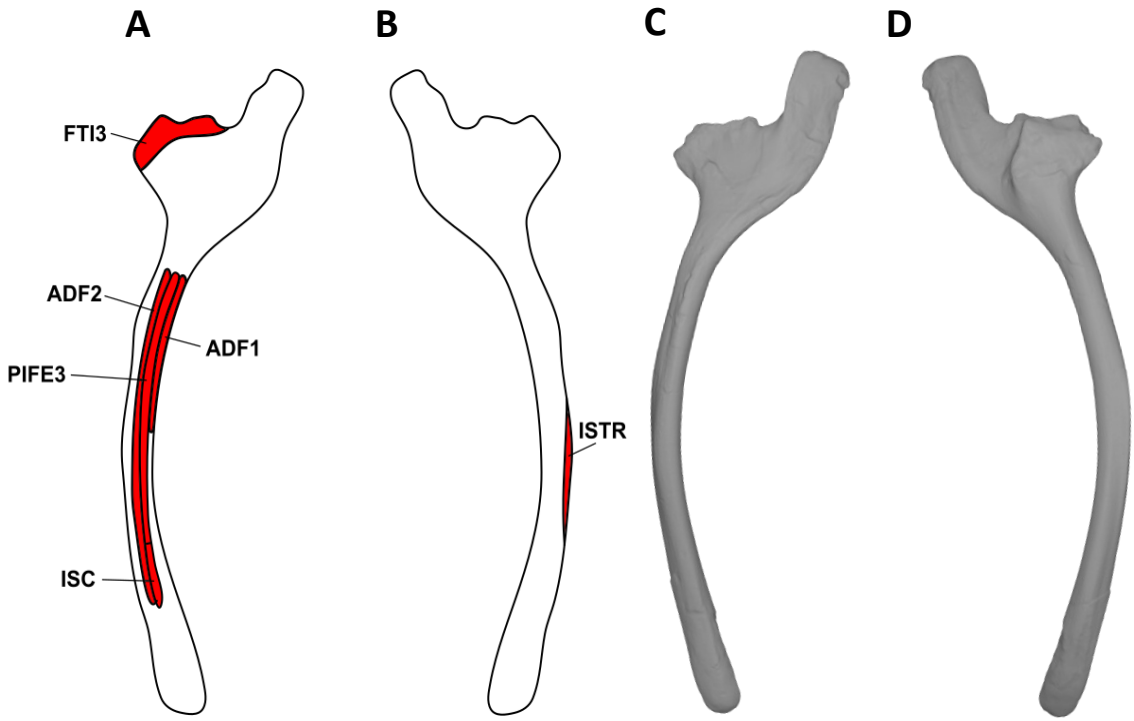

Figure 23. Myological reconstructions and scans of the right ischium of *Stegoceras validum.* (A) Lateral reconstruction, (B) medial reconstruction, (C) lateral scan, and (D) medial scan. Areas of red indicate muscle origins. Abbreviations: ADF1 - adductor femoralis 1, ADF2 - adductor femoralis 2, FTI3 - flexor tibialis internus 3, ISC - ischiocaudalis, ISTR - ischiotrochantericus, PIFE3 - puboischiofemoralis externus 3.

As discussed above, the insertions of the ISC are shared with the ILC. It is therefore assumed that the ISC of *S. validum* would have inserted on the caudal ribs and haemal arches of the anterior caudal vertebrae.

Puboischiofemoralis internus (PIFI). The puboischiofemoralis internus has two heads in crocodilians (Maidment & Barrett, 2011; Voegele *et al*., 2021). Homologous muscles in birds are the iliofemoralis internus and the iliotrochantericus cranialis and medius (Rowe, 1986; Maidment & Barrett, 2011). In crocodilians, PIFI 1 is the smaller of the two heads and originates on the medial surface of the preacetabular process of the ilium, ventral to the medial ridge and the anterior surface of the first sacral rib (Romer, 1923; Maidment & Barrett, 2011). PIFI 2 is larger and originates on the lateral faces of the dorsal vertebrae (Romer, 1923; Maidment & Barrett, 2011). The ventromedial ridge of the preacetabular process of the ilium in UALVP 2 is notably rugose, as is its ventral surface. It is therefore inferred that this served as the attachment for the PIFI 1 in *S. validum* as it does in crocodilians (Figure 22). This is a level 1 inference. The dorsal vertebrae of UALVP 2 likewise preserve a rugose texture on their lateral surfaces which would have served as the attachment sites for the PIFI 2.

PIFI 1 has been suggested to insert on the posteromedial surface of the femur near the insertion of the caudofemoralis longus (CFL) in dinosaurs (Maidment & Barrett, 2011; Piechowski & Talanda, 2020; Voegele *et al*., 2021). In crocodilians, the insertion surrounds that of the CFL mediodistally and extends to the distalmost extent of the fourth trochanter (Romer, 1923; George & Berger, 1966; Hutchinson, 2001; Fechner, 2009; Maidment & Barrett, 2011; Piechowski & Talanda, 2020). There is a distinct pit medial to the fourth trochanter on the femora of UALVP 2 which likely corresponds to the insertion of the CFL. The area medial and distal to the pit is highly rugose and is

attributed to the insertion of PIFI 1 in *S. validum* as a level 1 inference (Figure 24). This muscle would have acted to abduct and extend the femur (Schachner *et al*., 2011; Piechowski & Tałanda, 2019).

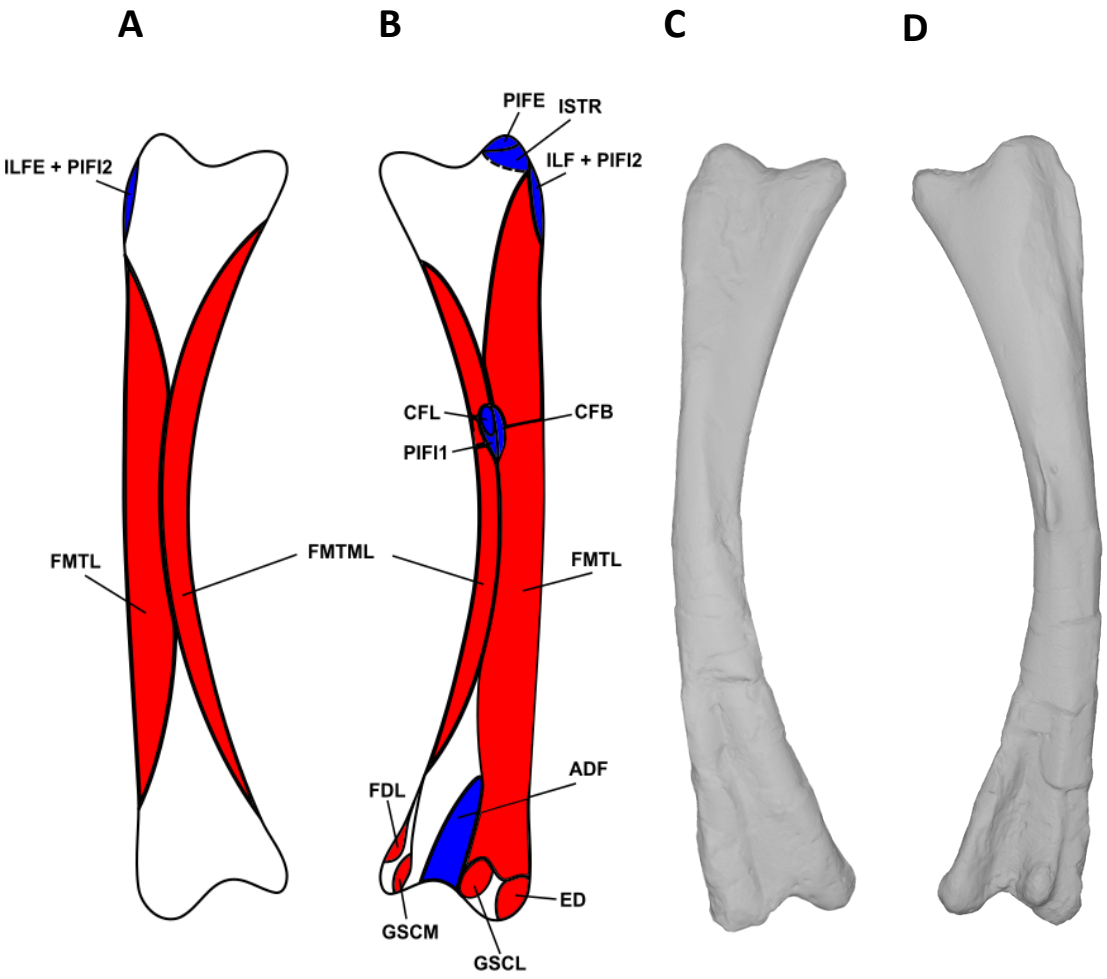

Figure 24. Myological reconstructions and scans of the right femur of *Stegoceras validum*. (A) Anterior reconstruction, (B) posterior reconstruction, (C) anterior scan, and (D) posterior scan. Areas of red indicate muscle origins. Areas of blue indicate muscle insertions. Dashed lines indicate muscles that were reconstructed entirely based on EPB comparisons. Abbreviations: ADF – adductores femores, CFB - caudofemoralis brevis, CFL - caudofemoralis longus, ED - extensor digitorum, FDL - flexor digitorum longus, FMTL - femorotibialis lateralis, FMTML - femorotibialis medialis, GSCL - gastrocnemius lateralis, GSCM - gastrocnemius medialis, ILFE - iliofemoralis, ISTR - ischiotrochantericus, PIFE - puboischiofemoralis externus, PIFI1 - puboischiofemoralis internus 1, PIFI2 - puboischiofemoralis internus 2.

PIFI 2 inserts on the anterolateral portion of the proximal femur in the EPB (Fechner, 2009; Maidment & Barrett, 2011; Piechowski & Talanda, 2020; Voegele *et al*., 2021). This area corresponds with the proximodistally elongate lesser trochanter of UALVP 2 (Figure 24). The surface of this feature is slightly rugose and is likely associated with the insertion of PIFI 2, a level 1 inference. This muscle complex would have acted to flex the hip (Schachner *et al*., 2011; Piechowski & Talanda, 2020).

Iliofemoralis (ILFE). The origin of the iliofemoralis is consistent across the EPB and is therefore unequivocal in dinosaurs (Dilkes, 2000; Carrano & Hutchinson, 2002; Maidment & Barrett, 2011; Otero & Vizcaíno, 2008; Ibiricu et al., 2018; Voegele *et al*., 2021). In the EPB, this muscle originates from the supracetabular region of the lateral ilium and usually does not leave a scar (Dilkes, 2000; Carrano & Hutchinson, 2002; Maidment & Barrett, 2011; Otero & Vizcaíno, 2008; Ibiricu et al., 2018; Voegele *et al*., 2021). This surface is smooth in UALVP 2, but it is assumed that it would be the origin site of the ILFE in *S. validum* based on the EPB, a level 1' inference (Figure 24).

The insertion(s) of the ILFE are equivocal in dinosaurs (Maidment & Barrett, 2011; Piechowski & Talanda, 2020; Voegele *et al*., 2021). Crocodilians possess a single-bodied ILFE which is homologous to the iliofemoralis externus (IFE) and iliotrochantericus (ITC) of birds (Rowe, 1986; Maidment & Barrett, 2011). In crocodilians, the ILFE inserts on the anterolateral femur between the attachments of the femorotibialis (FMT) internus and externus (Maidment & Barrett, 2011). The ITC of birds inserts on the proximal trochanteric crest of the femur and the IFE inserts on a ridge

distolateral to the trochanteric crest, which represents the fusion of the greater and lesser trochanters (Hutchinson, 2001; Maidment & Barrett, 2011). Since the only homologous feature to these on the femur of UALVP 2 is the lesser trochanter, the ILFE is reconstructed here as inserting on the lesser trochanter along with the insertion of the puboischiofemoralis internus 2, a level 1' inference, as there is no way to differentiate scarring on the feature (Figure 24). Such a morphology would have resulted in a muscle which abducted the hip (Schachner *et al*., 2011; Piechowski & Talanda, 2020)

Puboischiofemoralis externus (PIFE). The homology of the PIFE in archosaurs and its number of divisions are inconsistent in the literature (Romer, 1923, 1927; Walker, 1977; Hutchinson & Gatesy, 2000; Hutchinson, 2001; Maidment & Barrett, 2011). For simplicity and consistency, it is assumed here that the PIFE complex has three heads in crocodilians, two originating from the pubis and one from the ischium, and is homologous with the obturator in birds (Romer, 1927; Hutchinson & Gatesy, 2000; Maidment & Barrett, 2011). PIFE 1 attaches to the medial aspect of the pubis in crocodilians and PIFE 2 originates from the posterolateral pubis (Maidment & Barrett, 2011). As birds possess a retroverted pubis, the attachments of PIFE 1 and 2 have shifted to the postpubis (Maidment & Barrett, 2011). This structure, however, is extremely reduced in basal ornithischians and pachycephalosaurs, and was unlikely able to support major muscle attachments (Maryańska *et al*., 2004; Maidment & Barrett, 2011). As a result, it is difficult to interpret the origins of PIFE 1 and 2 in *S. validum*, especially since UALVP 2 lacks a preserved pubis. It has been hypothesized that the

pubic attachments of PIFE 1 and 2 shifted to the ischiadic apron in ornithischians (Galton, 1970a; Coombs, 1979; Norman, 1986; Maidment & Barrett, 2011), however, this structure is also heavily reduced in ornithischians and would result in an overall reduction of the PIFE musculature. There is also no osteological correlate present on this region of the ischium in UALVP 2. A second hypothesis is that the first and second heads of the PIFE complex were completely lost in ornithischians. Since there is no preserved pubis and no osteological correlate for PIFE 1 and 2 in UALVP 2, these attachments are not reconstructed here for *S. validum*. It is, however, still possible that these attachments were present in the animal.

The PIFE 3 of crocodilians originates from the lateral ischium and has no avian homologue (Maidment & Barrett, 2011). Romer (1927) reported, based on the embryonic development of birds, that the lack of a third head of the obturator complex was a derived character of the clade. Maidment & Barrett (2011) reconstructed the pelvic musculature of basal ornithischians as having a crocodilian morphology of the PIFE complex with all three heads. Similarly, Voegele *et al*. (2021) reconstructed the pelvis of *Dreadnoughtus* as having a PIFE 3 on the ventrolateral face of the distal shaft of the ischium, based on distinct striations in that region. UALVP 2 has a notably rugose ridge on the lateral surface of its ischium which descends distally from the base of the pubic peduncle, roughly halfway down the shaft. This ridge corresponds to the origin of the PIFE 3 in crocodilians and the above-mentioned dinosaurian muscle reconstructions. It is therefore presented here as the origin site for the PIFE 3 in *S. validum*, a level 2 inference (Figure 23).

All heads of the PIFE share one insertion in the EPB on the greater trochanter (Fechner, 2009; Maidment & Barrett, 2011; Voegele *et al*., 2021). The greater trochanter of the right femur of UALVP 2 displays rugose scarring on its posterolateral surface, which is attributed here to the insertion of the PIFE complex, a level 1 inference (Figure 24). Such a morphology would have resulted in a complex that flexed and adducted the hip (Schachner *et al*., 2011; Piechowski & Talanda, 2020).

Iliotibialis (ILT). The presence of the iliotibialis is unequivocal in dinosaurs based on EPB comparisons (Dilkes, 2000; Carrano & Hutchinson, 2002; Otero & Vizcaíno, 2008; Maidment & Barrett, 2011; Ibiricu *et al*., 2018; Piechowski & Talanda, 2020; Voegele *et al*., 2021). It attaches on the dorsolateral margin of the ilium in the EPB (Maidment & Barrett, 2011; Piechowski & Talanda, 2020; Voegele *et al*., 2021). Such an attachment has also been hypothesized in basal ornithischians (Maidment & Barrett, 2011) and sauropods (Borsuk-Bialynicka, 1977; Otero & Vizcíno, 2008; Klinkhamer *et al*., 2018; Voegele *et al*., 2021). In pachycephalosaurs, the dorsolateral margin of the ilium has been folded medially and is simply referred to as the dorsal margin of the ilium. The entirety of this surface in UALVP 2 is covered in prominent parallel striations, supporting this as the attachment site for the ILT in *S. validum*. Similar continuous striations extend onto the dorsal surface of the medial iliac flange in UALVP 2. No other muscles attach to the corresponding area in extant or extinct archosaurs (Dilkes, 2000; Carrano & Hutchinson, 2002; Otero & Vizcaíno, 2008; Maidment & Barrett, 2011; Ibiricu *et al*., 2018; Piechowski & Talanda, 2020; Voegele *et al*., 2021), making it difficult to assess what may have left these scars on the ilium of UALVP 2. It is possible that this area may

have served as an attachment site for sacro-iliac ligaments or perhaps for a muscle/belly unique to pachycephalosaurs. Since the EPB and no other dinosaurs display such a structure, no muscles can be confidently reconstructed as attaching here in *S. validum*. The ILT is reconstructed here with an origin covering the entire length of the dorsal margin of the ilium, a level 1 inference.

The iliotibialis unequivocally shares a tendinous insertion with the femorotibialis complex and the ambiens on the anteromedial surface of the cnemial crest in the EPB (Romer, 1923; Maidment & Barrett, 2011; Piechowski & Talanda, 2020; Voegele *et al*., 2021). This region of the tibia is densely striated in UALVP 2 and is therefore attributed as a level 1 inference to the insertion of this tendon in *S. validum* (Figure 25). This muscle would have acted to flex, extend, and abduct the hip (Schachner *et al*., 2011).

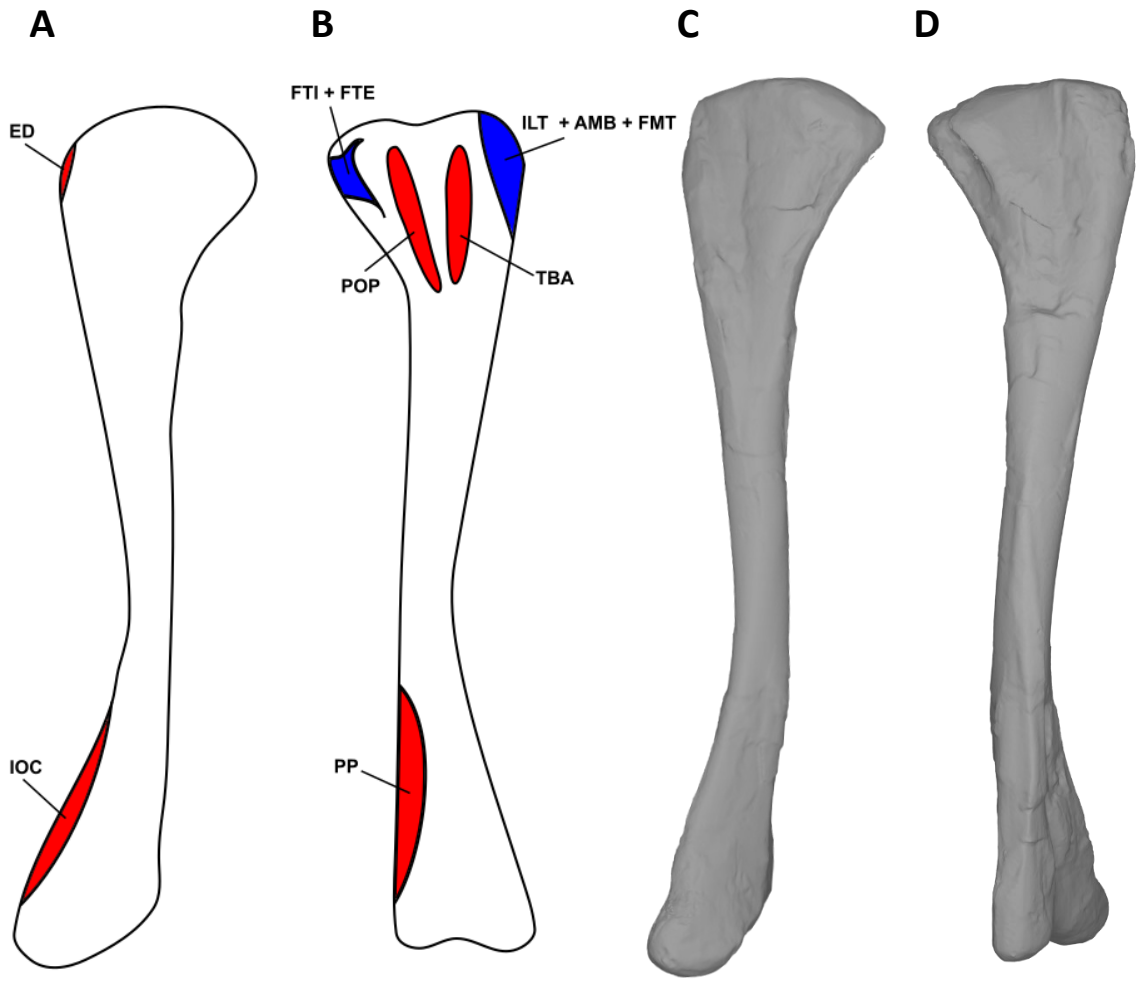

Figure 25. Myological reconstructions and scans of the left tibia of *Stegoceras validum*. (A) Lateral reconstruction, (B) medial reconstruction, (C) lateral scan, and (D) medial scan. Areas of red indicate muscle origins. Areas of blue indicate muscle insertions. Abbreviations: AMB - ambiens, ED - extensor digitorum, FMT - femorotibialis, FTE - flexor tibialis externus, FTI - flexor tibialis internus, ILT - iliotibialis, IOC - interosseus cruris, POP - popliteus, PP - pronator profundus, TBA - tibialis anterior.

Iliofibularis (ILF). The presence and structure of the iliofibularis is consistent across the EPB (Dilkes, 2000; Carrano & Hutchinson, 2002; Otero & Vizcíno, 2008; Maidment & Barrett, 2011; Ibiricu *et al*., 2018; Voegele *et al*., 2021). It attaches to the dorsolateral margin of the postacetabular process of the ilium in extant archosaurs

(Maidment & Barrett, 2011; Piechowski & Talanda, 2020, Voegele *et al*., 2021). This same morphology has been reconstructed over a wide variety of dinosaur taxa (Dilkes, 2000; Maidment & Barrett, 2011; Ibiricu *et al*., 2018; Klinkhamer *et al*., 2018; Piechowski & Talanda, 2020; Voegele *et al*., 2021). The entire length of the dorsolateral margin of the postacetabular process of UALVP 2 displays parallel linear striations which likely correspond to the origin of the ILF. As such, the ILF is reconstructed here as attaching to the lateral surface of the postacetabular process, anterior to the iliocaudalis, in *S. validum*, a level 1 inference (Figure 22).

The insertion site of the ILF is found on the lateral aspect of the proximal fibula in archosaurs (Dilkes, 2000; Carrano & Hutchinson, 2002; Dzik, 2003; Otero & Vizcaíno, 2008; Fechner, 2009; Maidment & Barrett, 2011; Schachner *et al*., 2011; Ibiricu *et al*., 2018; Piechowski & Talanda, 2020; Voegele *et al*., 2021). The anterolateral surface of the left fibula of UALVP 2 is heavily rugose and is attributed to this insertion as a level 1 inference in *S. validum* (Figure 26). This muscle would have acted to abduct the hip (Schachner *et al*., 2011; Piechowski & Talanda, 2020).

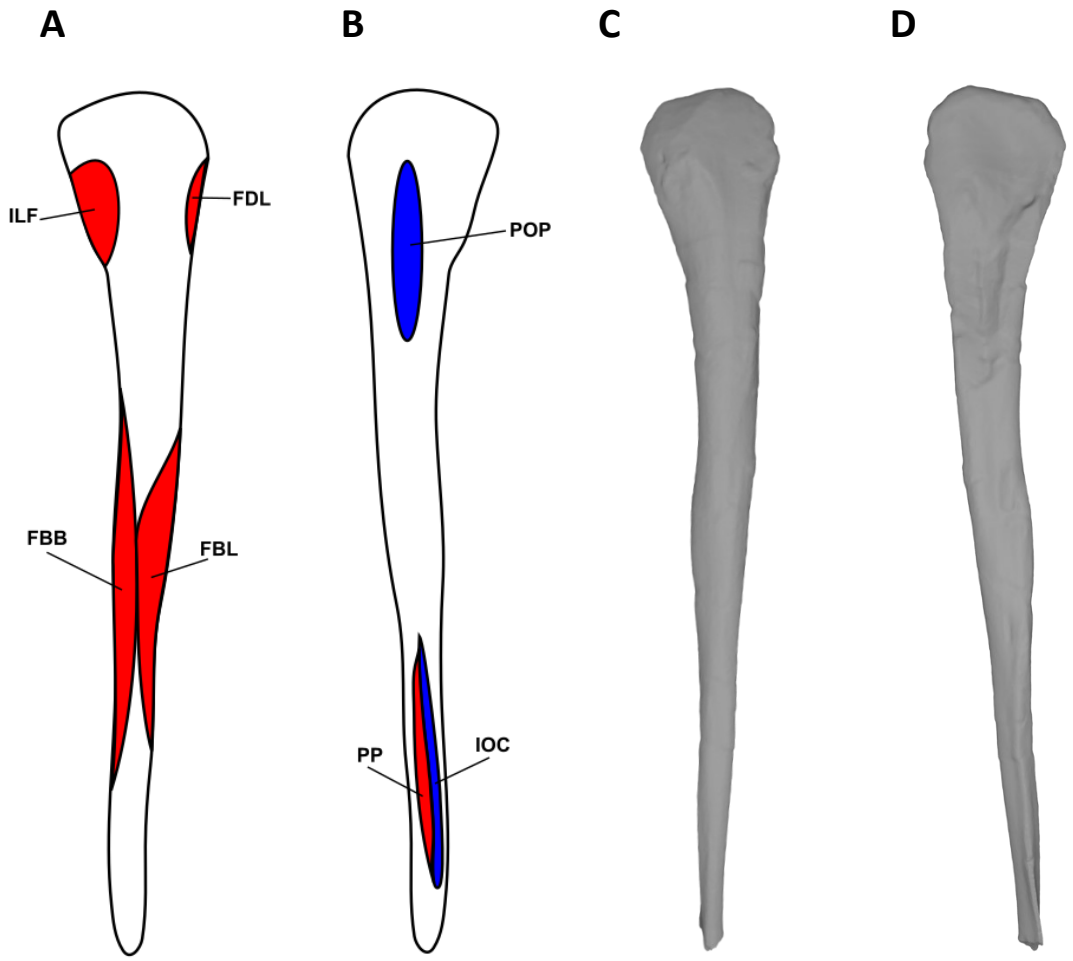

Figure 26. Myological reconstructions of the left fibula of *Stegoceras validum*. (A) Lateral reconstruction, (B) medial reconstruction, (C) lateral scan, and (D) medial scan. Areas of red indicate muscle origins. Areas of blue indicate muscle insertions. Abbreviations: FBB - fibularis brevis, FBL - fibularis longus, FDL - flexor digitorum longus, ILF - iliofibularis, IOC - interosseus cruris, POP - popliteus, PP - pronator profundus.

Flexor tibialis internus (FTI). The flexor tibialis internus is present in EPB taxa but the number of heads varies from four in crocodilians to just one in birds (Maidment & Barrett, 2011). FTI 1 is present in turtles, lepidosaurs, and crocodiles, but appears to have been lost in birds (Hutchinson, 2001; Maidment & Barrett, 2011). FTI 2 is only

present in crocodilians and has no avian homologue, and so it is likely that this represents a crocodilian autapomorphy (Hutchinson, 2001; Maidment & Barret, 2011). FTI 3 and 4 of crocodilians are suggested to be homologous to the flexor cruris medialis in birds and the FTI 2 of turtles and lepidosaurs (Hutchinson, 2001; Maidment & Barrett, 2011). FTI 4, however, has no osteological attachments and so cannot be confirmed in fossil taxa (Romer, 1923; Maidment & Barrett, 2011). Given the confusing phylogenetic origins of the FTI heads, only one head homologous to the FTI 3 of crocodilians will be considered here, as it is present in all modern taxa. This head originates on the proximolateral ischium in crocodilians and on the distal end of the ischium in birds (George & Berger, 1966; Gangl *et al*., 2004; Maidment & Barrett, 2011). It has been proposed that the FTI 3 of basal archosaurs originated on the ischial tuberosity near its attachment in crocodilians (Hutchinson, 2001; Maidment & Barrett, 2011), a direct osteological correlate on the lateral ischium just distal to the iliac peduncle. This area displays a heavy rugose texture in UALVP 2 and is inferred as the origin for the FTI 3 in *S. validum*, a level 1' inference (Figure 23).

The FTI musculature shares a tendinous insertion on the proximal posteromedial surface of the tibia with the flexor tibialis externus in the EPB (Schachner *et al*., 2011; Piechowski & Talanda, 2020; Voegele *et al*., 2021). This area displays a mildly striated texture on the tibia of UALVP 2, which is attributed here as a level 1 inference to the attachment of this tendon in *S. validum* (Figure 25). With such a morphology, the FTI musculature would have adducted and extended the hip, and flexed the knee (Schachner *et al*., 2011; Piechowski & Talanda, 2020).

Flexor tibialis externus (FTE). The attachment sites of the FTE are unequivocal in dinosaurs based on the EPB. It originates on the posterior margin of the lateral face of the postacetabular process in these animals and has been reconstructed as such in many dinosaurs (Dilkes, 2000; Carrano & Hutchinson, 2002; Maidment and Barret, 2011, Ibiricu *et al*., 2018; Piechowski & Talanda, 2020; Voegele *et al*., 2021). As stated above, the lateral surface of the postacetabular process of the ilium in UALVP 2 displays prominent striations over its entire length. There is no obvious way of discerning exactly which area of these striations is associated with the FTE versus the ILF or ILC, so the FTE is reconstructed here posterior and ventral to the ILF, as it is in crocodilians and *Silesaurus*, a level 1 inference (Figure 22) (Romer, 1923; George and Berger, 1966; Gangl et al. 2004; Schachner et al. 2011; Piechowski & Talanda, 2020).

As discussed above, the FTE would have shared a tendinous insertion with the FTI musculature on the proximal posteromedial surface of the tibia in *S. validum* (Figure 25). This muscle would have flexed the knee and extended and adducted the hip along with the FTI musculature (Schachner *et al*., 2011; Piechowski & Talanda, 2020).

Caudofemoralis brevis (CFB). In crocodilians and birds, the CFB originates on the ventral aspect of the lateral surface of the postacetabular blade (Romer, 1923; George & Berger, 1966; Gangl *et al*., 2004; Maidment & Barrett, 2011). This area of the ilium of UALVP 2 shows faint striations and is attributed to the attachment of the CFB, a level 1 inference, ventral to the ILF and anterior to the FTE (Figure 22).

The CFB of both EPB taxa inserts on the lateral surface of the fourth trochanter (Maidment & Barrett, 2011; Piechowski & Talanda, 2020; Voegele *et al*., 2021). There is no distinct texturing on this surface in UALVP 2. However, since the fourth trochanter is a direct osteological correlate to the CFB in archosaurs, it likely still served as its insertion site in *S. validum*, a level 1 inference (Figure 24). This muscle would have extended and adducted the hip (Schachner *et al*., 2011; Piechowski & Talanda, 2020)

Caudofemoralis longus (CFL). The caudofemoralis longus originates on the lateral surfaces of the caudal vertebrae in crocodilians and the base of the pygostyle in birds (Romer, 1923; George & Berger, 1966; Maidment & Barrett, 2011; Piechowski & Talanda, 2020; Voegele *et al*., 2021). Non-avian dinosaurs are usually reconstructed with the crocodilian condition, because the presence of a pygostyle is unique to birds (Maidment & Barrett, 2011; Piechowski & Talanda, 2020; Voegele *et al*., 2021). The preserved caudal centra of UALVP 2 display faint striations on their lateral surfaces, which likely correspond to the origin of the CFL, a level 1' inference.

The CFL inserts in a rugose pit medial to the proximal fourth trochanter in the EPB (Romer, 1923; George & Berger, 1966; Maidment & Barrett, 2011; Piechowski & Talanda, 2020; Voegele *et al*., 2021). This feature is present in UALVP 2, and so the CFL is reconstructed as inserting in this area, a level 1 inference (Figure 24). With such a morphology the CFB would have extended and adducted the hip along with the CFB (Schachner *et al*., 2011; Piechowski & Talanda, 2020).

Adductores femores (ADF). There are two ADFs unequivocally present in the EPB, although, their origin locations are equivocal (Dilkes, 2000; Carrano & Hutchinson, 2002; Otero & Vizcaíno; 2008 Maidment & Barrett, 2011; Voegele *et al*., 2021). In crocodilians, ADF 1 originates on the dorsolateral surface of the ischial shaft and ADF 2 originates on its ventrolateral surface, surrounding the PIFE 3 and ISC (Romer, 1023; Maidment & Barrett, 2011). In birds, origins are found on the lateral ischium, anterior pubis, and ilioischiadic membrane (George & Berger, 1966; Gangl *et al*., 2004; Maidment & Barrett, 2011). Because birds lack a PIFE 3, the origins of the ADF 1 and ADF 2 are found adjacent to each other on the ischium (Hutchinson, 2001; Maidment & Barrett, 2011). In UALVP 2, there are minor striations found dorsal and ventral to the ridge attributed as the origin of the PIFE 3. These are attributed to the origins of ADF 1 and ADF 2, a level 1' inference, based on the condition observed in the EPB (Figure 23).

ADF 1 and 2 insert together on the posterior surface of the femoral shaft in the EPB (Romer, 1923; Fechner, 2009; Maidment and Barrett, 2011; Piechowksi & Talanda, 2020), although their exact insertion is variable. In ornithischian dinosaurs, such as *Hypsilophodon*, *Dysalotosaurus*, *Kentrosaurus*, *Barilium*, and *Mantellisaurus*, there are clear muscle scars along the linea intermuscularis caudalis dorsal to the lateral femoral condyle which are attributed to the ADF musculature (Maidment & Barrett, 2011). Piechowski & Talanda (2020) place this attachment slightly more medial between the lateral and distal condyles based on scarring observed in the dinosauriform *Silesaurus*. In UALVP 2, there are distinct striations between the distal condyle of the left femur which extend proximally up to roughly one third of the femoral shaft. It is therefore

assumed that the ADF musculature of *S. validum* would have inserted here in the same area proposed by Piechowski & Talanda (2020), a level 1 inference (Figure 24). These muscles would have functioned in the adduction and extension of the hip (Schachner *et al*., 2011; Piechowski & Talanda, 2020)

Ischiotrochantericus (ISTR). The ischiotrochantericus originates on the medial ischial shaft in crocodilians and on the lateral surface in birds (Romer, 1923; Dilkes, 2000; Maidment & Barrett, 2011). It is likely that the crocodilian condition is ancestral, and that the lateral migration of the ISTR in birds is a result of the loss of PIFE 3, which attaches in the same location (Romer, 1927; Romer, 1942; Maidment & Barrett, 2011). There are no obvious scar textures preserved on the medial ischial shaft of UALVP 2, however, there is a smooth, distinct ridge on its dorsomedial surface. A similar ridge is reported in *Dreadnoughtus* (Voegele *et al*., 2021) and is recognized as the origin of the ISTR. This ridge is also attributed here as the origin site of the ISTR in *S. validum*, a level 1' inference (Figure 23).

The ISTR of crocodilians inserts on the proximolateral face of the femur, just distal to the insertion of the PIFE complex (Romer, 1923; Maidment & Barrett, 2011). In birds, it inserts on the trochanteric crest of the femur (Hutchinson, 2001; Maidment & Barrett, 2011). In dinosaurs and basal archosaurs, this attachment may be found on either the proximal posterolateral surface of the femur, as in crocodiles, or on the greater and lesser trochanters, which are homologous to the trochanteric crest of birds. Both conditions have been previously reconstructed (Otero & Vizcaíno, 2008; Maidment & Barrett, 2011; Piechowski & Talanda, 2020; Voegele *et al*., 2021). Without any

definitive osteological correlates in these regions of the femora of UALVP 2, the insertion of the ISTR is tentatively reconstructed here just distal to the insertion of the PIFE complex as in crocodilians, a level 1' inference (Figure 24). This muscle would have acted to supinate and retract the hip (Schachner *et al*., 2011; Piechowski & Talanda, 2020).

Ambiens (AMB). The ambiens is unequivocal in archosaurs but its number of divisions varies in the EPB. Crocodilians possess a two-headed AMB, a unique condition among modern reptiles, while birds display only a single head (Romer, 1923; Romer, 1927; George & Berger, 1966; Hutchinson, 2001; Maidment & Barrett, 2011; Voegele *et al*., 2021). In crocodilians, the muscle originates proximomedially on the pubis; it originates anteriorly in birds (Romer, 1923; George & Berger, 1966; Maidment & Barrett, 2011). Since a two-headed AMB is an autapomorphy of crocodilians, its is likely that dinosaurs had a single-headed AMB. It is thought that basal archosaurs would have had an AMB attachment on the proximoanterior pubic tubercle (Romer, 1956; Walker, 1977; Hutchinson, 2001; Maidment & Barrett), a direct osteological correlate for this muscle. However, since ornithischians display a retroverted pubis, the pubic tubercle is located ventrally on the pubis (Hutchinson, 2001; Maidment & Barrett, 2011). Given the drastic change of this attachment site, it is unlikely that the AMB still attached to it in ornithischians, such as *Stegoceras*. It has been hypothesized that the AMB instead arises from the prepubis in ornithischians, which is supported by osteological correlates found in *Heterodontosaurus* and *Hypsilophodon* (Galton, 1969; Santa-Luca *et al*., 1976; Maidment & Barrett, 2011). Although the pubis of UALVP 2 is not preserved, it is

unlikely that the AMB still attached to the pubic tubercle due to the retroversion of the pubis and its extreme reduction in other pachycephalosaurs (Chapter 2; Maryańska *et al*., 2004). As such, the AMB of *S. validum* is tentatively reconstructed here as originating from the proximolateral prepubis, a level 2 inference, as it did in *Hypsilophodon* and *Heterodontosaurus*. Given that the pubis and prepubis of pachycephalosaurs are both highly reduced (Maryańska *et al*., 2004), it is likely that muscles which attached to it, such as the AMB, would have been reduced as well.

The ambiens would have shared a tendinous insertion with the femorotibialis and iliotibialis musculature as described above (Figure 25).

Hindlimb Musculature

Femorotibiales (FMT). The FMT musculature is unequivocal in archosaurs, however, the number of heads differs in the EPB (Romer, 1923; Maidment & Barrett, 2011; Piechowski & Talanda, 2020). Crocodilians possess two heads, the femorotibialis externus (FMTE) and the femorotibialis internus (FMTI) (Romer, 1923; Maidment & Barrett, 2011). The FMTE originates on the posteromedial femoral shaft between the adductors and fourth trochanter, and the FMTI originates over most of the anterior and medial femoral shaft. Birds possess an additional head, the femorotibialis medius (FMTM) (Romer, 1923; Maidment & Barrett, 2011). The avian FMTE originates on the posterolateral femoral shaft, the FMTI originates on the posteroventral aspect of the shaft, and the FMTM originates on the anterior and medial surfaces of the shaft (Maidment & Barrett, 2011). In both birds and crocodilians, these muscles are clearly

separated from each other by intermuscular lines (Maidment & Barrett, 2011; Piechowski & Talanda, 2020). The femora of UALVP 2 display an intermuscular line on their posterior surfaces, extending proximally and distally from the fourth trochanter, which would have mediolaterally divided the FMT musculature. A ridge dividing the medial and lateral aspects of the anterior shaft is also present. As such, it is proposed here that there were only two heads of the FMT in *S. validum*; the femorotibialis lateralis (FMTL), which occupied the lateral surfaces of the anterior and posterior femoral shaft, and the femorotibialis medialis (FMTML), which occupied the medial surfaces of the anterior and posterior femoral shaft (Figure 24). This is a level 1' inference.

As discussed above, the FMT complex would have shared a single tendinous insertion with the ambiens and iliotibialis on the cnemial crest of *S. validum* (Figure 25).

Gastrocnemii (GSC). The EPB displays at least two divisions of the gastrocnemius, the gastrocnemius lateralis (GSCL), which originates from the posteromedial aspect of the lateral condyle of the femur, and the gastrocnemius medialis (GSCM), which originates from the medial surface of the proximal tibia (Hutchinson, 2002; Fechner, 2009; Schachner, 2011; Piechowski & Jalanda, 2020; Voegele *et al*., 2021). Birds possess a third division, the gastrocnemius intermedialis (GSCI), which originates on the posteromedial aspect of the medial femoral condyle (Piechowski & Talanda, 2020). Both femora of UALVP 2 display highly rugose texturing on their distal condyles, supporting the presence of the GSCL and the GSCI. Their attachments are proposed to originate on

the posteromedial aspects of the femoral condyles in *S. validum*, a level 1 inference (Figure 24).

The gastrocnemius musculature shares common tendinous insertions on the ventral surfaces of metatarsals II-IV in the EPB (Gadow, 1882; Hudson et al. 1959; McGowan, 1979; Nickel et al. 2003; Gangl et al. 2004; Fechner, 2009; Schachner et al. 2011; Piechowski & Talanda, 2020). These elements are preserved in UALVP 2 and display rugose texturing on their proximoventral surfaces. This scarring is attributed here to the insertions of the gastrocnemius tendons in *S. validum*, a level 1 inference (Figure 27). With such a morphology, the gastrocnemius would have extended the ankle and flexed the knee (Schachner *et al*., 2011; Piechowski & Talanda, 2020).

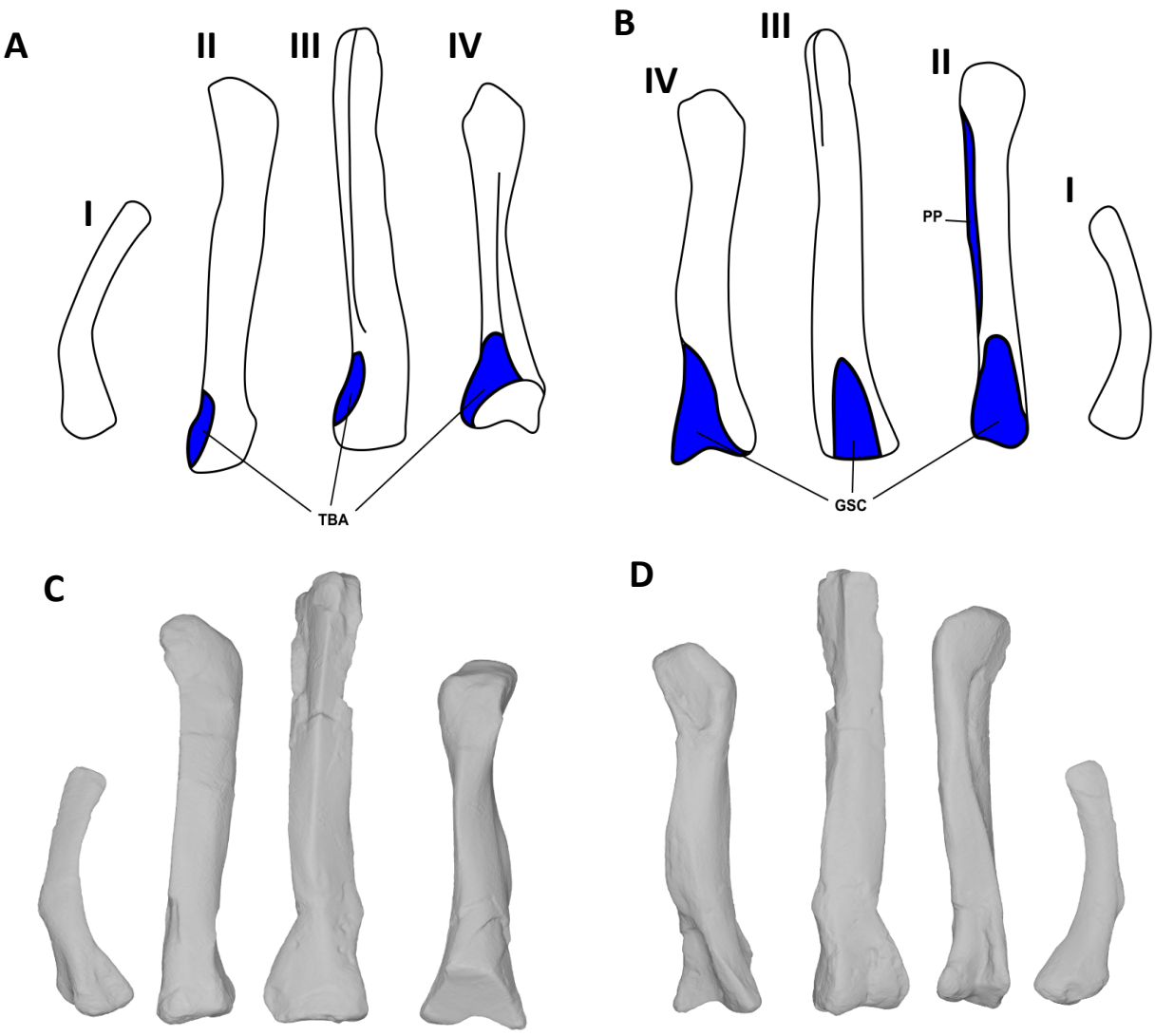

Figure 27. Myological reconstructions and scans of the left Metatarsals I-IV of *Stegoceras validum*. (A) Dorsal reconstruction, (B) ventral reconstruction, (C) dorsal scan, and (D) ventral scan. Areas of blue indicate muscle insertions. Abbreviations: GSC - gastrocnemius, PP - pronator profundus, TBA - tibialis anterior.

Fibularis (FB). The presence of the fibularis is unequivocal in dinosaurs, however, its area of origin is equivocal. Crocodilians possess both a fibularis longus (FBL) and a fibularis brevis (FBB) attaching to the lateral fibular shaft, with the former posterior to the latter. Because birds have a highly reduced and fused fibula, the FBL has migrated

and attaches to the cristae of the tibia (Fechner, 2009; Schachner et al. 2011; Piechowski & Talanda, 2020). Because the tibia possesses no such structures in UALVP 2, and the fibula is not heavily reduced, it is likely that *S. validum* displayed the crocodilian origins of the FB musculature, a level 1' inference. Additionally, faint striations are visible on the antero- and posterolateral shaft of the left fibula of UALVP 2, which likely correspond to the FBB and FBL, respectively (Figure 26).

These muscles insert on the ventral calcaneum and distoventral metatarsal V in the EPB (Piechowski & Talanda, 2020). Neither of these elements are preserved in UALVP 2, and so the FBL is tentatively reconstructed here as attaching to the ventral calcaneum, while the FBB is reconstructed as attaching to the distoventral surface of metatarsal V based on EPB comparisons, a level 1 inference. These muscles would have acted to flex the ankle (Schachner *et al*., 2011; Piechowski & Talanda, 2020).

Extensor digitorum (ED). The origin of the extensor digitorum longus is equivocal in dinosaurs, based on the EPB (Dilkes, 2000; Carrano & Hutchinson, 2002; Ibiricu *et al*., 2018; Piechowski & Talanda, 2020; Voegele *et al*., 2021). In crocodilians, the origin is found on the lateral aspect of the lateral distal condyle of the femur (Dilkes, 2000; Carrano & Hitchinson, 2002; Voegele *et al*., 2021). In birds, it is found on the anterior surface of the cnemial crest (Dilkes, 2000; Carrano & Hitchinson, 2002; Piechowski & Talanda, 2020). The lateral condyles of the femora of UALVP 2 both display heavy rugose texturing on their lateral surfaces, however, the cnemial crest of the tibia also displays a striated texture on its anterior surface. There is no way of distinguishing which of these osteological correlates corresponds to the origin of the EDL. As such, the

origin is tentatively reconstructed here as originating from both areas, a level 1' inference, as in the reconstructions of Dilkes (2000), Carrano & Hutchinson (2002), and Voegele *et al*. (2021) (Figures 24 & 25). It is most likely that the EDL would have had only one of these origins, but without more data, it is impossible to determine which is more likely. The extensor digitorum brevis (EDB) originates from the dorsal surface of the proximal tarsals in crocodilians and is fused with the EDL in birds (Hutchinson & Garcia, 2002; Piechowski & Talanda, 2020). Since the tarsals are not preserved in UALVP 2, it is tentatively reconstructed as a level 1' inference originating from the same location as crocodilians in *S. validum*, as birds possess a highly modified tibiotarsus and pes.

Whether these muscles shared insertions on the dorsal unguals and phalanges or had individual insertions in *S. validum* is impossible to know, as these elements are not preserved in UALVP 2. However, it is likely that these muscles both inserted somewhere on these elements because they do in both crocodilians and birds (Gadow, 1882; Hudson et al. 1959; McGowan, 1979; Tarsitano, 1981; Vanden Berge and Zweers, 1993; Carrano and Hutchinson, 2002; Nickel et al. 2003; Fechner, 2009; Schachner et al. 2011; Piechowski & Talanda, 2020). With such a morphology, both muscles would have acted to extend the digits of the pes (Schachner *et al*., 2011; Piechowski & Talanda, 2020).

Flexor digitorum longus (FDL). The origins of the flexor digitorum longus are equivocal in dinosaurs based on the EPB, however, osteological correlates for this muscle are consistently found on the posterolateral aspect of the lateral femoral condyle (Carrano & Hutchinson, 2002; Dilkes, 2000; Klinkhamer et al., 2017; Ibiricu *et al*., 2018; Piechowski & Talanda, 2020; Voegele *et al*., 2021). The femora of UALVP 2 also

display a distinct rugose scarring on the lateral aspect of the lateral condyles. *S. validum* is therefore reconstructed as having an origin for the FDL in this location (Figure 24). The fibular origin of the FDL is lost in birds as a result of their highly modified tibiotarsus. In crocodilians, this origin is found on the posterolateral surface of the proximal fibula (Piechowski & Talanda, 2020). There is a striated texture on this region of the left fibula of UALVP 2, which likely corresponds to the origin of the FDL. As such, *S. validum* is reconstructed here as possessing a fibular head of the FDL originating from the proximal posteromedial surface of the fibula, a level 1' inference (Figure 26).

The insertion of the FDL occurs on the ventral unguals and phalanges II-IV in the EPB (Hudson et al. 1959; Kriegler, 1961; McGowan, 1979; Tarsitano, 1981; Dilkes, 2000; Nickel et al. 2003; Gangl et al. 2004; Fechner, 2009; Schachner et al. 2011; Piechowski & Talanda, 2020). Because these elements are not present in UALVP 2, FDL insertions are assumed to be the same in *S. validum* as they are in the EPB, a level 1 inference. This muscle would have acted to extend the ankle and flex the pedal digits (Schachner *et al*., 2011; Piechowski & Talanda, 2020).

Popliteus (POP). The origin of the popliteus on the tibia is somewhat variable in the EPB, but the muscle generally originates from the proximal lateral surface of the cnemial pocket (Carrano & Hutchinson, 2002; Piechowski & Talanda, 2020; Voegele *et al*., 2021). This area also gives rise to the tibialis anterior, which is generally found anterior to the POP attachment (Piechowski & Talanda, 2020). UALVP 2 displays subtle striations across this entire region. As such, striations on the anterior side of the cnemial

pocket are attributed to the origin of the tibialis anterior whereas the posterior striations are attributed as a level 1' inference to the POP (Figure 25).

The insertion of the POP is found on the proximal medial surface of the fibula in archosaurs and is often denoted by a scarred concavity (Harris, 2007; Canudo *et al*., 2008; RoyoTorres *et al*., 2012; Piechowski & Talanda, 2020). The left fibula of UALVP 2 has been taphonomically mediolaterally flattened and displays no such concavity, but it is present in the right fibula. As such, the POP is reconstructed here as having a fibular insertion in this cavity of the fibula in *S. validum*, a level 1 inference (Figure 26). This muscle would have acted to rotate the fibula (Schachner *et al*., 2011; Piechowski & Talanda, 2020).

Tibialis anterior (TBA). As previously discussed, the TBA originates from the anterior aspect of the cnemial pocket of the tibia in *S. validum*, based on the condition observed in the EPB and osteological correlates on the tibia of UALVP 2 (Figure 25). This is a level 1 inference.

The TBA inserts on the proximolateral surfaces of metatarsals II-IV in the EPB (Hudson *et al*. 1959; McGowan, 1979; Dilkes, 2000; Nickel et al. 2003; Gangl et al. 2004; Fechner, 2009; Schachner et al. 2011; Piechowski & Talanda, 2020). Faint striations are present on these surfaces of the metatarsals of UALVP 2. As such, the TBA is reconstructed here as inserting on the proximolateral surfaces of metatarsals II-IV in *S. validum*, a level 1 inference (Figure 27). This muscle would have acted to flex the ankle (Schachner *et al*., 2011; Piechowski & Talanda, 2020).

Interosseus cruris (IOC). The presence of the IOC is unequivocal in dinosaurs, based on the EPB. The muscle originates from the lateral tibia and attaches to the distomedial fibula (Gadow, 1882; Kriegler, 1961; Vanden Berge and Zweers, 1993; Carrano and Hutchinson, 2002; Hutchinson and Garcia, 2002; Fechner, 2009; Piechowski & Talanda, 2020). The tibia of UALVP 2 displays striations on its distal anterolateral surface, which are attributed here as a level 1 inference to the tibial origin of the IOC in *S. validum* (Figure 25). Distinct rugose ridges also occur on the distomedial fibular surfaces of UALVP 2, which likely correspond to the insertion of the IOC (Figure 26). This muscle would have acted to flex the ankle (Piechowski & Talanda, 2020).

Pronator profundus (PP). The pronator profundus is unequivocally present in dinosaurs, however, its number of divisions is equivocal (Gadow 1882; Tarsitano, 1981; Hutchinson and Garcia, 2002; Fechner, 2009; Piechowski & Talanda, 2020). Crocodilians possess both a tibial and fibular head; birds possess only a tibial head because the fibula has been drastically reduced and fused to the tibiotarsus (Gadow 1882; Tarsitano, 1981; Hutchinson and Garcia, 2002; Fechner, 2009; Piechowski & Talanda, 2020). In crocodilians, the tibial head of the PP originates from the distal half of the posteromedial surface of the tibia (Piechowski & Talanda, 2020). There are notable striations on this surface in UALVP 2, which are attributed here to the origin of the PP, a level 1 inference (Figure 25). The fibular origin of the PP is located on the distal posteromedial surface of the fibular shaft posterior to the IOC in crocodilians and is often marked by scarring or a small ridge (Gadow 1882; Tarsitano, 1981; Hutchinson and Garcia, 2002; Fechner, 2009; Piechowski & Talanda, 2020). Such a ridge is present on

both fibulae of UALVP 2, however, it has slightly shifted to the anteromedial surface of the fibula. The posterior aspect of this ridge is attributed here to the fibular origin of the PP in *S. validum*, a level 2 inference (Figure 26).

The PP inserts on the ventromedial surface of metatarsals I and II in extant archosaurs (Gadow, 1882; Kriegler, 1961; Fechner, 2009; Piechowski & Talanda, 2020). Metatarsal I of UALVP 2 is somewhat reduced and displays no osteological correlates of the pronator profundus. Metatarsal II, however, displays a rugose texture on its ventromedial surface which is attributed here as a level 1 inference to the insertion of the pronator profundus in *S. validum* (Figure 27). Such a morphology would have resulted in a muscle which flexed the ankle (Piechowski & Talanda, 2020).

Discussion

Pectoral and forelimb musculature

The pectoral and forelimb myology of pachycephalosaurs is generally unremarkable. All muscles present in modern archosaurs which were presumably also present in dinosaurs display osteological correlates at the expected areas. Differences between *S. validum* and the EPB are easily accounted for by large scale morphological differences. For example, the bipedal stance of pachycephalosaurs means that their forelimbs did not need to support their body weight. The bipedal stance of pachycephalosaurs differs significantly from the quadrupedal stance of crocodilians. Additionally, the avian forelimb has been highly modified for flight in most taxa, but pachycephalosaurs possess no such modifications (Romer, 1923; Meers, 2003; Jasinoski

et al., 2006; Maidment & Barrett, 2011; Burch, 2014). When comparing *S. validum* to other bipedal dinosaurs, several slight differences become apparent (Langer *et al*., 2007; Maidment & Barrett, 2011; Burch, 2014). For example, basal saurischians exhibit a larger deltopectoral crest than pachycephalosaurs and ornithischians in general, resulting in a longer moment arm for the supracoracoideus and a larger insertion area for the deltoideus clavicularis (Langer *et al*., 2007; Burch, 2014). This would have resulted in a greater capacity for protraction and abduction of the humerus in saurischians. When compared to other ornithischians, the deltopectoral crest of pachycephalosaurs is also diminutive (Gilmore, 1924; Dilkes, 2000; Maidment & Barrett, 2011). This is likely because pachycephalosaurs are bipedal and have much reduced forelimbs. As a result, the forelimb musculature attaching to the deltopectoral crest would not have needed to be as robust as in quadrupedal ornithischians. Basal theropods also display a longer scapular blade than pachycephalosaurs, providing a more distal attachment area for the deltoideus scapularis (Burch, 2014). This along with a more distal insertion of the latissimus dorsi on the humerus results in stronger humeral extension in basal theropods, which likely aided in hunting and catching prey (Burch, 2014). Since pachycephalosaurs were herbivorous dinosaurs, such adaptations would be unnecessary. Pachycephalosaurs also display a more slender scapula than most other ornithischians (Gilmore, 1924; Maidment & Barrett, 2011), which display a broad and robust scapular blade. This is likely due to pachycephalosaurs being relatively small, bipedal dinosaurs. As they did not use their forelimbs for locomotion, they did not need well-developed pectoral muscles. The rest of the forelimb musculature of

pachycephalosaurs is quite similar to other bipedal dinosaurs (Jasinoski *et al*., 2006; Langer *et al*., 2007; Maidment & Barrett, 2011; Burch, 2014), and likely functioned in grasping and manipulating small food items.

Pelvic and hindlimb musculature

Pachycephalosaurs display several odd modifications of the pelvis and hindlimb which likely affected their appendicular musculature. As described above, pachycephalosaurs are unique among dinosaurs in having a transversely wide pelvis (Maidment & Barrett, 2014). This would have increased the available volume for the pelvic musculature and contributed to a wider gate. Such morphologies may have been beneficial for these animals if they indeed participated in their proposed head-butting or flank-butting behaviour (Colbert, 1955; Galton, 1970a; Sues, 1978; Bakker *et al*., 2006; Snively & Cox, 2008; Lehman, 2010; Longrich *et al*., 2010; Snively & Theodor, 2011; Peterson *et al*., 2013). The wider gate and stronger pelvis would have given pachycephalosaurs a more stable stance to stay upright during such competitions. Pachycephalosaurs also possess the unique medial iliac flange. The dorsal aspect of the flange displays distinct striations which are continuous with those present across the entire dorsal margin of the ilium and attributed to the ILT. Given that the flange is unique to pachycephalosaurs, it is difficult to determine what may have attached to it. No other muscle attaches to a similar area of the ilium in the EPB. It is perhaps possible that the medial flange represented an attachment site for a muscle unique to pachycephalosaurs, however, this is impossible to determine with any accuracy as there is no extant or extinct point of comparison. It may have also served as an attachment

site for various sacro-iliac ligaments, but this is speculative and is again difficult to determine without similar structures for comparison in the EPB.

The preacetabular process of the ilium of pachycephalosaurs also displays an odd morphology among dinosaurs. It is distally and transversely broadened, dorsoventrally flattened somewhat like those of anylosaurs and ceratopsids (Carpenter *et al*., 2013; Carpenter & Cifelli, 2016), laterally deflected, and has minimal lateral surface area for the attachment of the PIFI 1 (Maryańska & Osmólska, 1974; Maryańska *et al*., 2004). Such a reduced attachment area would indicate a reduced PIFI 1, and therefore its function in abducting and extending the femur would be diminished. However, its insertion surrounding the fourth trochanter is located quite distally in UALVP 2. This would create a higher leverage system and possibly compensate for the reduction in muscle mass.

A second odd morphology of the pachycephalosaur pelvis is the extreme reduction of the pubis (Maryańska *et al*., 2004). Although the pubis of *S. validum* is not preserved, this character is observable in pachycephalosaurs such as *Pacycephalosaurus*, CMN 22039, and *Homalocephale* (Chapter 2). Assuming that *S. validum* displayed this same condition, the reduction of the pubis would have certainly affected the muscles which attached to it. Most notably, the puboischiofemoralis externus 1 and 2 muscles, which function in the flexion and adduction of the hip (Schachner *et al*., 2011; Piechowski & Talanda, 2020), would have either been lost or relocated to the ischium in pachycephalosaurs (Galton, 1970a; Coombs, 1979; Norman, 1986; Maidment & Barrett, 2011). Because there is no definitive osteological correlate

for PIFE 1 or 2 on the ischium of UALVP 2, it is more likely that these muscles were lost in *S. validum*. As a result, their functions would have had to have been compensated for by some other structure. However, these inferences are speculative and cannot be confirmed without further examination of the pubic musculature of pachycephalosaurs. This could be accomplished in future studies by examining the preserved pubis of pachycephalosaurs such as *Pachycephalosaurus sp.* (ROM 73555) and *H. calathocercos* (MPC-D 100/1201) for osteological correlates.

Another muscle that may have been influenced by the structure of the pachycephalosaur pubis is the ambiens. The retroversion of the pubis in ornithischians would have resulted in a shift of the pubic attachment from the pubic tubercle to the proximolateral prepubis (Galton, 1969; Maryańska & Osmólska, 1974; Santa-Luca *et al*., 1976; Maidment & Barrett, 2011). It is impossible to confirm if this is the case in *S. validum* without a preserved pubis, however, since the prepubis of pachycephalosaurs does not display the same reduction as the pubis, it is likely that this structure served as the attachment site of the AMB.

A final muscle group that merits further discussion includes those muscles which attach to the posterior ilium and base of the tail. These are the caudofemoralis, iliocaudalis, and ischiocaudalis. As discussed above, the pelvis and anterior portion of the tail of pachycephalosaurs are transversely broad due to the medial iliac flange and long sacral ribs (Mayańska *et al*., 2004; Maidment & Barrett, 2011). This creates more volume for the muscles which attach in this area. These muscles were therefore likely stronger and better developed in pachycephalosaurs than other dinosaurs, resulting in

improved strength and stability of the hip and tail. The caudofemoralis musculature would have been further affected by the form and position of the fourth trochanter. As noted in the previous chapter, the position and morphology of the fourth trochanter varies in pachycephalosaurs. Individuals such as CMN 22039 and MPC-D 100/1204 (*Pr. prenes*) display a weakly pendant fourth trochanter while others display a simple non-pendant morphology. Additionally, pachycephalosaurs including *Pachycephalosaurus sp.* (ROM 73555), *H. calathocercos* (MPC-d 100/1201), and *Pr. prenes* (MPC-D 100/1204) possess a more distally positioned fourth trochanter when compared to other members of the clade. UALVP 2 displays a more distally positioned, non-pendant fourth trochanter. A proximal, pendant fourth trochanter is the basal condition among dinosaurs and basal archosaurs (Persons & Currie, 2020). It is thought that the pendant process of this structure provided a larger area of attachment for the caudofemoralis brevis in early ornithischians, resulting in a high leverage system and an increased locomotive capability of the hip (Persons & Currie, 2020). This would have supported an active foraging lifestyle as early ornithischians transitioned to herbivory (Persons & Currie, 2020). As many groups became larger, the fourth trochanter migrated distally down the femoral shaft to provide further leverage for the CFB to the point where a pendant process was no longer needed and was lost (Persons & Currie, 2020). It is also hypothesized that the pendant process of the fourth trochanter is an osteological correlate to bipedality in ornithischians (Maidment & Barrett, 2014). Bipedal ornithischians are generally smaller than their quadrupedal counterparts and would not have needed the extra leverage provided by a distal migration of the fourth trochanter

(Maidment & Barrett, 2014; Persons & Currie, 2020). As such, many retain the basal condition (Persons & Currie, 2020). Pachycephalosaurs appear to retain an intermediate condition. The position of the fourth trochanter in UALVP 2 is relatively distal compared to other pachycephalosaurs, however, it is still relatively proximal compared to larger ornithischians such as ankylosaurs (Persons & Currie, 2020). Additionally, although the fourth trochanter of *S. validum* displays a non-pendant morphology, this is not the case for pachycephalosaurs which retain a more proximally positioned fourth trochanter. These observations suggest that *S. validum* represents an intermediate stage of the distal migration of the femoral fourth trochanter in ornithischians. This would have resulted in a higher functionality of the caudofemoralis musculature in extending and adducting the hip and provided more retractive power which may have been beneficial during intraspecific combat (Schachner *et al*., 2011; Piechowski & Talanda, 2020; Persons & Currie, 2020). The improved caudofemoralis muscles may have also allowed pachycephalosaurs to compensate for the reduced PIFE musculature and provided stability to their stance.

Conclusions

By examining the appendicular skeleton of UALVP 2 for osteological correlates and comparing them to the musculature of the EPB, the appendicular myology of *S. validum* was reconstructed. Furthermore, by comparing the reconstructed myology of *S. validum* to other pachycephalosaurs and unique pachycephalosaur skeletal morphologies, conclusions were made about the functionality of several of these previously mysterious structures. The medial iliac flange of pachycephalosaurs remains

enigmatic, however, it is certain that some muscle or ligaments attached to its dorsal surface based on observable scarring. Unfortunately, since there are no comparable structures resembling the flange present in the EPB, it is impossible to accurately determine what exactly would have attached to its dorsal surface. The pachycephalosaur pelvis and base of the tail are transversely wide, resulting in large and strong iliocaudalis, ischiocaudalis, and caudofemoralis muscles. Additionally, a distally located femoral fourth trochanter in *S. validum* would have given more leverage to the caudofemoralis musculature, further contributing to the stability of the pelvis (Persons & Currie, 2020). Finally, the reduced pubis of pachycephalosaurs likely resulted in a significant reduction of the puboischiofemoralis externus complex (Maidment & Barrett, 2011), which would have been compensated for by the enlarged iliotibialis and the improved caudofemoralis musculature. This, however, is impossible to confirm in *S. validum* without a preserved pubis. The myology of the pectoral girdle and forelimb of *St. validum* were found to be generic and consistent with previous myological reconstructions of bipedal dinosaurs (Jasinoski *et al*., 2006; Burch, 2014).

The myological reconstruction presented here provides functional explanations for the odd postcranial adaptations of pachycephalosaurs including a transversely wide pelvis and extreme reduction of the pubis. However, additional myological studies of pachycephalosaurs are required to confirm if the conditions observed in *S. validum* are consistent across the clade and if they indeed support the theorized intraspecific head-butting behaviour of these animals.

Chapter 4: Conclusions

Pachycephalosaurs are a poorly understood group of small (~2 to 3 m in length), bipedal, ornithischian dinosaurs (Maryańska *et al*., 2004). They are best known for the characteristic frontoparietal skull dome which defines the clade (Cooper, 2004; Goodwin & Horner, 2004; Maryańska *et al*., 2004). This striking feature is unique among dinosaurs and as such, it is often the focus of pachycephalosaur research (Colbert, 1955; Galton, 1970; Sues; 1978, Bakker *et al*., 2006; Snively & Cox, 2008; Lehman, 2010; Longrich *et al*., 2010; Snively & Theodor, 2011; Peterson *et al*., 2013). Not only is it an interesting structure to study, but it is also the most often preserved element of the skeleton, since it is thickened and robust while the rest of the skeleton is gracile (Snively & Theodor, 2011; Williamson & Brusatte, 2016). This has led to a biased understanding of pachycephalosaurs in the literature largely skewed towards the cranial skeleton. When examining the characters used to study the phylogenetics of pachycephalosaurs, remarkably few of them (less than 30%) relate to the postcranial skeleton (Longrich *et al*., 2010; Schott, 2011; Evans *et al*., 2013; Williamson & Brusatte; 2016). As a result, little is known about the phylogenetic signal(s) of the postcranial skeleton and whether it aligns with that of the cranial skeleton. Additionally, the postcranial skeleton of pachycephalosaurs is poorly understood functionally. It displays unique features such as a transversely broad hip and base of the tail, a pubis that is reduced and largely excluded from the acetabulum, a double ridge and groove articulation of the dorsal vertebrae, and a caudal basket of ossified tendons (Maryańska *et al*., 2004; Brown *et al*., 2012). Despite having a variety of unique characters, almost no research has been

dedicated to the pachycephalosaur postcranial skeleton and understanding the function of these features. This is largely due to the poor fossil record of pachycephalosaurs.

In this study, the problems surrounding the phylogenetics and functional morphology of pachycephalosaurs were addressed by examining the best preserved pachycephalosaur postcranial skeletons from around the world. To better understand the impact of postcranial characters on the phylogenetic relationships of pachycephalosaurs, a new postcranial pachycephalosaur skeleton (CMN 22039), which was originally identified as a juvenile *Thescelosaurus* (Russell & Manabe, 2002), was reidentified, described, and compared to all other pachycephalosaur skeletons with comparable postcranial material and relevant outgroup taxa (Gilmore, 1913, 1915, 1924; Perle *et* al., 1982; Sues & Galton, 1982; Sereno, 1987; Sereno *et al*., 1988; Maryańska *et al*., 2004; Butler & Sullivan, 2009; Brown *et al*., 2011). The observations collected by studying these specimens were then used to identify new postcranial characters of possible phylogenetic importance. In turn, these newly identified postcranial characters were added to the most recent pachycephalosaur phylogenetic character matrix (Williamson & Brusatte, 2016) to create an updated strict consensus tree and determine their impact on the evolutionary relationships of these animals. CMN 22039 was also coded into this matrix to aid in its identification and establish its phylogenetic position.

Upon re-examining CMN 22039, its taxonomic identity was reinterpreted as a juvenile pachycephalosaur. It displays pachycephalosaur synapomorphies such as: (1) a double ridge and groove articulation of the pre- and postzygapophyses of the dorsal

vertebrae; (2) a medially projecting flange on the postacetabular process of the ilium; and (3) a highly reduced pubis that barely contributes to the margin of the acetabulum (Maryańska et al., 2004). Any further identification is impossible without more material. A juvenile life stage for the animal is supported by: (1) its small size; (2) unfused neurocentral sutures of the caudal vertebrae; (3) woven bone texture of the tibia and fibula; and (4) a lack of any secondary mature osteohistological features (Francillon-Vieillot *et* al., 1990; Castanet *et al*., 2000; de Margerie *et al*., 2002; Lamm & Werning, 2013; Prieto-Márquez *et al*., 2016a; Prieto-Márquez *et al*., 2016b).

By comparing CMN 22039 to pre-existing pachycephalosaur postcranial material, new postcranial characters were discovered to vary between taxa. These were: (1) the angle of projection of the medial iliac flange, (2) the shape of the femoral fourth trochanter, and (3) the proximodistal position of the fourth trochanter along the femoral shaft. It is, however, impossible to determine if these characters vary with ontogeny or taxonomy without a larger collection of pachycephalosaur postcranial specimens for comparison.

New postcranial data from existing pachycephalosaur specimens and CMN 22039 were added to the character matrix of Williamson and Brusatte (2016) to assess the affect of postcranial characters on pachycephalosaur phylogenetic relationships. CMN 22039 was placed in a large polytomy of taxa more derived than *S. validum* and more basal to the sister-taxon pairs of *Homalocephale* and *Goyocephale*, *Acrotholus* and *Prenocephale*, and *Pachycephalosaurus* and *Alaskacephale*. As it is a young individual, CMN 22039 may well occupy a more derived position (Kluge, 1985; Barrantes &

Everhard, 2010; Carballido & Sander, 2014), but this is impossible to know without further study.

Examining the strict consensus tree of this study alongside that of Williamson and Brusatte (2016) reveals that our understanding of phylogenetic relationships of pachycephalosaurs has changed with the addition of postcranial characters. A new monophyly for *Stegoceras validum* was established, the previous sister taxon-pair of *Sphaerotholus goodwini* and *Sphaerotholus buchholtzae* has degraded into a polytomy, and *Homalocephale calthocercos* once again forms a clade with *Goyocephale latimorei*. More generally, the resolution of the pachycephalosaur phylogeny remains the same, however, isolated areas show shifts in resolution. The base of the tree displays a higher resolution and separates *Yinlong downsi* Xu *et al*., 2006 and *Wannanosaurus yansiensis* from a large polytomy into their own respective monophylies. More derived taxa such as *Foraminacephale brevis, Tylocephale gilmorei*, and *Amtocephale gobiensis*, however, have degraded into an unresolved polytomy. These results, however, must be considered with caution.

As not many pachycephalosaur postcranial skeletons are known, and those that are known are not all the same growth stage, it is difficult to determine if the new postcranial characters used in this study vary with ontogeny. Ideally, all taxa used in any phylogenetic analysis would occupy the same growth stage to eliminate differences due to ontogenetic variations. Unfortunately, this is impossible for pachycephalosaurs and most fossil taxa in general. By adding postcranial characters which may vary through ontogeny to a strict consensus analysis including taxa of different growth stages, the

observed results may not represent true phylogenetic relationships. This problem is likely accentuated by the addition of a known juvenile (CMN 22039) to the analysis. As such, the observed differences between the strict consensus analysis of this study and that of Williamson and Brusatte (2016) could very well be due to the ontogenetic variation within pachycephalosaurs available to study. This is not to say that the observed phylogenetic shifts could not also be due to true taxonomic variation, it is simply impossible to determine the cause without further study. Future osteohistological analyses on pachycephalosaurs used in similar studies to determine their exact ontogenetic ages would aid to remedy this problem. Then, specimens which vary drastically in their ontogeny could be fully accounted for.

To better understand the functional morphology of the pachycephalosaur postcranial skeleton, I performed a pachycephalosaur appendicular myological reconstruction. The appendicular myology of *S. validum* was reconstructed by examining Canada's most complete pachycephalosaur (UALVP 2) for osteological correlates and comparing them to previous dinosaur muscle reconstructions and the musculature of the extant phylogenetic bracket (EPB). Pectoral and forelimb musculature of *S. validum* was found to be generic and consistent with prior reconstructions of bipedal dinosaurs (Jasinoski *et al*., 2006; Burch, 2014).

The pelvic and hindlimb musculature of *S. validum*, to the contrary, was unusual in several aspects relating to odd pachycephalosaur skeletal morphologies. Striations were found on the dorsal surface of the medial iliac flange, however, it is still unclear as to what this scarring corresponds to. The pachycephalosaur hip is transversely broad,

creating a more stable stance and allowing for a larger pelvic muscle volume (Maidment & Barrett, 2014). Such adaptations may have been beneficial for the proposed intraspecific headbutting behaviour of these animals (Colbert, 1955; Galton, 1970a; Sues; 1978, Bakker *et al*., 2006; Snively & Cox, 2008; Lehman, 2010; Longrich *et al*., 2010; Snively & Theodor, 2011; Peterson *et al*., 2013; Maidment & Barrett, 2014).

The femoral fourth trochanter of UALVP 2 was found more distally than in other pachycephalosaurs. This structure served as the attachment site for the caudofemoralis musculature which functioned in the extension and adduction of the femur (Schachner *et al*., 2011; Piechowski & Talanda, 2020). A more distal femoral insertion for these muscles would have provided them with more leverage, further stabilizing the pachycephalosaur stance (Persons & Currie, 2020).

Although the pubis of UALVP 2 is not preserved, it can be assumed that it was highly reduced and largely excluded from the acetabulum based on the condition observed in every other preserved pachycephalosaur pubis (Maryańska *et al*., 2014). The reduced structure would have resulted in a severe reduction of the puboischiofemoralis externus complex (Maidment & Barrett, 2011), which would have been compensated for by the enlarged iliotibialis and improved caudofemoralis musculature.

Characters such as the position of the fourth trochanter along the femoral shaft, the shape of the fourth trochanter, and the projection angle of the medial iliac flange vary between individuals, however, it is still uncertain whether these variations are a

result of ontogenetic or taxonomic differences. To remedy this, more pachycephalosaur postcranial skeletons must be discovered and analyzed for comparison and existing pachycephalosaur specimens should be histologically studied to determine their exact ontogenetic stage. Pachycephalosaur phylogenetics should also continue to be studied, however, the ontogenetic age of the specimens being used should be identified and any specimens with significant ontogenetic variations from the majority should be excluded from analysis.

The myological reconstruction of *S. validum* provides insight into the function of unique pachycephalosaur appendicular skeletal adaptations but is of limited use without other reconstructions for comparison. Additional myological reconstructions of other pachycephalosaurs are needed for a broader understanding of the musculature of these animals as a clade. Furthermore, UALVP 2 does not preserve its entire appendicular skeleton. Most notably, the pubis is not preserved. By examining the appendicular skeletons of pachycephalosaurs which preserve these missing elements, the inferences made here based solely on the EPB may be further supported or opposed. Since there is limited pachycephalosaur postcranial material to work with, performing myological reconstructions of better-known bipedal dinosaurs (e.g., *Thescelosaurus*, *Parksosaurus*, and basal theropods) and comparing them to pachycephalosaurs may provide an alternative solution to aid in understanding the functional morphology of the pachycephalosaur postcranial skeleton. Studying the axial myology of pachycephalosaurs would also be beneficial to understanding their postcranial anatomy and functional morphology. By studying more of the postcranial skeleton along with the

myological reconstruction presented here for the appendicular myology of *S. validum*, a better understanding of how the different muscle systems of these animals interacted with each other may emerge. Studying axial musculature may also provide insight into the function of structures which could not be discerned by studying appendicular myology alone. For example, it is still unclear as to what muscle/ligament may have attached to the dorsal aspect of the medial iliac flange in *S. validum*. If an axial muscle were to attach here, surely studying the axial myology of pachycephalosaurs would confirm this.

Much of the uncertainty surrounding the evolution and functional morphology of the pachycephalosaur postcranial skeleton remains unresolved. This work puts forth hypotheses as to how this part of the skeleton developed and what purpose(s) it may have served. More research is still required to fully understand how these animals evolved and lived, but the results presented here provide important steps toward achieving that goal.

References

Abdala, V. Diogo, R. 2010. Comparative anatomy, homologies and evolution of the pectoral and forelimb musculature of tetrapods with special attention to extant limbed amphibians and reptiles. *Journal of Anatomy*. **217**: 536-573.

Abdala, V., Manzano, A.S., Herrel, A. 2008. The distal forelimb musculature in aquatic and terrestrial turtles: phylogeny of environmental constraints? *Journal of Anatomy*. **213**: 159-172.

Baadsgaard, H., Lerbekmo, J.F. 1980. A Rb/Sr age for the Cretaceous – Tertiary boundary (Z coal), Hell Creek, Montana. *Canadian Journal of Earth Sciences*. **17**: 671-673.

Baadsgaard, H., Lerbekmo, J.F., McDougall, I. 1987. A radiometric age for the Cretaceous – Tertiary boundary based upon K – Ar, Rb – Sr, and U – Pb ages of bentonites from Alberta, Saskatchewan, and Montana. *Canadian Journal of Earth Sciences*. **25**: 1088-1097.

Bakker, R.T., Sullivan, R.M., Porter, V., Larson, P., Saulsbury, S.J. 2006. *Dracorex hogwartsia*, N. Gen., N. SP., A Spiked, Flat-Headed Pachycephalosaurid Dinosaur from the Upper Cretaceous Hell Creek Formation of South Dakota. *Late Cretaceous Vertebrates from the Western Interior, Bulletin 35*. 331-345.

Bamforth, E.L., Button, C.L., Larsson, H.C.E. 2014. Paleoclimate estimates and fire ecology immediately prior to the end-Cretaceous mass extinction in the Frenchman Formation (66 Ma), Saskatchewan, Canada. *Palaeogeography, Palaeoclimatology, Palaeoecology*. **401**: 96-110.

Barrantes, G., Everhard, W.G. 2010. Ontogeny repeats phylogeny in *Steatoda* and *Latrodectus* spiders. *The Journal of Arachnology*. **38**: 485-494.

Baumel, J.J., Jing, A.S., Breazile, J.E., *et al*. 1993. Handbook of Avian Anatomy: Nomina Anatomica Avium, 2nd edn. *Cambridge: Nuttall Ornithological Club*. 779.

Behrensmeyer, A.K., Kidwell, S.M., Gastaldo, R.A. 2000. Taphonomy and Paleobiology. *Paleobiology*. **26**: 103-147.

Bell, P.R., Currie, P.J., Russell, D.A. 2015. Large caenagnathids (Dinosauria, Oviraptosauria) from the uppermost Cretaceous of western Canada. *Cretaceous Research*. **52**: 101-107.

Benton, M.J., Shishkin, M.A., Unwin, D.M., Kurochkin, E.N. 2003. The Age of Dinosaurs in Russia and Mongolia. *Cambridge University Press*.

Berger-Dell'Mour, H.A.E. 1983. Der Übergang von Echse zu Schleiche in der Gattung Tetradactylus Merrem. *Zoologische Jahrbücher. Abteilung für Anatomie und Ontogenie Tiere.* **110**: 1–152.

Bever, G.S., Gauthier, J.A., Wagner, G.P. 2011. Finding the frame shift: digit loss, developmental variability, and the origin of the avian hand. *Evolution and Development*. **13**: 269–279.

Borsuk-Bialynicka, M. 1977. A new camasaurid sauropod *Opisthocoelicaudia skarzynskii* gen. n., sp. n. from the Upper Cretaceous of Mongolia. *Palaeontologica Polonica*. **37**: 1-64.

Boyd, C.A., Brown, C.M., Scheetz, R.D., Clarke, J.A. 2009. Taxonomic Revision of the Basal Neornithischian Taxa *Thescelosaurus* and *Bugenasaura*. *Journal of Vertebrate Paleontology*. **29**: 758-770.

Brochu, C.A. 1996. Closure of neurocentral sutures during crocodilian ontogeny: implications for maturity assessment in fossil archosaurs. *Journal of Vertebrate Paleontology*. **16**: 49-62.

Brooks, D.R., Wiley, E.O. 1985. Theories and methods in different approaches to phylogenetic systematics. *Cladistics*. **1**: 1-11.

Brown, C.M. 2009. *Thescelosaurus* (Dinosauria: Ornithischia) and related taxa from the Late Cretaceous of Alberta and Saskatchewan. *ProQuest Dissertations Publishing*. MR54512.

Brown, C.M., Boyd, C.A., Russell, A.P., 2011. A new basal ornithopod Dinosaur (Frenchman Formation, Saskatchewan, Canada), and implications for late Maastrichtian ornithischian diversity in North America. *Zoological Journal of the Linnean Society*. **163** (4): 1157–1198.

Brown, C.M., Evans, D.C., Campione, N.E., O'Brien, L.J., Eberth, D.A. 2013. Evidence for taphonomic size bias in the Dinosaur Park Formation (Campanian, Alberta), a model Mesozoic terrestrial alluvial-paralic system. *Palaeogeography, Palaeoclimatology, Palaeoecology*. **372**: 108-122.

Brown, C.M., Russell, A. 2012. Homology and Architecture of the Caudal Basket of Pachycephalosauria (Dinosauria: Ornithischia): The First Occurrence of Myorhabdoi in Tetrapoda. *PLoS One*. **7**: e30212.

Bryant, H.N., Seymour, K.L. 1990. Observations and Comments on the Reliability of Muscle Reconstruction in Fossil Vertebrates. *Journal of Morphology*. **206**: 109-117.

Burch, S.H. 2014. Complete forelimb myology of the basal theropod dinosaur *Tawa hallae* based on a novel robust muscle reconstruction method. *Journal of Anatomy*. **225**: 271-297.

Butler, R.J., Sullivan, R.M. 2009. The Phylogenetic Position of the Ornithischian Dinosaur *Stenopelix valdensis* from the Lower Cretaceous of Germany and the Early Fossil Record of Pachycephalosauria. *Acta Palaeontologica Polonica*. **54**: 21-34.

Butler, R.J., Upchurch, P., Norman, D.B. 2008. The Phylogeny of the Ornithischian Dinosaurs. *Journal of Systematic Palaeontology*. **6**: 1-40.

Butler, R.J., Zhao, Q. 2009. The small-bodied ornithischian dinosaurs *Micropachycephalosaurus hongtuyanensis* and *Wannanosaurus yansiensis* from the Late Cretaceous of China. *Cretaceous Research*. **30**: 63-77.

Carballido, J.L., Sander, P.M. 2014. Postcranial axial skeleton of *Europasaurus holgeri* (Dinosauria, Sauropoda) from the Upper Jurassic of Germany: implication for sauropod ontogeny and phylogenetic relationships of basal Macronaria. *Journal of Systematic Palaeontology*. **12**: 335-387.

Carpenter, K., Cifelli, R.L. 2016. A possible juvenile ceratopsid ilium from the Cenomanian of central Utah, U.S.A. *Cretaceous Research*. **60**: 167-175.

Carpenter, K., DiCroce, T., Kinneer, B., Simon, R. 2013. Pelvis of *Gargoyleosaurus* (Dinosauria: Ankylosauria) and the Origin and Evolution of the Ankylosaur Pelvis. *PLoS One*. **8**: e79887.

Carrano, M.T., Hutchinson, J.R. 2002. Pelvic and Hindlimb Musculature of *Tyrannosaurus rex* (Dinosauria: Theropoda). *Journal of Morphology*. **253**: 207-228.

Castanet, J., Curry, R.K., Cubo, J., Boisard, J.J. 2000. Periosteal bone growth rates in extant ratites (ostrich and emu). Implications for assessing growth in dinosaurs. *Comptes Rendus de l'Académie des Sciences*. **323**: 543-550.

Colbert, E.H. 1955. Evolution of the vertebrates: a history of the backboned animals through time. Wiley, New York, NY. 479.

Coombs, W.P., Jr. 1978. Forelimb muscles of the Ankylosauria (Reptilia, Ornithischia). *Journal of Paleontology.* **52**: 642-657.

Coombs, W.P., Jr. 1979. Osteology and myology of the hindlimb in the Ankylosauria (Reptilia, Ornithischia). *Journal of Paleontology.* **53**: 666-684.

Cooper, J.E. 2004. Pachycephalosaur Cranial Morphology and Species Definition. *University of Alabama*.

Crawford, N.G., Parham, J.F., Sellas, A.B., Faircloth, B.C. Glenn, T.C., Papenfuss, T.J. 2015. A phylogenetic analysis of turtles. *Molecular Phylogenetics and Evolution*. **83**: 250-257.

de Margerie, E., Cubo, J., Castanet, J. 2002. Bone typology and growth rate: testing and quantifying "Amprino's rule" in the mallard (*Anas platyrhynchos*). *Comptes Rendu Biologies*. **325**: 221-230.

Curry Rogers, K. 2009. The postcranial osteology of *Rapetosaurus krausei* (Sauropoda: Titanosauria) from the Late Cretaceous of Madagascar. *Journal of Vertebrate Paleontology*. **29**: 1046-1086.

De Queiroz, K. 1985. The ontogenetic method for determining character polarity and its relevance to phylogenetic systematics. *Systematic Zoology*. **34**: 280-299.

Dieudonné, P.E., Cruzado-Caballero, P., Godefroit, P., Tortosa, T. 2020. A new phylogeny of cerapodan dinosaurs. *Historical Biology*. DOI: 10.1080/08912963.2020.1793979.

Dodson, P. 1971. Sedimentology and taphonomy of the Oldman formation (Campanian), dinosaur provincial park, Alberta, Canada. *Palaeogeography, Palaeoclimatology, Palaeoecology*. **10**: 21-74.

Dilkes, D.W. 2000. Appendicular myology of the hadrosaurian dinosaur *Maiasaura peeblesorum* from the Late Cretaceous (Campanian) of Montana. *Transactions of the Royal Society of Edinburgh: Earth Sciences*. **90**: 87-125.

Dilkes, D.W., Hutchinson, J.R., Holiday, C.M., Witmer, L.M. 2012. Reconstructing the musculature of dinosaurs. In: Brett-Surman, M.K., Holtz, T.R. Jr., Farlow, J.O. (Eds.) The complete dinosaur. Bloomington: *Indiana University Press*. 151-190.

Dodson, P. 1983. A faunal review of the Judith River (Oldman) Formation, Dinosaur Provincial Park, Alberta. *Mosasaur*. **1**: 89-118.

Dzik, J. 2003. A beaked herbivorous archosaur with dinosaur affinities from the early Late Triassic of Poland. *Journal of Vertebrate Paleontology*. **23**: 556–574.

Eberth, D.A. 2018. Stratigraphy and paleoenvironmental evolution of the dinosaur-rich Baruungoyot-Nemegt succession (Upper Cretaceous), Nemegt Basin, southern Mongolia. *Palaeogeography, Palaeoclimatology, Palaeoecology*. **494**: 29-50.

Evans, D.C., Brown, C.M., Ryan, M.J., Tsogtbaatar, K. 2011. Cranial ornamentation and ontogenetic status of *H. calathocercos* (Ornithischia: Pachycephalosauria) from the Nemegt Formation, Mongolia. *Journal of Vertebrate Paleontology*. **31**: 84-92.

Evans, D.C., Hayashi, S., Chiba, K., Watabe, M., Ryan, M.J., Lee, Y., Currie, P.J., Tsogtbaatar, K., Barsbold, R. 2018. Morphology and histology of new cranial specimens of Pachycephalosauridae (Dinosauria: Ornithischia) from the Nemegt Formation, Mongolia. *Palaeogeography, Palaeoclimatology, Palaeoecology*. **494**: 121-134.

Evans, D.C., Schott, R.K. 2012. Squamosal Ontogeny and Variation in the Pachycephalosaurian Dinosaur *S. validum* Lambe, 1902, from the Dinosaur Park Formation, Alberta. *Journal of Vertebrate Paleontology*. **32**: 903-913.

Evans, D.C., Schott, R.K., Larson, D.W., Brown, C.M., Ryan, M.J. 2013. The oldest North American pachycephalosaurid and the hidden diversity of small-bodied ornithischian dinosaurs. *Nature Communications*. DOI: 10.1038/ncomms2749.

Fastovsky, D.E., Weishampel, D.B. 1996. The Evolution and Extinction of the Dinosaurs. *Cambridge University Press*.

Fastovsky, D., Weishampel, D., Watabe, M., Barsbold, R., Tsogtbaatar, K., Narmandakh, P. 2011. A nest of Protoceratops andrewsi (Dinosauria, Ornithischia). *Journal of Paleontology*. **85**: 1035–1041.

Fechner, R. 2009. Morphofunctional evolution of the pelvic girdle and hindlimb of Dinosauromorpha on the lineage to Sauropoda. *PhD Dissertation, Fakultät für Geowissenschaften, Ludwig-MaximiliansUniversität, Munich*.

Francillon-Vieillot, H., de Buffrenil, V., Castanet, J., Géraudie, J., Meunier, F-J., Sire, J-Y., Zylbergberg, L., de Ricqlès, A. 1990. Microstructure and mineralization of vertebrate skeletal tissues. In: Carter, J.G., ed. *Skeletal Biomineralization: Patterns, Processes and Evolutionary Trends.* New York: Van Nostrand Reinhold. 471-530.

Frankel, V.H., Nordin, M. 2001. Biomechanics of bone. In: Nordin, M., Frankel, V.H. (Eds.) Basic Biomechanics of the musculoskeletal system. Baltimore: *Lippincott Williams and Wilkins*. 26-59.

Fraser, F.J., McLearn, F.H., Russell, L.S., Warren, P.S., Wickenden, R.T.D. 1935. Geology of southern Saskatchewan. *Geological Survey of Canada Memoirs*. **176**: 1–137.

Fricke, H.C., Foreman, B.Z., Sewall, J.O. 2010. Integrated climate model-oxygen isotope evidence for a North American monsoon during the Late Cretaceous. *Earth and Planetary Science Letters*. **289**: 11-21.

Furnival, G.M. 1946. Cypress Lake map-area, Saskatchewan. *Geological Survey of Canada Memoirs*. **242**: 1–161.

Gadow, H. 1882. Beiträge zur Myologie der hinteren Extremität der Reptilien. *Morphologisches Jahrbuch*. **7**: 329–466.

Galton, P.M. 1969. The pelvic musculature of the dinosaur *Hypsilophodon* (Reptilia: Ornithischia). *Postilla.* **131:** 1-64.

Galton, P.M. 1970a. Ornithischian dinosaurs and the origin of birds. *Evolution*. **24**: 448-462.

Galton, P.M. 1970b. Pachycephalosaurids – Dinosaurian Battering Rams. *Discovery*. **6**: 23–32.

Gangl, D., Weissengruber, G.E., Egerbacher, M., Forstenpointner, G. 2004. Anatomical description of the muscles of the pelvic limb in the Ostrich (*Struthio camelus*). *Anatomy, Histology, Embryology.* **33**: 100-114.

George, J.C., Berger, A.J. 1966. Avian myology. *New York: Academic Press*.

Giffin, E.B. 1989. Pachycephalosaur paleoneurology (Archosauria: Ornithischia). *Journal of Vertebrate Paleontology*. **9**: 67-77.

Gilmore, C.W. 1913. A new dinosaur from the Lance Formation of Wyoming. *Smithsonian Miscellaneous Collections*. **61**: 1-5.

Gilmore, C.W. 1915. Osteology of *Thescelosaurus*, an orthopodus dinosaur from the Lance Formation of Wyoming. *Proceedings of the United States National Museum*. **49**: 591-628.

Gilmore, C.W. 1924. On Troodon Validus: An Orthopodous Dinosaur from the Belly River Cretaceous of Alberta, Canada. *University of Alberta, Department of Geology, Bulletin No. 1*. 1-58.

Goloboff, P.A., Catalano, S.A. 2016. TNT version 1.5, including a full implementation of phylogenetic morphometrics. *Cladistics*. **32**: 221-238.

Goodwin, M. B. 1990. Morphometric landmarks of pachycephalosaurid cranial material from the Judith River Formation of northcentral Montana. Pp. 189–201 in K. Carpenter and P. Currie, eds. Dinosaur systematics: perspectives and approaches. Cambridge University Press, London.

Goodwin, M.B., Buchholtz, E.A., Johnson, R.E. 1998. Cranial anatomy and diagnosis of *Stygimoloch spinifer* (Ornithischia: Pachycephalosauria) with comments on cranial siplay structures in agonistic behavior. *Journal of Vertebrate Paleontology*. **18**: 363-375.

Goodwin, M.B., Evans, D.C. 2016. The early expression of squamosal horns and parietal ornamentation confirmed by new end-stage juvenile *Pachycephalosaursus* fossils from the Upper Cretaceous Hell Creek Formation, Montana. *Journal of Vertebrate Paleontology*. **36**: 1-8.

Goodwin, M.B., Horner, J.R. 2004. Cranial histology of pachycephalosaurs (Ornithischia: Marginocephalia) reveals transitory structures inconsistent with head-butting behavior. *Paleobiology*. **30**: 253-267.

Gradzinsky, R. 1970. Sedimentation of dinosaur-bearing Upper Cretaceous deposits of the Nemegt Basin, Gobi Desert. *Palaeontologica Polonica*. **21**: 147-229.

Gradzinsky, R., Jerzykiewicz, T. 1974. Dinosaur- and mammal-bearing aeolian and associated deposits of the Upper Cretaceous in the Gobi Desert (Mongolia). *Sedimentology and Geology*. **12**: 249-278.

Gradzinsky, R., Kielan-Jaworowska, Z., Maryańska, T. 1977. Upper Cretaceous Djadokhta, Baron Goyot and Nemegt formations of Mongolia, including remarks on previous subdivisions. *Acta Geologica Polonica*. **27**: 281-318.

Haines, R.W. 1950. The flexor muscles of the forearm and hand in lizards and mammals. *Journal of Anatomy*. **84**: 13–29.

Haines, R.W. 1939. A revision of the extensor muscles of the forearm in tetrapods. *Journal of Anatomy*. **73**: 211-233.

Harris, J. 2007. The appendicular skeleton of *Suuwassea emilieae* (Sauropoda: Flagellicaudata) from the Upper Jurassic Morrison Formation of Montana (USA). *Geobios*. **40**: 501-522.

Hilton, R.P., Kirkland, K., Dodson, P., Osmolska, H., Weishampel, D.B. 2004. The Dinosauria. *University of California Press*. 464-477.

Hone, D.W.E., Naish, D. 2013. The 'species recognition hypothesis' does not explain the presence and evolution of exaggerated structures in non-avian dinosaurs. *Journal of Zoology*. doi:10.1111/jzo.12035.

Hoffman, R., Sander, P.M. 2014. The first juvenile specimens of *Plateosaurus engelhardti* from Frick, Switzerland: isolated neural arches and their implication for developmental plasticity in a basal sauropodomorph. *PeerJ*. 2:e458; DOI 10.7717/peerj.458.

Horner, J. R., Goodwin, M.B. 2009. Extreme Cranial Ontogeny in the Upper Cretaceous Dinosaur *Pachycephalosaurus*. *PLoS One*. https://doi.org/10.1371/journal.pone.0007626.

Howell, A.B. 1937. Morphogenesis of the shoulder architecture: Aves. *Auk*. **54**: 364-375.

Hudson, G.E., Schreiweis, D.O., Wang, S.Y.C., *et al*. 1972. A numerical study of the wing and leg muscles of Tinamous (Tinamidae). *Northwest Science*. **46**: 207–255.

Hudson, G.E., Hoff, K.M., Vanden Berge, J.C., *et al*. 1959. A numerical study of the wing and leg muscles of Lari and Alcae. *Ibis.* **111**: 459–524

Hutchinson, J.R. 2001. The evolution of femoral osteology and soft tissues on the line to extant birds (Neornithes). *Zoological Journal of the Linnean Society.* **131**: 169-197.

Hutchinson, J.R., Garcia, M. 2002. *Tyrannosaurus* was not a fast runner. *Nature*. **415**: 1018–1021.

Hutchinson, J.R., S.M. Gatesy. 2000. Adductors, abductors, and the evolution of archosaur locomotion. *Paleobiology.* **26**: 734- 751.

Ibiricu, L.M., Martínez, R.D., Casal, G.A. 2018. The pelvic and hind limb myology of the basal titanosaur *Epachthosaurus sciuttoi* (Sauropoda: Titanosauria). *Historical Biology*. https://doi.org/10.1080/08912 963.2018.1535598

Jasinski, S., Sullivan, R.M. 2011. Re-evaluation of Pachycephalosaurids from the Fruitland-Kirkland Transition (Kirtlandian, Late Campanian), Sand Juan Basin, New Mexico, with a description of a new species of *Stegoceras* and a reassessment of *Texacephale langstoni*. *Fossil Record 3: New Mexico Museum of Natural History and Science, Bulletin 53*. 202-215.

Jasinoski, S.C., Russell, A.P. Currie, P.J. 2006. An integrative phylogenetic and extrapolatory approach to the reconstruction of dromaeosaur (Theropoda: Eumaniraptora) shoulder musculature. *Zoological Journal of the Linnean Society*. **146**: 301-344.

Kilbourne, B.M., Makovicky, P.J. 2010. Limb bone allometry during postnatal ontogeny in non-avian dinosaurs. *Journal of Anatomy*. **217**: 135-152.

Klinkhamer, A.J., Mallison, H., Poropat, S.F., Sinapius, G.H.K., Wroe, S. 2018. Three-dimensional musculoskeletal modeling of the sauropodomorph hind limb: the effect of postural change on muscle leverage. *Anatomical Record*. **301**: 2145-2163.

Klinkhamer, A.J., Mallison, H., Poropat, S.F., Sloan, T., Wroe, S. 2019. Comparative three-dimensional moment arm analysis of the sauropod forelimb: implications for the transition to a wide gauge stance in titanosaurs. *Anatomical Record*. **302**: 794-817.

Klinkhamer, A.J., Wilhite, D.R., White, M.A., Wroe, S. 2017. Digital dissection and three-dimensional interactive models of limb musculature in the Australian estuarine crocodile (*Crocodylus porosus*). *PLoS ONE*. **12**: e0175079.

Kluge, A.G. 1985. Ontogeny and phylogenetic systematics. *Cladistics*. **1**: 13-27.

Kluge, A.G., Strauss, R.E. 1985. Ontogeny and Systematics. *Annual Review of Ecology and Systematics*. **16**: 247-268.

Knell, R.J., Sampson, S. 2011. Bizarre structures in dinosaurs: species recognition or sexual selection? A response to Padian and Horner. *Journal of Zoology.* 283: 18–22.

Kolaceke, A., Velez, M.I., Coulson, I.M., Barbi, M., Tokaryk, T. 2018. Lithostratigraphy of Sections in the Vicinity of the Excavation Site of a Nearly Complete *Tyrannosaurus rex* Skeleton (Scotty) in Southwestern Saskatchewan, Canada. *Summary of Investigations*. **1**: 1-12.

Kriegler, W. 1961. Zur Myologie des Beckens und der Hinterextremität der Reptilien. *Morphologisches Jahrbuch*. **101**: 541–625.

Kundrát, M. 2009. Primary chondrification foci in the wing basipodium of *Struthio camelus* with comments on interpretation of autopodial elements in Crocodilia and Aves. *Journal of Experimental Zoology*. **312B**: 30–41.

Kundrát, M., Cruickshank A.R., Manning T.W., Nudds, J. 2008. Embryos of therizinosauroid theropods from the Upper Cretaceous of China: diagnosis and analysis of ossification patterns. *Acta Zoologica*. **89**: 231–251.

Kupsch, W.O. 1956. Geology of eastern Cypress Hills (Knollys and Dollard quadrangles). *Saskatchewan Department of Mineral Resources, Geological Society Report*. **20**: 1–30.

Kupsch, W.O. 1957. Frenchman formation of Eastern Cypress Hills, Saskatchewan, Canada. *GSA Bulletin*. **68** (4): 413–420.

Lamm, E-T., Werning, S. 2013. Bone Histology of Fossil Tetrapods: Advancing Methods, Analysis, and Interpretation. *University of California Press*. Berkeley and Los Angeles, California.

Langer, M.C., França, M.A.G., Gabriel, S. 2007. The pectoral girdle and forelimb anatomy of the stem-sauropodomorph *Saturnalia tupiniquim* (Upper Triassic, Brazil). *Special Papers in Paleontology*. **31**: 614-638.

Lehman, T. 2010. Pachycephalosauridae from the San Carlos and Aguja Formations (Upper Cretaceous) of West Texas, and Observations of the Frontoparietal Dome. *Journal of Vertebrate Paleontology*. **30**: 786-798.

Lerbekmo, J.F., Sweet, A.R., St. Louis, R.M. 1987. The relationship between the iridium anomaly and palynological floral events at three Cretaceous – Tertiary boundary localities in western Canada. *Geological Society of America Bulletin*. **99**: 325-330.

Livezey, B.C. 1990. Evolutionary morphology of flightlessness in the Aukland Islands Teal. *Condor.* **92**: 639–673.

Longrich, N.R., Sankey, J., Tanke, D. 2010. *Texacephale langstoni*, a new genus of pachycephalosaurid (Dinosauria: Ornithischia) from the upper Campanian Aguja Formation, southern Texas, USA. *Cretaceous Research*. **31**: 274-284.

Lundberg, J.G. 1973. More on primitiveness, higher level phylogenies, and ontogenetic transformations. *Systematic Zoology*. **22**: 327-329.

Mabee, P.M. 2000. The Usefulness of Ontogeny in Interpreting Morphological Characters. In *Phylogenetic Analysis of Morphological Data*. *Smithsonian Institution Press*. 84-114.

Maidment, S.C.R., Barrett, P.M. 2011. The locomotor musculature of basal ornithischian dinosaurs. *Journal of Vertebrate Paleontology*. **31**: 1265-1291.

Maidment, S.C.R., Barrett, P.M. 2014. Osteological correlates for quadrupedality in ornithischian dinosaurs. *Palaeontologica Polonica*. **59**: 53-70.

Mallon, J.C., D.C. Evans. 2014. Taphonomy and habitat preference of North American pachycephalosaurids (Dinosauria, Ornithischia). Lethaia. **47**: 567-578.

Mallon, J.C., Evans, D.C., Tokaryk, T.T., Currie, M.L. 2014. First pachycephalosaurid (Dinosauria: Ornithischia) from the Frenchman Formation (upper Maastrichtian) of Saskatchewan, Canada. *Cretaceous Research*. **56**: 426-431.

Mallon, J.C., Ryan, M.J., Campbell, J.A. 2015. Skull ontogeny in *Arrhinoceratops brachyops* (Ornithischian: Ceratopsidae) and other horned dinosaurs. *Zoological Journal of the Linnean Society*. **75**: 910-929.

Maryańska T., Osmólska H. 1974. Pachycephalosauria, a new suborder of ornithischian dinosaurs. *Palaeontologia Polonica*. **26**: 133–182.

McGowan, C. 1979. The hind limb musculature of the Brown Kiwi, *Apteryx australis mantelli*. *Journal of Morphology*. **160**: 33–74.

McGowan, C. 1982. The wing musculature of the Brown Kiwi, *Apteryx australis mantelli* and its bearing on ratite affinities. *Journal of Zoology*. **197**: 173–219.

McGowan, C. 1986. The wing musculature of the Weka (*Gallirallus australis*), a flightless rail endemic to New Zealand. *Journal of Zoology, London*. **210**: 305-346.

McIntosh J.S. 1990. Sauropoda. In: Weishampel, D., Dodson, P., Osmólska, H., editors. The dinosauria. Berkeley, CA: *University of California Press*. 345–401.

McIver, E.E. 2002. The paleoenvironment of Tyrannosaurus rex from southwestern Saskatchewan, Canada. *Canadian Journal of Earth Sciences*. **39** (2), 207–221.

Meers, M.B. 2003. Crocodylian Forelimb Musculature and Its Relevance to Archosauria. *The Anatomical Record Part A*. **274**: 891-916.

Mossop, G., Shetsen, I. 1994. Geological Atlas of the Western Canada Sedimentary Basin. *Canadian Society of Petroleum Geologists and Alberta Research Council, Calgary*.

Mounce, R.C.P., Sansom, R., Wills, M.A. 2016. Sampling diverse characters improves phylogenies: Craniodental and postcranial characters of vertebrates often imply different trees. *Evolution*. **70**: 666-686.

Nelson, G.J. 1973. The higher-level phylogeny of vertebrates. *Systematic Zoology*. **22**: 87-91.

Nelson, G.J. 1978. Ontogeny, phylogeny, paleontology, and the biogenetic law. *Systematic Zoology*. **27**: 324-345.

Nickel, R., Schummer, A., Seiferle, E., Habermehl, K.H. 2003. Lehrbuch der Anatomie der Haustiere I: Bewegungsapparat: Bd I. *Stuttgart: Parey Verlag*.

Norman, D.B., 1986. On the anatomy of *Iguanodon atherfieldensis* (Ornithischia: Ornithopoda). *Buletin de l'Institut Royal des Sciences Naturelle de Belgique: Sciences de la Terre*. **56**: 281-372.

Otero, A. 2018. Forelimb musculature and osteological correlates in Sauropodamorpha (Dinosauria: Saurischia). *PLoS ONE*. **13**: e0198988.

Otero, A., Gallina, P.A., Herrera, Y. 2010. Pelvic musculature of *Caiman latirostris*. *Herpetological Journal*. **20**: 173-184.

Otero, A., Vizcaíno, S.F. 2008. Hindlimb musculature and function of *Neuquensaurus australis* (Sauropoda: Titanosauria). *Ameghiniana*. **45**: 333-348.

Padian, K. 2004. Basal Avialae. In: *The Dinosauria*, 2nd edn. (eds Weishampel D.B., Dodson, P., Osmolska, H.). *Berkeley: University of California Press*. 210-231.

Padian, K., Horner, J.R. 2010. The evolution of 'bizarre structures' in dinosaurs: biomechanics, sexual selection, social selection or species recognition? *Journal of Zoology*. **283**: 3-17.

Parker, W.G. 2016. Revised phylogenetic analysis of the Aetosauria (Archosauria: Pseudosuchia); assessing the effects of incongruent morphological character sets. *PeerJ*. 4:e1583; DOI 10.7717/peerj.1583.

Perales-Gogenola, L. Elorza, J., Canudo, J.I., Pereda-Suberbiola, X. Taphonomy and palaeohistology of ornithischian dinosaur remains from the Lower Cretaceous bonebed of La Cantalera (Teruel, Spain). *Cretaceous Research*. **98**: 316-334.

Perle, A., Maryańska, T., Osmolska, H. 1982. *Goyocephale Lattimorei* Gen. ET SP. N., A New Flat-Headed Pachycephalosaur (Ornithischia, Dinosauria) From the Upper Cretaceous of Mongolia. *Acta Palaeontologica Polonica*. **27**: 115-132.

Persons, W.S., Currie, P.J. 2011. The Tail of *Tyrannosaurus*: Reassessing the Size and Locomotive Importance of the *M. caudofemoralis* in Non-Avian Theropods. *The Anatomical Record*. **294**: 119-131.

Persons, W.S., Currie, P.J. 2020. The Anatomical and Functional Evolution of the Femoral Fourth Trochanter in Ornithischian Dinosaurs. *The Anatomical Record*. **303**: 1146-1157.

Peterson, J.E., Bigalke, C.L. 2013. Hydrodynamic Behaviors of Pachycephalosaurid Domes in Controlled Fluvial Settings: A Case Study in Experimental Dinosaur Taphonomy. *Palaios*. **28**: 285-292.

Peterson, J.E., Dischler, C., Longrich, N.R. 2013. Distributions of cranial pathologies provide evidence for head-butting in dome-headed dinosaurs (Pachycephalosauridae). *PLoS One*. **8**: e68620.

Pfretzschner, H., Tutken, T. 2011. Rolling bones – Taphonomy of Jurassic dinosaur bones inferred from diagenetic microcracks and mineral infillings. *Palaeogeography, Palaeoclimatology, Palaeoecology*. **310**: 117-123.

Piechowski, R., Tałanda, M. 2020. The locomotor musculature and posture of the early dinosauriform *Silesaurus opolensis* provides a new look into the evolution of Dinosauromorpha. *Journal of Anatomy*. **236**: 1044-1100.

Poore, S.O., Sanchez-Haiman, A., Goslow, G.E. 1997. Wing upstroke and the evolution of flapping flight. *Nature*. **387**: 799-802.

Poroporat, S.F., Upchurch, P., Mannion, P.D., Hocknull, S.A., Kear, B.P., Sloan, T., Sinapius, G.H.K., Elliott, D.A. 2015. Revision of the sauropod dinosaur *Diamantinasaurus matildae* Hocknull *et al*. 2009 from the mid-Cretaceous of Australia: Implications for Gondwanan titanosauriform dispersal. *Gondwana Research*. **27**: 995-1033.

Prieto-Márquez, A., Erickson, G.A., Ebersole, J.A. 2016. A primitive hadrosaurid from southern North America and the origin and early evolution of “duck-billed” dinosaurs. *Journal of Vertebrate Paleontology*. e1054495 DOI 10.1080/02724634.2015.1054495.

Prieto-Márquez, A., Erickson, G.A., Ebersole, J.A. 2016. Anatomy and osteohistology of the basal hadrosaurid dinosaur *Eotrachodon* from the uppermost Santonian (Cretaceous) of Southern Appalachia. *PeerJ*. 4:e1872; DOI 10.7717/peerj.1872.

Redelstorff, R., Sander, P.M. 2009. Long and Girdle Bone Histology of *Stegosaurus*: Implications for Growth and Life History. *Journal of Vertebrate Paleontology*. **29**: 1087-1099.

Redman, C.M., Gardner, J.D., Scott, C.S., Braman, D.R. 2015. Geological setting of vertebrate microfossil localities across the Cretaceous-Paleogene boundary in southwestern Saskatchewan, Canada. *Canadian Journal of Earth Sciences*. **52**: http://dx.doi.org/10.1139/cjes-2015-0038.

Romer, A.S. 1923. Crocodilian pelvic muscles and their avian and reptilian homologues. *Bulletin of the American Museum of Natural History.* **48**: 533-552.

Romer, A. S. 1927. The development of the thigh musculature of the chick. *Journal of Morphology.* **43**: 347-385.

Romer, A.S. 1944. The development of tetrapod limb musculature – the shoulder region of *Lacerta*. *Journal of Morphology*. **74**: 1-41.

Romer, A.S. 1956. Osteology of the Reptiles. *Krieger Publishing Company, Malabar, Florida*. 771.

Rowe, T. 1986. Homology and evolution of the deep dorsal thigh musculature in birds and other Reptilia. *Journal of Morphology*. **189**: 327-346.

Russell, A.P., Bauer, A.M. 2008. The appendicular locomotor apparatus of *Sphenodon* and normal-limbed squamates. In: *Biology of the Reptilia 24, Morphology 1.* (eds Gans, C., Gaunt, A.S., Adler, K.). *Ithaca, NY: Society for the Study of Amphibians and Reptiles*. 1–466.

Russell, D., Manabe, M. 2002. Synopsis of the Hell Creek (uppermost Cretaceous) dinosaur assemblage. *Geological Society of America*. **361**: 169-176.

Santa-Luca, A.P., Crompton, A.W., Charig, A.J. 1976. A complete skeleton of the Late Triassic ornithischian *Heterodontosaurus tucki*. *Nature.* **264**: 324-328.

Sanz, J.L., Powell, J.E., Le Loeuff, J., Martinez, R., Pereda Suberbiola, X. 1999. Sauropod remains from the Upper Cretaceous of Laño (northcentral Spain). Titanosaur phylogenetic relationships. *Estudios del Museo de Ciencias Naturales de Álava*. **14**: 235-255.

Schachner, E.R., Manning, P.L., Dodson, P. 2011. Pelvic and hindlimb myology of the basal Archosaur *Poposaurus gracilis* (Archosauria: Poposauroidea). *Journal of Morphology.* **272**: 1464–1491

Schott, R.K. 2011. Ontogeny, Diversity, and Systematics of Pachycephalosaur Dinosaurs from the Belly River Group of Alberta. *University of Toronto*. MR76231.

Schott, R.K., Evans, D.A. 2012. Squamosal ontogeny and variation in the pachycephalosaurian dinosaur *Stegoceras validum* Lambe, 1902, from the Dinosaur Park Formation, Alberta. *Journal of Vertebrate Paleontology*. **32**: 903-913.

Schott, R.K., Evans, D.C. 2016. Cranial variation and systematic of *Foraminacephale brevis* gen. nov. and the diversity of pachycephalosaurid dinosaurs (Ornithischia: Cerapoda) in the Belly River Group of Alberta, Canada. *Zoological Journal of the Linnean Society*. **179**: 865-906.

Schott, R.K., Evans, D.C., Goodwin, M.B., Horner, J.R., Brown, C.M. 2011. Cranial Ontogeny in *Stegoceras validum* (Dinosauria: Pachycephalosauria): A Quantitative Model of Pachycephalosaur Dome Growth and Variation. *PLoS One*. **6**: e21092. DOI:10.1371/journal.pone.0021092.

Schott, R.K., Evans, D.C., Williamson, T.E., Carr, T.D., Goodwin, M.B. 2009. The anatomy and systematic of *Colepiocephale lambei* (Dinosauria: Pachycephalosauridae). *Journal of Vertebrate Paleontology*. **29**: 771-786.

Senter, P. 2006. Scapular orientation in theropods and basal birds, and the origin of flapping flight. *Acta Palaeontological Polonica*. **51**: 305-313.

Sereno, P.C. 1987. The ornithischian dinosaur *Psittacosaurus* from the Lower Cretaceous of Asia and the relationships of the Ceratopsia. *Proquest Dissertations Publishing*. 8710225.

Sereno, P.C. 1997. The Origin and Evolution of Dinosaurs. *Annual Review of Earth and Planetary Sciences*. **25**: 435-489.

Sereno, P.C. 2000. The fossil record, systematics and evolution of pachycephalosaurs and ceratopsians from Asia. *The Age of Dinosaurs in Russia and Mongolia*. 480-516.

Snively, E., Cox, A. 2008. Structural mechanics of pachycephalosaur crania permitted head-butting behavior. *Palaeontologica Electronica*. **11**: 17.

Sereno, P.C., Shichin, C., Zhengwu, C., Chenggang, R. 1988. *Psittacosaurus meileyingensis* (Ornithischia: Ceratopsia), a new psittacosaur from the Lower Cretaceous of Northeastern China. *Journal of Vertebrate Paleontology*. **8**: 366-377.

Simpson, G.G. 1950. The Meaning of Evolution: A study of the History of Life and of its Significance for Man. *New Haven*: *Yale University Press*, **363**.

Slowiak, J., Tereshchenko, V.S., Fostowicz-Frelik, L. 2019. Appendicular skeleton of *Protoceratops andrewsi* (Dinosauria, Ornithischia): comparative morphology, ontogenetic changes, and the implications for non-ceratopsid ceratopsian locomotion. *PeerJ*. 7:e7324 DOI 10.7717/peerj.7324

Snively, E., Theodor, J.M. 2011. Common functional correlates of head-strike behavior in the pachycephalosaur *Stegoceras validum* (Ornithischia, Dinosauria) and combative artiodactyls. *PLoS One*. **6**: e21422.

Spies, M.J., Gibbon, V.E., Finaughty, D.A. 2018. Forensic taphonomy: Vertebrate scavenging in the temperate southwestern Cape, South Africa. *Forensic Science International*. **290**: 62-69.

Storer, J.E., 1989. Geological History of Saskatchewan. Saskatchewan Museum of Natural History. *Government of Saskatchewan, Canada*.

Straus, W.L., 1942. The homologies of the forearm flexors: urodeles, lizards, mammals. *American Journal of Anatomy*. **70**: 281-316.

Sues, H.D. 1978. Functional morphology of the dome in pachycephalosaurid dinosaurs. *Neues Jahrbuch fur Geologie und Palaontologie Monatshefte*. **8**: 459– 472.

Sues, H., Galton, P.M. 1982. The Systematic Position of *Stenopelix valdensis* (Reptilia: Ornithischia) from the Wealden of North-Western Germany. *Palaeontographica*. **178**: 183-190.

Sues, H., Galton, P.M. 1987. Anatomy and classification of the North American Pachycephalosauria (Dinosauria: Ornithischia). *Palaeontographica*. **198**: 1-48.

Sullivan, G.E. 1962. Anatomy and embryology of the wing musculature of the domestic fowl (*Gallus*). *Australian Journal of Zoology*. **10**: 458-518.

Sullivan, R.M. 2003. Revision of the dinosaur *Stegoceras* Lambe (Ornithischia, Pachycephalosauridae). *Journal of Vertebrate Paleontology*. **23**: 181-207.

Sullivan, R.M. 2006. A taxonomic review of the Pachycephalosauridae (Dinosauria; Ornithischia). *Late Cretaceous Vertebrates from the Western Interior, Bulletin 35*.

Sullivan, P.M., Lucas, S.G. 2006. The Pachycephalosaurid Dinosaur *Stegoceras Validum* from the Upper Cretaceous Fruitland Formation, San Juan Basin, New Mexico. *Late Cretaceous Vertebrates from the Western Interior, Bulletin 35*. 329-330.

Tarsitano, S.F. 1981. Pelvic and hindlimb musculature of archosaurian reptiles. *PH.D., City University, New York.*

Tokaryk, T.T., 1997. First evidence of juvenile ceratopsians (Reptilia: Ornithischia) from the Frenchman Formation (late Maastrichtian) of Saskatchewan. *Canadian Journal of Earth Sciences*. **34** (10): 1401–1404.

Tokaryk, T.T., 2009. Head-hunting in Saskatchewan: the history of Triceratops. *Frenchman Formation Terrestrial Ecosystem Conference. Eastend, Saskatchewan: Royal Saskatchewan Museum Contribution to Science*. **12**: 61–62.

Tokaryk, T.T., Brinkman, D., 2009. Turtles from the Frenchman Formation and latitudinal patterns of distribution of turtles in the late Maastrichtian. *Gaffney Turtle Symposium. Royal Tyrrell Museum, Drumheller, Alberta*. 178–179.

Tokaryk, T.T., Bryant, H.N., 2004. The fauna from the Tyrannosaurus rex excavation, Frenchman Formation (late Maastrichtian), Saskatchewan summary of investigations. *Saskatchewan Geological Survey, Saskatchewan Industry Resources, Misc. Rep*. **1**: 1–12.

Tokaryk, T.T., James, P.C., 1989. Cimolopteryx sp. (Aves, Charadriiformes) from the Frenchman Formation (Maastrichtian), Saskatchewan. *Canadian Journal of Earth Sciences*. **26** (12): 2729–2730.

Tschopp, E., Mateus, O. 2013. The skull and neck of a new flagellicaudatan sauropod from the Morrison Formation and its implication for the evolution and ontogeny of diplodocid dinosaurs. *Journal of Systematic Palaeontology*. **11**: 853-888.

Tsuihiji, T. 2010. Reconstructions of the axial muscle insertions in the occipital region of dinosaurs: evaluations of past hypotheses on marginocephalia and Tyrannosauridae using the extant phylogenetic bracket approach. *The Anatomical Record*. **293**: 1360-1386.

Vanden Berge, J.C., Zweers, G.A. 1993. Myologia In: Handbook of Avian Anatomy: Nomina Anatomica Avium. (eds Baumel, J.J., King, A.S., Breazile, J.E., Evans, H.E., Vanden Berge, J.C.). *Cambridge: Nuttall Ornithological Club*. 189-247.

Vazquez, R.J. 1994. The automating skeletal and muscular mechanisms of the avian wing (Aves). *Zoomorphology*. **114**: 59-71.

Voegele, K.K., Ullmann, P.V., Lamanna, M.C., Lacovara, K.J. 2020. Appendicular myological reconstruction of the forelimb of the giant titanosaurian sauropod dinosaur *Dreadnoughtus schrani*. *Journal of Anatomy*. **237**: 133-154.

Voegele, K.K., Ullmann, P.V., Lamanna, M.C., Lacovara, K.J. 2021. Myological reconstruction of the pelvic girdle and hind limb of the giant titanosaurian sauropod dinosaur *Dreadnoughtus schrani*. *Journal of Anatomy*. **238**: 576-597.

von Huene, F. 1929. Los saurisquios y ornithisquios del Cretacéo Argentino. *An Museo de La Plata*. **3**: 1-196.

Walker, A.D. 1977. Evolution of the pelvis in birds and archosaurs. In S.M. Andrews, R.S. Miles, A.D. Walker (eds.), Problems in Vertebrate Evolution. *Academic Press, New York*. 319-357

Walker, J.W.F. 1973. The locomotor apparatus of testudines. In: *Biology of the Reptilia 4.* (eds Gans, C., Parsons, T.S.). *New York: Academic Press*. 1–100.

Wang, C., Scott, R.W., Wan, X., Graham, S.A., Huang, Y., Wang, P., Wu, H., Dean, W.E., Zhang, L. 2013. Late Cretaceous climate changes recorded in Eastern Asian lacustrine deposits and North American Epieric sea strata. *Earth-Science Reviews*. **126**: 275-299.

Weishampel, D.B., Norman, D.B. 1989. Vertebrate herbivory in the Mesozoic; Jaws, plants and evolutionary metrics. *Geological Society of America*. **238**: 87-101.

Werning. S. 2012. The Ontogenetic Osteohistology of *Tenontosaurus tilletti*. *PLoS One*. https://doi.org/10/1371/journal.pone.0033539.

Williamson, T.E., Brusatte, S.L. 2016. Pachycephalosaurs (Dinosauria: Ornithischia) from the Upper Cretaceous (upper Campanian) of New Mexico: A reassessment of *Stegoceras novomexicanum*. *Cretaceous Research*. **62**: 29-43.

Williamson, T.E., Carr, T.D. 2002. A new genus of derived pachycephalosaurian from western North America. *Journal of Vertebrate Paleontology*. **22**: 779-801.

Williamson, T.E., Carr, T.D. 2006. First Record of a Pachycephalosaurine (Ornithischia: Pachycephalosauria) From the Dinosaur Park Formation, Alberta, Canada. *Late Cretaceous Vertebrates from the Western Interior, Bulletin 35*. 323-327.

Witmer, L.M. 1995. The extant phylogenetic bracket and the importance of reconstructing soft tissues in fossils. In: Thompson, J. (Ed.) Functional morphology in vertebrate paleontology. London: *Cambridge University Press*. 19-33.

Woodward, H.N. 2019. Maiasaura (Dinosauria: Hadrosauridae) Tibia Osteohistology Reveals Non-annual Cortical Vascular Rings in Young of the Year. *Frontiers in Earth Science*. DOI 10.3389/feart.2019.00050.

Zusi, R.L. Bentz, G.D. 1978. The appendicular myology of the Labrador Duck (*Camptorhynchus labradorius*). *Condor*. **80**: 407–418.

Appendix

Supplementary Table 1. Character-Taxon matrix used in the phylogenetic analysis of pachycephalosaurs.

	1	**2**	**3**	**4**	**5**	**6**	**7**	**8**	**9**
Psittacosaurus mongoliensis	0	0	0	0	0	0	0	0	0
Yinlong downsi	0	0	0	?	1	0	0	?	0
Wannanosaurus yansiensis	?	?	1	1	0	?	?	?	?
Goyocephale lattimorei	1	1	1	1	1	1	1	1	1
Homalocephale calathocercos	1	1	?	?	?	1	1	1	1
Tylocephale gilmorei	?	?	?	?	?	?	?	?	?
Prenocephale prenes	1	1	?	?	1	1	1	?	1
Foraminacephale brevis	?	?	?	?	?	?	?	?	?
Hanssuesia sternbergi	?	?	?	?	?	?	?	?	?
Colepiocephale lambei	?	?	?	?	?	?	?	?	?
Stegoceras validum	?	1	1	1	1	1	1	1	0
Pachycephalosaurus wyomingensis	?	1	?	?	?	1	1	?	1
Alaskacephale gangloffi	?	?	?	?	?	?	?	?	?
Sphaerotholus goodwini	?	?	?	?	?	?	?	?	?
Sphaerotholus buchholtzae	?	?	?	?	?	?	?	?	?
Acrotholus audeti	?	?	?	?	?	?	?	?	?
Stegoceras novomexicanum	?	?	?	?	?	?	?	?	?
Amtocephale gobiensis	?	?	?	?	?	?	?	?	?
CMN 22039	?	1	?	?	?	1	?	?	1

	10	**11**	**12**	**13**	**14**	**15**	**16**	**17**	**18**
Psittacosaurus mongoliensis	0	0	0	0	0	0	0	0	0
Yinlong downsi	0	0	0	?	0	0	1	0	0
Wannanosaurus yansiensis	?	?	?	?	1	?	1	0	1
Goyocephale lattimorei	1	0	?	?	1	1	1	1	1
Homalocephale calathocercos	2	1	0	1	1	?	1	1	1
Tylocephale gilmorei	?	?	?	?	1	?	1	1	1
Prenocephale prenes	2	1	0	1	1	1	1	1	1
Foraminacephale brevis	?	?	?	?	1	?	1	1	1
Hanssuesia sternbergi	?	?	?	?	1	?	1	1	1
Colepiocephale lambei	?	?	?	?	1	?	?	?	1
Stegoceras validum	2	0	1	1	1	0	1	1	1
Pachycephalosaurus wyomingensis	2	1	1	1	1	?	1	1	1
Alaskacephale gangloffi	?	?	?	?	1	?	1	1	?
Sphaerotholus goodwini	?	?	?	?	1	?	1	1	1
Sphaerotholus buchholtzae	?	?	?	?	1	?	1	1	1
Acrotholus audeti	?	?	?	?	1	?	1	1	1
Stegoceras novomexicanum	?	?	?	?	1	?	?	?	1
Amtocephale gobiensis	?	?	?	?	1	?	?	?	1
CMN 22039	2	0	1	1	?	?	?	?	?

	19	20	21	22	23	24	25	26	27
Psittacosaurus mongoliensis	0	0	0	0	0	0	0	0	0
Yinlong downsi	1	0	0	0	?	?	0	0	?
Wannanosaurus yansiensis	1	0	1	?	?	?	?	?	?
Goyocephale lattimorei	1	1	?	?	1	?	?	0	1
Homalocephale calathocercos	1	1	1	1	1	0	1	0	2
Tylocephale gilmorei	1	1	1	1	?	1	?	0	2
Prenocephale prenes	1	1	1	1	1	0	1	0	2
Foraminacephale brevis	?	1	?	?	?	?	?	?	?
Hanssuesia sternbergi	?	1	?	?	?	?	?	?	?
Colepiocephale lambei	?	1	?	?	?	?	?	?	?
Stegoceras validum	1	1	1	1	1	0	1	0	1
Pachycephalosaurus wyomingensis	1	1	1	1	?	0	1	1	2
Alaskacephale gangloffi	?	1	?	?	?	?	?	?	?
Sphaerotholus goodwini	1	1	?	?	1	?	?	?	2
Sphaerotholus buchholtzae	?	1	?	?	?	?	?	?	?
Acrotholus audeti	?	1	?	?	?	?	?	?	?
Stegoceras novomexicanum	?	1	?	?	?	?	?	?	?
Amtocephale gobiensis	?	1	?	?	?	?	?	?	?
CMN 22039	?	?	?	?	?	?	?	?	?

	28	**29**	**30**	**31**	**32**	**33**	**34**	**35**	**36**
Psittacosaurus mongoliensis	0	0	0	0	0	0	0	0	0
Yinlong downsi	0	0	0	0	0	0	0	0	0
Wannanosaurus yansiensis	0	?	?	?	0	0	0	0	?
Goyocephale lattimorei	0	?	0	1	0	0	0	0	1
Homalocephale calathocercos	0	?	0	?	0	0	0	0	1
Tylocephale gilmorei	1	?	0	?	2	1	?	0	2
Prenocephale prenes	1	2	0	1	2	1	1	0	1
Foraminacephale brevis	1	1	1	2	2	1	1	0	1
Hanssuesia sternbergi	0	1	1	2	2	1	?	?	?
Colepiocephale lambei	0	1	1	2	1	1	0	?	?
Stegoceras validum	1	1	1	2	2	1	0	0	1
Pachycephalosaurus wyomingensis	1	2	0	1	2	2	1	0	?
Alaskacephale gangloffi	1	2	?	?	?	?	1	?	1
Sphaerotholus goodwini	1	2	0	1	2	2	1	1	2
Sphaerotholus buchholtzae	1	2	0	1	2	2	1	1	2
Acrotholus audeti	1	2	0	1	2	1	1	?	?
Stegoceras novomexicanum	0	1	1	2	1	1	0	?	?
Amtocephale gobiensis	1	2	?	2	2	1	1	?	?
CMN 22039	?	?	?	?	?	?	?	?	?

	37	**38**	**39**	**40**	**41**	**42**	**43**	**44**	**45**
Psittacosaurus mongoliensis	0	0	0	0	0	0	0	0	0
Yinlong downsi	0	0	1	0	0	0	0	0	0
Wannanosaurus yansiensis	0	0	1	?	0	0	0	0	0
Goyocephale lattimorei	2	0	1	1	1	?	1	1	1
Homalocephale calathocercos	2	0	1	0	1	1	1	1	1
Tylocephale gilmorei	?	0	1	0	1	?	0	1	0
Prenocephale prenes	1	0	1	0	0	0	0	1	0
Foraminacephale brevis	2	0	1	1	0	1	0	1	0
Hanssuesia sternbergi	?	?	?	?	?	?	?	?	?
Colepiocephale lambei	?	?	?	?	?	?	?	?	?
Stegoceras validum	1	0	1	1	1	[01]	1	0	0
Pachycephalosaurus wyomingensis	2	0	2	0	0	?	?	1	0
Alaskacephale gangloffi	?	0	2	0	0	?	0	?	0
Sphaerotholus goodwini	1	0	1	0	0	0	0	1	0
Sphaerotholus buchholtzae	2	0	1	0	0	1	0	1	0
Acrotholus audeti	1	?	?	?	?	0	?	?	?
Stegoceras novomexicanum	1	0	?	?	?	0	?	?	?
Amtocephale gobiensis	2	0	?	?	?	?	?	?	?
CMN 22039	?	?	?	?	?	?	?	?	?

	46	**47**	**48**	**49**	**50**	**51**	**52**
Psittacosaurus mongoliensis	0	0	0	0	0	0	0
Yinlong downsi	0	0	0	0	0	?	?
Wannanosaurus yansiensis	0	0	?	0	0	?	2
Goyocephale lattimorei	0	?	1	1	1	?	?
Homalocephale calathocercos	0	0	?	1	1	1	2
Tylocephale gilmorei	0	0	?	?	0	?	?
Prenocephale prenes	0	0	1	1	1	1	1
Foraminacephale brevis	0	?	?	0	1	?	?
Hanssuesia sternbergi	?	?	?	?	?	?	?
Colepiocephale lambei	?	?	?	?	?	?	?
Stegoceras validum	0	0	0	0	0	2	2
Pachycephalosaurus wyomingensis	0	1	2	1	0	1	2
Alaskacephale gangloffi	0	?	?	?	?	?	?
Sphaerotholus goodwini	0	?	?	0	1	?	?
Sphaerotholus buchholtzae	0	?	?	0	1	?	?
Acrotholus audeti	?	?	?	?	?	?	?
Stegoceras novomexicanum	?	?	?	?	?	?	?
Amtocephale gobiensis	?	?	?	?	?	?	?
CMN 22039	?	?	?	?	?	1	1

Supplementary Note 1. List of characters used in the phylogenetic analysis of pachycephalosaurs (Modified from Evans *et al*., 2013 and Williamson & Brusatte, 2016).

1. Posterior sacral rib length: short and subrectangular (0); strap-shaped and elongate (1).

2. Preacetabular process, shape of distal end: tapered and subvertically oriented (0); dorsoventrally flattened and expanded distally (1).

3. Humeral length: more (0), or less than (1), 50% of femoral length (2).

4. Humeral shaft form: straight (0); bowed (1).

5. Deltopectoral crest development: strong (0); rudimentary (1).

6. Zygapophyseal articulations, form: flat (0); grooved (1).

7. Ossified tendons: bundled, rodlike (0); caudal basket, fusiform (1).

8. Sternal shape: plate-shaped (0); shafted (1).

9. Iliac blade, lateral deflection of preacetabular process weak (0); marked (1).

10. Iliac blade, position of medial tab: absent (0); above acetabulum (1); on postacetabular process (2).

11. Postacetabular process of ilium: elongate and subrectangular (0); deep and downturned distally, with an arcuate dorsal margin (1).

12. Ischial pubic peduncle, shape: dorsoventrally (0), or transversely (1); flattened

13. Pubic body: substantial (0); reduced, nearly excluded from acetabulum (1).

14. Frontal and parietal thickness: thin (0); thick (1).

15. Arched premaxilla-maxilla diastema: absent (0); present (1).

16. Postorbital-squamosal bar, form: strap-shaped with a narrow dorsal margin (0); broad, flattened (1).

17. Squamosal exposure on occiput: restricted (0); broad (1).

18. Supraorbital bones 1 and 2: absent (0); present, and exclude the frontal from the orbital rim (1).

19. Postorbital-jugal bar, position of descending process of postorbital: extends to the ventral margin of the orbit (0); terminates above the ventral margin of the orbit, interdigitate postorbital-jugal contact (1).

20. Parietal septum, form: narrow and smooth (0); broad and rugose, has dorsal ornamentation (1).

21. Infratemporal fenestra size: larger than orbit, lower temporal bar long (0); smaller than orbit, lower temporal bar greatly shortened, jugal and quadrate in close proximity or have a small contact (1).

22. Pterygoquadrate rami, posterior projection of ventral margin: weak, jaw joint at the approximate level of occusal surface (0); pronounced, jaw joint below occlusal surface (1).

23. Prootic-basisphenoid plate: absent (0); present (1).

24. Quadratojugal fossa: absent (0); present (1).

25. Quadrate, posterior ramus in lateral view: subvertical or gently curved dorsally (0); sinuous, quadrate strongly inclined dorsally, posterior ramus embayed (1).

26. Skull: relatively short, rostrum has a convex profile (0); relatively long, rostrum has a concave dorsal profile (1).

27. Epaxial muscle attachment scars on ventrocaudal margin of paroccipital process, caudal view: absent or indistinct (0); broad extending from ventrocaudal margin of paroccipital process and including region above foramen magnum (1); restricted to area dorsolateral to foramen magnum (2).

28. Supratemporal fenestra: open (0); closed (1).

29. Roof of temporal chamber as manifest on parietal in lateral view: absent (0); small, roof horizontal (1); enlarged, dorsally arched (2).

30. Grooves in frontal: absent (0); present (1).

31. Contact of anterior supraorbital with frontal: absent (0); restricted (1); extensive (2).

32. Doming of frontoparietal: absent (0); does not include supraorbital lobes (1); includes supraorbital lobes (2).

33. Dorsal margins of postorbital and posterior supraorbital sutural surfaces on dome: postorbital and supraorbital II do not form part of a dome (0); dorsally arched such that

there is a distinct diastema between the two (1); both are straight and continuous, diastema absent (2).

34. Frontoparietal dome in lateral view, caudal margin of parietal dome blends with parietosquamosal shelf along a curve: absent (0); present (1).

35. Parietosquamosal bar in caudal view (viewed perpendicular to shelf): horizontal or slopes at a shallow ventrolateral angle (0); slopes at a steep ventrolateral angle (1).

36. Parietosquamosal bar beneath the primary node row: absent (0); maintains approximately the same depth or slightly deepens laterally (1); shallows laterally (2).

37. Exposure of posteromedian (intersquamosal) process between squamosals: caudolateral wings well developed (0); restricted (1); broad (2).

38. Extensive intersquamosal joint posterior to parietal: absent (0), present (1).

39. Parietosquamosal bar primary (enlarged) nodes: absent (0); in a single row (1); in two or more rows sometimes appearing clustered (2).

40. Number of nodes in the primary parietosquamosal node row: 5 or less (0) 6 or more (1).

41. Irregular tuberculate ornamentation on caudal surface of squamosal below the primary node row: absent (0); present (1).

42. Parietal, parietosquamosal nodes: absent (0); medial most nodes of the primary node row occur largely or completely on the parietal (1).

43. Medialmost nodes in primary parietosquamosal node row, enlarged relative to all other nodes: absent (0); present (1).

44. Enlarged corner node on squamosal ventrolateral to primary node row of parietosquamosal bar: absent (0); present (1).

45. Secondary corner node, medial to the lateroventral corner node: absent (0); present (1).

46. Squamosal, several nodes drawn out into long spikes: absent (0); present (1).

47. Large, conical node projects laterally from jugal: absent (0); present (1).

48. Rostral nodes: absent (0); continue from the supraorbital shelf onto the dorsal region of the rostrum (1); cover the dorsal surface of rostrum and form series of 'half rings' (2).

49. Postorbital node row: absent (0); present (1).

50. Posterolateral edge of skull formed by squamosal and postorbital in dorsal view: straight (0); convex (1).

51. Medial iliac tab projects: directly horizontally (0); dorsomedially at an angle of at least 30^{o} from the horizontal (1).

52. Fourth trochanter shape: strongly pendant (0); weakly pendant (1); not pendant (2).